E V A L U A T I O N   A N D   D E V E L O P M E N T   O F   A N

I N - V I V O   B O N E   D E N S I T O M E T E R

B Y

M O H A M M E D   I B R A H I M   A L - J A R A L L A H

A thesis submitted for the degree of

DOCTOR OF PHILOSOPHY

Department of Physics

The University of Aston in Birmingham

JULY 1976

SUMMARY

Archer-Hall et al, 1973, have described an in-vivo bone densitometer (scanning machine) which employs a conventional X-ray set and has many merits. The scanning machine was designed to give a scan of the ulna. The work described in this thesis is a continuation of this work.

Various improvements have been made on the machine to make it more accurate and reproducible in clinical use.

An artificial bone reference material has been made which is homogeneous, machinable and has attenuation coefficients similar to a real compact bone. It serves to calibrate the output signals in scanning measurements.

An optical transform system has been designed to give a linear area representation of the quantity of bone mineral shown non-linearly on the trace. The total mineral in a scanned bone section can be determined by the use of a planimeter on this area transform.

In a series of an in-vitro measurements on post mortem ulnar sections, good correlations were found between the scan areas and the following weights: total bone, dry fat-free bone and ash. The scan areas were also correlated to calcium content of the bone as found by neutron activation. The effect of arm repositioning errors on scans were also studied.

Measurements have been made using the scanning machine in-vivo, on volunteers and in several cases involving metabolic bone diseases.

ACKNOWLEDGEMENTS

TO MY FAMILY

<div dir="rtl">

وما أُوتيتم مِّنَ العِلمِ إلا قليلا.

الفرقان ـ سورة الإسـراء .

</div>

You have been given of knowledge nothing except a little

ALFORGAN-SURAH XVII

Part of verse 85

CONTENTS

NOTATION

AB	artificial bone
A_n	transform area corresponding to nth step
a	diameter of powder $\left[Ca_3(PO_4)_2 \right]$ particle
B	bone mineral mass per unit area in radiation beam path
$\int Bdw$	total mineral content in the bone site scanned
b	thickness of bone in g/cm^2
$\bar{b}$	slit width
C_1, C_2	constants
C_o	count rate at the start of count $(t = 0)$
c	mean cortical thickness of bone
D	total standard deviation
D_1, D_2	standard deviations of counts
D_3, D_4	fractional errors
d	distance from the anode to the detector
F	constant
$\bar{F}$	load
f	focal length
$\bar{f}$	frequency
g	gravitational force per unit mass
h_n	signal height of the nth step measured from step five (y_5)
h_n^*	signal height of nth step in the image, measured from step five (y_5^*)

h_1, h_2 — peaks in ulna trace representing 1st and 2nd maximum attenuations of X-rays

I_o — count rate of unattenuated photon beam

I_1 — count rate of attenuated photon beam in soft tissue

I_2 — count rate of attenuated photon beam in soft tissue and bone

$\bar{I}_o$ — X-ray intensity reaching the detector when anode is vertically above the slit

$\bar{I}$ — X-ray intensity reaching the detector when anode is at any possible position (x from normal position)

I_o^* — X-ray intensity for zero thickness

I^* — X-ray intensity transmitted through thicknesses of uranium and tungsten

I — measured count rate

I_Z — current at depth x

K — force constant

K^* — viscosity constant

$\bar{K}$ — constant

l — total thickness of bone and soft tissue

M — constant

m_2 — mass of powder particle

m_1 — mass of an equivalent size of molten araldite

$m = m_2 - m_1$

n — step number

PR — planimeter

r — radius of artificial bone specimen

$\bar{S}$ — total displacement of powder particle

S_1	photon current from the monitor detector
S_2	photon current from the second detector ('detector')
SA_n or SA	total scan area
$\triangle SA_n$	scan area corresponding to step number n
S	thickness of soft tissue in g/cm^2
T	'actual' counting time
t	recorded decay time
$t\grave{}$	time of 'mean count rate'
$t + t\grave{}$	total decay time
$t_{1/2}$	half life
$\bar{t}$	thickness of slab forming the slit
t_u	thickness of uranium
t_w	thickness of tungsten
u	distance of object from lens principle plane
V	volume of powder particle
v	distance of image from lens principle plane
W	weight of bone, mineral or calcium
W_i	weight percentage of ith element
$\bar{W}$	preset voltage value of the monitor detector
$\bar{w}$	angular speed
w	bone width
w_o	bone width in the trace
w_i	bone width in the image transform
d_w	an element width of bone in the site scanned
x	depth of penetration of current

$\bar{x}$	axial anode movement
x^{*}	$\mu_u t_u + \mu_w t_w$
$\bar{y}$	decrease in width of the detector slit
$y_{(n)}$	the function of signal heights
y_n^{*}	signal height of the nth step
y_n	signal height of the nth step in the image transform
$\propto$	$\sqrt{j\,\sigma\,\bar{\mu}\,\bar{w}}$
β	constant
δ	depth at which penetration current decreased to $\frac{1}{e}$ ($-$ 37%)
η	viscosity of molten araldite
σ	electric conductivity
λ	radioactive decay constant
μ or μ_1	linear attenuation coefficient
μ_m	mass attenuation coefficient
μ_b	linear attenuation coefficient of bone
μ_s	linear attenuation coefficient of soft tissue
μ_u	linear attenuation coefficient of uranium
μ_w	linear attenuation coefficient of tungsten
$\bar{\mu}$	magnetic permeability
ρ	density
ρ_s	density of soft tissue
ρ_b	density of bone
ρ_2	density of powder particle
ρ_1	density of araldite
θ	angle of tilt

CHAPTER ONE

Introduction and Literature Survey

1.1   Introduction

A reliable and accurate measure of mineral content of bones in
the living subject is essential to both the diagnosis and the treat-
ment of bone diseases. Quantification of loss of bone mineral may
permit an early diagnosis of certain bone diseases such as osteoporosis
and osteomalacia and it may be useful in the evaluation of therapeutic
measures. It could be used to observe the effects of sustained lack
of stress on bones, such as those resulting from prolonged bed rest,
disuse or weightless flight in space. The effect of diet, pregnancy
and lactation could be studied.

For many years skeletal status has been evaluated by estimation
of a radiograph either visually or with an optical densitometer.
Other techniques like bone biopsy and calcium balance by tracer
isotopes are less commonly used.

A number of new techniques have been evolved recently to
replace   the less sensitive techniques. Among these techniques
are bone densitometry using monochromatic or polychromatic photon
sources and a detector and neutron activation analysis. These
techniques are now in use in a number of centres. The use of
acoustic techniques was also investigated.

The main literature survey in this chapter is about the main
techniques used now, namely, bone densitometry using monochromatic
and polychromatic photon sources, whole body and partial body neutron
activation analysis. A specific investigation is made into the
different aspects of the techniques with a view to evaluating and
comparing them. These aspects are reproducibility and accuracy,
patient dose, cost and ease of measurement and patient amenity.

.../

Archer-Hall et al 1973 have developed a technique which employs
a conventional X-ray set but avoids the difficulty associated with
radiographic methods and minimises the uncertainties in the tube
output which occur due to the variation in the mains supply voltage.
The technique has other advantages such as negligible statistical
error and fast scan. The work described in this thesis is a continua-
tion of this work.

Chapter Two discusses different improvements carried out to
the scanning machine. The improvements are twofold; work done to
overcome weak points in the machine and addition of extra parts
which proved to be important partly from clinical experience.

In order to calibrate the signal of the transmitted photons
in the techniques using polychromatic photon sources, it is necessary
to have a calibration standard. It is also desirable to have some
absolute reference standard in order to calibrate and intercompare
results from different scanning systems and from different laboratories.
Due to the lack of a suitable bone standard, work was carried out to
make a standard and this is discussed in Chapter Three.

In the Aston technique and all other techniques using poly-
chromatic photon sources, it is not possible to do a straightforward
integration to measure the scan area of the trace which represents
total mineral content in the scanned site. This is because one needs
to know the attenuation coefficients of bone and soft tissue for the
energy range applied, together with the photon intensities. Chapter
Four discusses an optical transform system made to give a linear area
representation to the scan area of the trace which is then measured
by a planimeter.

Chapter Five discusses the measurements carried out on post mortem bone pieces to find the relation between the scan areas and various in-vitro measurements made on the bone. It also discusses the measurements made on post mortem ulnas in order to obtain an idea of the significance of arm repositioning errors on scan areas and to determine the measurement on the trace giving least variation of measured parameters. A survey of bone indices and best measurements to make on traces is also discussed.

Chapter Six discusses some traces collected from the application of the scanning technique in-vivo to volunteers and to several cases involving metabolic bone diseases. It also discusses other clinical experience from the usage of the scanning machine.

Chapter Seven contains final conclusions on the main work done, together with some suggestions for future work.

1.2   Literature survey
1.2.1   Bone radiography

Almost from the earliest use of diagnostic radiography, radiologists have wished to estimate the degree of bone mineralisation from radiographs. The idea behind using X- or γ-rays in bone radiography is the difference in absorption of these radiations in bone and soft tissue. The absorption in a compound or a mixture is preferentially greater in the higher atomic numbered elements and higher density.

.../

The main mineral in the human bone is calcium hydroxyapatite $3Ca_3(PO_4)$ $Ca(OH)_2$ (Fourman and Royer, 1968, Harris and Heaney, 1970). Thus the main heavy elements in bone are calcium and then phosphorus. The percentages of calcium and phosphorus, in the human skeleton, are about 14% and 7% respectively (see Table 3.3). The proportion of calcium to phosphorus varies according to the amount of calcium carbonate $CaCO_3$ present. This calcium carbonate accounts for about 10 - 15% of total bone calcium (Fourman and Royer, 1968).

The simplest radiographic technique for estimating bone density involves only the taking of a good radiograph. X-rays from a normal clinical X-ray set are directed at the chosen body site and a proportion of the transmitted rays is detected by the photographic film emulsion. On subsequent development the film represents a shadowgraph of the subject with the bones lighter than the surrounding soft tissue. As the optical density of the photographic plate is dependent on the transmitted X-ray flux, which in turn is dependent on the bone density of the subject and its size, the more material in the bone, the lighter will be the image. Thus comparison of the picture obtained with that of the same site in a normal subject should give some indication of the relative bone densities (West, R, 1969). Virtama, 1957, and other earlier workers tried measuring the density of photographic emulsion in terms of the metallic silver produced. Virtama, 1957, removed the silver from the exposed and developed emulsion with diluted nitric acid. Silver weight was then determined by titration.

The method of estimating relative changes in bone density by visual inspection of a radiograph was, and still is, frequently used. The criteria used in the visual assessment of bone radiography are first, photographic blackening of the X-ray image of the bone examined and second, morphological signs, that is to say, changes in the thickness of the cortical layer of long bones like the ulna and the radius, rarefaction of the trabecular pattern of the cancellous bones like the vertebrae and the oscalcis or the concavity of the vertebrae.

It was realised by many workers, such as Ardran, 1951, Virtama, 1957, Harris and Heaney, 1970, that the many variables in a radiograph make the method inaccurate. The main factors affecting the accuracy of a radiograph are:

a) variability in X-ray high tension (voltage and current)

b) variability in the photographic emulsion and film development

c) the variation in X-ray intensity due to the angle of emergence of the X-rays from the X-ray generator, i.e. the heel effect (Glasser et al, 1961)

d) the complication of non-monochromatic radiation

e) photon scattering

f) the effect of soft tissue on photon absorption and its contribution to scattered photons.

Due to these reasons, bone radiography by visual inspection of standard radiographs was found to be unreliable in detecting changes in mineral content of less than 30 - 40% (Simon, 1973, Sorenson, Cameron and Wisconsin, 1967, Camberlain et al, 1968).

1.2.1.1   The improvements in bone radiography

Quite a number of improvements entered in old bone radiography to decrease the effect of the above-mentioned sources of error and to give more quantitative measurement of bone mineral.

The variations in photographic emulsion cause a considerable image density variation. This was decreased to a certain extent by using high definition, non-screened film.

The variation in film development are reduced by the use of automatic film processing.

The variation of the X-rays due to the angle of emergence of the X-ray generator might be partially solved by standardising the X-ray source-film geometry.

There are several factors causing variability in X-ray intensity of a normal clinical X-ray set. The high tension applied to the tube can vary with time by $\pm$ 5%. The variation of the X-ray intensity is proportional to the square of the high tension (Meredith and Massy, 1972). This also affects the quality of the X-ray beam. This factor and the variability in the photographic emulsion and film development can be reduced by the simultaneous exposure of a reference standard with the limb.

For a quantitative estimation of bone density, the overlaying soft tissue should be corrected for because of its significant attenuation, even at low X-ray energies. The second and more complex effect of soft tissue is the scattering of the primary X-ray beam (West, R, 1969). The immersion of the limb in a bath of water or soft tissue equivalent liquid gives nearly uniform attenuation by the soft tissue and fairly constant scattering mass for all radiographs.

The new techniques which broke through as a substitute of the visual assessment of a radiograph could be divided into two basic categories; the comparison of the passage of light through bone images on X-ray film with a standard index image appearing on the same film using optical densitometer and in osteoporosis by measuring the reduction in cortical thickness of long bones (Helela and Virtama, 1970, Virtama and Mahoven, 1960, McCrace, Glas and Sweet, 1967), and the reduction in the thickness of the cortex of the vertebrae or its bioconcavity (Barnett and Nordin, 1960, 1961, Virtama, Gastrin and Telkka, 1962).

Attempts have been made to use monochromatic radiations from various nuclei in medical radiography. Carl Henrikson, 1967, has written a literature review in this field. The main defect of using X or 𝛾 radioactive source in bone radiography is the difficulty in obtaining a strong source of small dimensions. Because of this and other drawbacks radioactive sources are rarely used.

Sorenson, Cameron and Wisconsin, 1967, said that with modified bone radiography techniques it has not been conclusively demonstrated that any of the modified techniques give results that are reproducible (able to detect changes in mineral content) to within 10% when in routine use over long periods of time. They continued that a more reliable technique is required to demonstrate the smaller changes resulting from less severe diseases and from such cases as normal growth, aging, pregnancy and lactation.

1.2.2 Bone densitometry using monochromatic X- or γ rays

The fundamental principle, on which most in-vivo measurements of bone density are dependent, involves the difference between the attenuation coefficients of bone and soft tissue for low energy X- or γ-radiation.

To overcome some of the disadvantages associated with X-ray tube and film, many workers (Cameron and Sorenson, 1963, Reed, West and Atkinson, 1970, Smith, Johnson and Pao-Lo Yo, 1972) have used low energy X- or γ - radioactive sources and a counter. Garn, S M, 1962, has published an annotated bibliography on bone densitometry which includes references to direct measurements using scintillation counters.

In bone densitometry techniques the radiation beam generated by the radioactive source is well collimated. The collimated beam passes through a moving limb or vice versa and a point by point count of the transmitted photons is made by using a scintillation crystal and a photomultiplier system.

.../
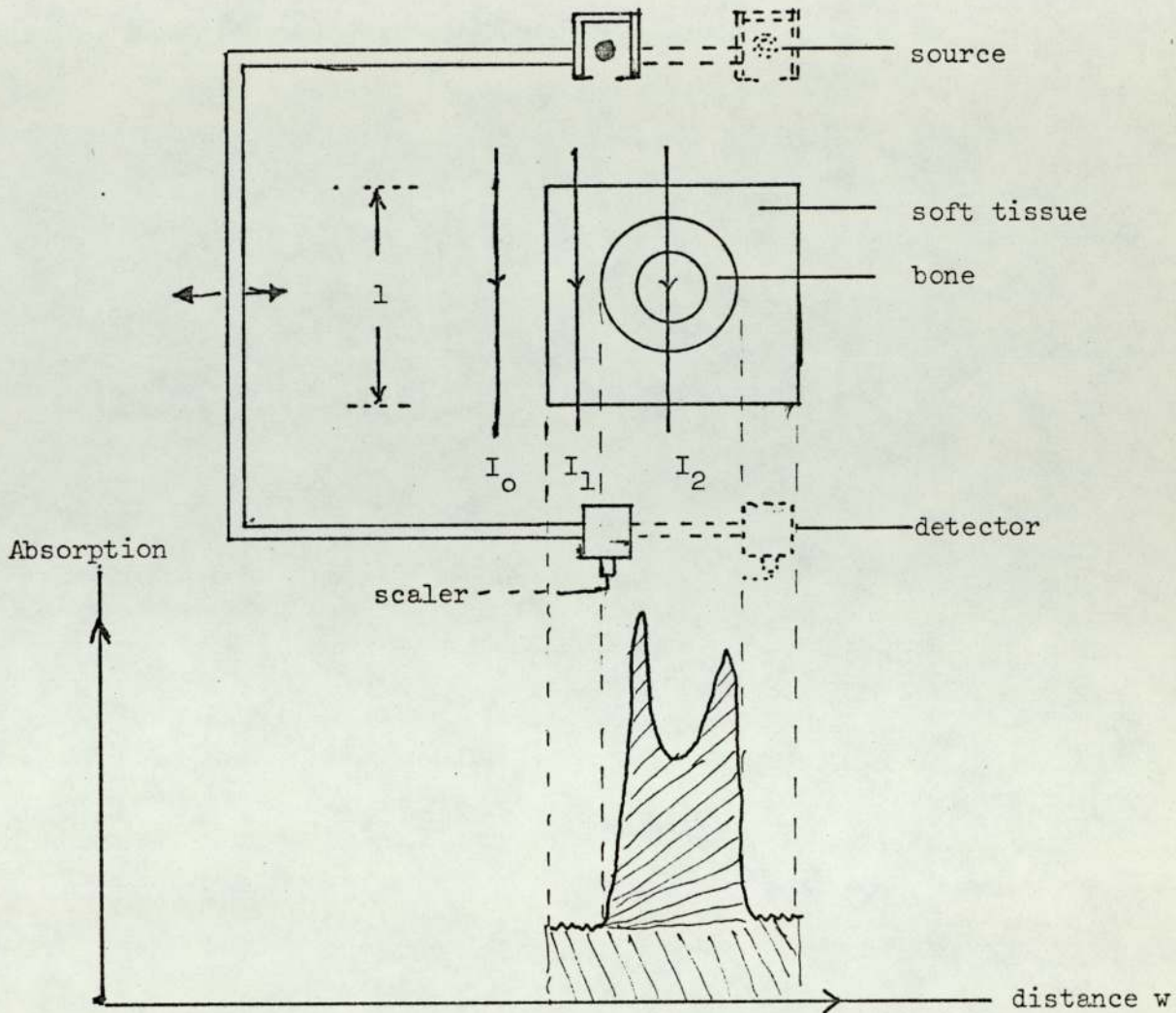
Fig. 1.1   A simple diagram of apparatus and
transmitted photons through a bone surrounded
         by soft tissue of equithickness

The absorption is then plotted against distance across the limb as
shown in figure 1.1.   The amount of mineral in the path of the
photon could be calculated using these two equations.

$$I_1 = I_o e^{-\mathcal{M}_s l} \qquad\qquad 1.1$$

$$I_2 = I_o e^{-\frac{\mathcal{M}_s}{P_s} S - \frac{\mathcal{M}_b}{P_b} B} \qquad\qquad 1.2$$

Where I_o is the count rate when there is no soft tissue

or bone in the way of the photons,

I_1 is the count rate when there is only soft tissue

of thickness l (cm) in the way of the photons,

I_2 is the count rate when there is soft tissue of

thickness S (gm/cm^2) and bone of thickness B (gm/cm^2)

in the way of the photons,

l is the total thickness of bone and soft tissue,

$\mathcal{M}_s$ and $\mathcal{M}_b$ are the linear attenuation coefficients

in cm^{-1} of soft tissue and bone respectively,

and P_s and P_b are the density in g/cm^3 of soft tissue

and bone respectively.

$$\frac{S}{P_s} + \frac{B}{P_b} = 1 \qquad\qquad 1.3$$

From equations 1.1, 1.2 and 1.3, it can be easily shown that

$$B = P_b \frac{\ln I_2/I_1}{\mathcal{M}_b - \mathcal{M}_s} \qquad\qquad 1.4$$

Where B is the bone thickness in g/cm^2, i.e. the bone

mineral mass per unit area in the radiation beam path.

Bone densitometry measurements do not, by themselves, tell about bone density, since density can only be determined when both mass and volume of bone are known. It measures total bone mineral in the site scanned. By integrating across the scanned bone, the total mineral content in the site scanned can be found.

$$\int B \, dw = \frac{\rho_b}{\mu_b - \mu_s} \int \ln \frac{I_2}{I_1} \, dw \text{ (in g/cm)} \qquad 1.5$$

Different radioactive sources have been used in bone densitometry. Selecting a suitable source for scanning depends on both the bone to be scanned and the bone site. Several small bone sites like ulna, radius and fingers have been studied using iodine-125 sources which emit γ-rays of energy 27.4 keV (Strandjord et al, 1966, Cameron and Sorenson, 1963). In the case of large bones, however, like femur, os calcis and head of the humerus (West, 1973, Nilsson, 1970, Atkinson, 1970, Strandjord et al, 1970, Lundberg and Nilsson, 1968) or for body sites which involve a long total path-length for the photon beam like vertebrae, the attenuation is considerable and the transmission count rate correspondingly small. In such cases a higher photon energy will give better detection statistics in spite of the poorer discrimination. Amercium-241 and cesium-137 of photon energies 60 keV and 660 keV respectively were found to be suitable for bone mineral measurements in those sites (West and Reed, 1970, Reed, West and Atkinson, 1970).

A dual isotope technique is used for determination of bone mineral assuming that the absorption of the monochromatic beams takes place in a two component system, bone mineral and soft tissue (Cameron and Sorenson, 1963, Reed, West and Atkinson, 1970). In this case the total thickness of bone and soft tissue (1 in fig. 1.1) does not need to be known as is the case in the one isotope technique. A further development is described by Jacobson, B, 1964, whereby a three component object is analysed by three characteristic secondary X-rays and compared with wedges of the three standard components in an integrated analog computer.

Different bones and different sites have been used for measuring bone mineral. The choice of site for bone density studies depends on the parts which are most affected by the different bone disorders and are easy to relocate again. It has been argued that disorders such as osteoporosis are observed primarily in cancellous bones since the higher surface to volume ratio renders it more accessible than cortical bone to calcium metabolic processes (West and Reed, 1970). The cancellous sites used for mineral measurement are os calcis and distal end of radius and femur. These sites are chosen because of the little overlaying soft tissue.

Because of the difficulties in relocating the same measuring site in repeated measurements and the less discrimination between bone and soft tissue with high energy photons, most measurements of bone mineral or of parameters describing it have been made at cortical sites in small bones.

Table 1.1 shows values of reproducibility, photon source, dose, bones and other information in bone densitometry using monochromatic sources which were quoted in different publications in this field.

1.2.2.1 Reproducibility and accuracy

The measurements in bone densitometry using monochromatic sources involve generally measuring the scan area which is drawn from the counted photons transmitted through bone across the scanned site (see fig. 1.1). This area represents bone mineral derived from the scan and is called the scan area (or bone index). It may be determined simply by measuring the area enclosed between the bone thickness profile and the soft tissue base line. Bone width is also measured to give a rough indication of the bone size.

Cameron and Sorenson, 1963, reported a mean reproducibility of 3% in measuring scan area on patients. Evens et al, 1969, quoted a mean of 2% reproducibility from two measurements on ten subjects. The reproducibility on a single patient may go higher than the mean reproducibility, i.e. Sorenson, Cameron and Wisconsin, 1967, reported a mean reproducibility of 2.2% while in two site measurements of the radius of two patients the reproducibilities were $\pm 2\%$, $\pm 3\%$ and $\pm 4\%$, $\pm 6\%$. Most of the errors in bone densitometry are statistical and due to patient movement and relocation. A possible solution to the relocation error is to measure mineral content at closely spaced intervals, a few millimeters apart along the length of the bone and to integrate the result (Sorenson, Cameron and Wisconsin, 1967).

.../

Cameron and Sorenson, 1963, tested the accuracy of estimating the percentage by weight of two compounds mixed homogeneously in phantom specimen s. Two radioactive sources were used ^{125}I - 27.3 keV and ^{241}Am - 59.6 keV. The material used was blocks of paraffin and calcium carbonate ($CaCO_3$). The average accuracy in determining the percentage by weight of $CaCO_3$ was within 3%.

In all bone densitometry, the size of source and detector slits are fairly large (a few millimeters) compared with the bone widths (see Table 1.1). Wide slits are needed in order to collect sufficient counts but this has the disadvantages of causing a distortion in the viewed profile and giving poor spatial resolution and also increasing the error due to scattering.

1.2.2.2   Patient dose

The dose in a bone densitometry measurement is very small, (generally less than 0.2 r.e.m. per scan) and is restricted to the small region scanned. So radiation dose is no problem in bone densitometry and measurements can be repeated as much as is needed without risk of subjecting the patient to an unsafe dose. The maximum I.C.R.P. dose limit for members of the public for hands, feet, forearms or ankles is 7.5 r.e.m. (Coggle, J E, 1971).

1.2.2.3   Cost and ease of measurement

The main apparatus required in bone densitometry are the radioactive sources, limb fixer and a monitor system. To get fast and

accurate values of the integration (scan area) and bone width, a
small computer is needed (Shimmins et al, 1972, Mazes, R B, 1968,
Sorenson and Cameron, 1970). A complete bone scanner with a small
computer, made for measuring mineral content in the lower arm
(ulna and radius) and in the heel, costs little more than £6,000
(Atomoenergi isotop service, Sweden) which is less than one fourth
of the price of 14 ^{238}Pu/Be sources used for whole body neutron
activation (Cohn et al, 1973).

1.2.2.4   Patient amenity

In bone densitometry the time needed to fix the limb and take
a scan does not exceed a few minutes (Table 1.1). Generally the
distress caused to the patient, either by fixing or during scanning,
is negligible. This should be compared with neutron activation
measurements where a longer time is required with the patients being
isolated in most cases.

1.2.2.5   Summary

The advantages of using monochromatic radioactive sources and
a detector in bone mineral measurement are:

    1)   cheap apparatus combined with low
running cost and ease of measurement,

    2)   direct relation between count rate
and bone mineral in the way of the
photon-beam,

3) very low dose to the patient,

4) the photon output for a long-lived isotope is substantially constant

5) spatial resolution which depends upon detector slit size

6) reduced error due to photon scattering

The disadvantages are:

1) unknown correlation of the mineral changes in the site scanned with the total mineral changes in the skeleton in bone disorders,

2) generally, there is a considerable statistical error due to the low detected count rate,

3) a relatively long scanning time, of a few minutes, is required to perform a scan and this increases the possible error due to limb movement,

4) poor spatial resolution since a broad beam of a few millimeters is needed to collect sufficient photons which will also increase the error due to scattering.

1.2.3 Bone densitometry using polychromatic X-rays

X-rays from diagnostic X-ray sets have been used in mineral measurement instead of radioactive sources (Vose, 1958, 1959,

.../

Mayer et al, 1960, Mason, 1965). The principle of this technique is similar to bone densitometry using monochromatic radioactive sources with the difference that in this case polychromatic photons are used.

The use of this technique eliminates the error of the X-ray film in bone radiography and reduces the error due to scattering through collimation. The technique still has a number of drawbacks. The most important of these is the variation in the mains voltage. A small change in the mains voltage causes a large variation in the total X-ray intensity (see section 1.2.1).

The technique which has been developed at Aston University uses a clinical X-ray set and minimises the error due to X-ray fluctuations. This has been achieved by the use of a monitor detector and an electronic switching technique (Archer-Hall et al, 1973). The technique has other advantages like high spatial resolution and negligible statistical error which will be discussed in the following sections.

In the Aston technique and all other techniques using poly-chromatic X-rays it is not possible to do a straightforward integration to measure total mineral content from the scan area of the trace of the bone site scanned, since to do this it is required to know the attenuation coefficients of bone and soft tissue for the energy range applied together with the X-ray intensities at these energies. This information is not easily measurable. For this reason a calibration standard in a stepwedge shape is used (see fig. 2.13). With the aid of the signals representing the standard

.../

steps in the trace, an optical transform system was developed to give a linear area representation to the scan area of the trace with good accuracy (Chapter Four).

1.2.3.1 Reproducibility and accuracy

The scanning machine measures the attenuation of X-rays by the soft tissue and bone in the site scanned. Two repeated scans of dead ulnas and subjects were done, with an interval of time between the two scans, in order to check the reproducibility of the scanning machine. The two traces were superimposed (fig. 6.10). The reproducibility in the measurement of the patients' scan areas using the optical transform system is 2.1%.

The scanning machine has good spatial resolution (0.25 mm) which compares favourably with that achieved in bone densitometry using monochromatic radioactive sources.

1.2.3.2 Patient dose

The dose per scan to the small site scanned in the arm (2 x 2 cm) was found to be about 0.15 r.e.m. (Archer-Hall et al, 1973). The scattered dose to the subject's body which is mainly due to radiation leakage through the tube head is negligible (Edwards, J, 1973). For this reason scans could be safely performed to observe calcium changes in the different patients as frequently as is the case in bone densito-metry using monochromatic sources.

1.2.3.3   Cost and ease of measurement

The scanning machine was made to fit onto the X-ray head of the tube of a conventional X-ray set without the need to make any alteration.   A commercial model of the scanning machine might cost approximately £4,000 to £5,000 (Edwards, J, 1973).   The running cost of the machine is negligible since only one 12.5 x 10 cm sheet of X-ray film is required per scan together with the cost of the small quantities of salts required to make the tissue equivalent liquid (section 3.2) which could be used for a few days.

The ease with which the scanning machine may be used is comparable with monochromatic sources techniques and compares favourably with neutron activation analysis where a special equipment is needed, requiring skilled staff to operate.

1.2.3.4   Patient amenity

The trolley speed is 1 cm/sec and the ulna width in the front end (near ulnar styloid) generally does not exceed 1.5 cm; therefore the actual scan takes only a few seconds.   The time needed for making a scan, including fixing the arm, is only two minutes with little discomfort to the patient.

1.2.3.5   Summary

The advantages of this technique are:

.../

1)   it can provide accurate analysis of
     the site scanned due to the high spatial
     resolution of the slit and the number
     of readings done in the scan (one
     reading every 0.1 mm movement),

2)   the X-ray dose to the patient is very
     small,

3)   cheap apparatus with very low running
     cost and ease of measurement,

4)   it compensates for the variation in
     the X-ray intensity and the statistical
     error is negligible (Edwards, J, 1973),

5)   short scanning time is required to
     perform a scan ($\sim$2 seconds) which
     minimises possible distortions of the
     observed profile due to limb movement,

6)   the apparatus is made to fit an un-
     modified clinical X-ray set.

The disadvantages of the technique are:

1)   unknown correlation of the mineral
     changes in the site scanned with the
     total mineral changes in the skeleton
     in bone disorders,

2)   it is not possible to do a straight-
     forward integration to measure total
     mineral content in the site scanned
     from the trace and therefore another

.../

instrument is required to do this

integration (i.e. the optical

transform system).

1.2.4 Neutron activation analysis

A completely different approach to the estimation of calcium

in bone is by in-vivo neutron activation analysis (N.A.A.). The

principle of N.A.A. is that when certain elements are exposed to

neutrons there is a probability that a small fraction of stable

atoms may be transmuted to a radioactive form often giving γ-rays

of a particular energy and half life. The activity produced is

proportional to the amount of elements present in the irradiated

subject.

The application of neutron activation analysis to measuring

calcium in bones rests on the fact that almost all calcium in the

body is in the skeleton (98 - 99%, Nelp et al, 1972). So any

significant change in calcium indicates a change in total mass of

skeletal mineral (Palmer et al, 1968).

For calcium measurements use is made of the reaction

^{48}Ca (n, γ) ^{49}Ca. The γ-ray from the subsequent decay of ^{49}Ca is

of 3.1 Mev energy. The high energy photon emitted in this reaction

decreases the effect of photon attenuation by the body tissues.

Even though N.A.A. is regarded as a very sensitive technique

in detecting small quantities, first considerations suggest that

calcium is an unsuitable element for detection by neutron activation.

This is because the only suitable isotope produced is ^{49}Ca (with a half life of 8.8 minutes) from ^{48}Ca which forms only 0.18% of the element and which is not a strong absorber of neutrons (1 barn for a neutron of 0.025 eV energy, Bethard et al, 1967).

To perform a neutron activation in-vivo the patient is subjected to a neutron flux from a neutron source. Immediately after irradiation the patient is taken to a monitor system and the characteristic γ-rays from ^{49}Ca decay are counted by a scintillation counter. Usually in a whole body neutron activation a whole body counter is used to measure the radioactivity.

The neutron sources mostly used in in-vivo neutron activation are accelerators of various types and radioactive sources (α, n). These sources differ in their neutron energies and outputs. The requirements of neutron sources for total body in-vivo activation measurements of calcium include uniform thermal neutron flux throughout the body, acceptable dose, reproducibility of the thermal neutron flux throughout the body, irradiation procedure causing as little inconvenience as possible to the patient and acceptable cost.

In selecting the neutron source for neutron activation analysis a number of factors have to be considered. The dose per incident neutron increases with neutron energy and, the activation produced by the (n, γ) reaction is proportional to the thermal flux. The thermal neutron flux produced is also decreased with increase in the energy of the incident neutrons due to the increase in penetration (escaped neutrons). However, a compromise must be made between the advantages and the desired uniformity of the thermal neutron flux distribution which increases with neutron energy. Cohn, Fairchild

and Shukla, 1973, considered all the above factors and showed that 4.5 MeV neutrons have an overall advantage over 14 MeV neutrons in total body N.A.A.

For the measurement of calcium - 48, the ^{37}Cl (n, P) ^{37}S reaction is the principal interfering reaction. Sulphur - 37 emits photons of the same energy as ^{49}Ca and its half life is close to that of ^{49}Ca (5.1 minutes). This reaction has a threshold energy of 10 MeV so using a neutron source of less than 10 MeV eliminates the interference due to this reaction (Cohn et al, 1973).

The requirements of the counter for measuring the induced γ-rays in whole body N.A.A. include: high sensitivity throughout the body, minimum distress to the patient, acceptable cost and high stability.

In the following sections more discussion will be given of whole body and partial body N.A.A. separately.

1.2.4.1 Whole body neutron activation analysis

Studies involving total body in-vivo activation analysis are in progress in several centres. Cohn and Dombrowski, 1968, using 14 MeV neutrons from a generator $\left[^{3}H \text{ (d, n) } ^{4}H \right]$ moderated with polythene, reported measurements of ^{49}Ca, ^{24}Na, ^{38}Cl and other elements.

Chamberlain et al, 1968, have carried out neutron activation on phantoms, cadavers and in-vivo using a 60 inch cyclotron and the ^{7}Li (p, n) ^{7}Be reaction. The mean neutron energy produced was

.../

approximately 3 MeV (range 0.1 to 8 MeV). The authors reported in 1970 the results of regular measurements done on a large group of patients.

Palmer et al, 1968, have carried out irradiations on human cadavers and on phantoms filled with tissue equivalent solution to measure a number of body elements including calcium. A Van de graaff and the ^{3}H (d, n) ^{4}He reaction was used to produce 14 Mev neutrons, also a cyclotron $\left[^9\text{Be (d, n) } ^{10}\text{B}\right]$ was used to produce a wide energy range of neutrons of a lower mean energy ($\sim$2 MeV).

Nelp et al, 1970, 1972, reported calcium examinations on a large number of patients with various metabolic bone diseases and on normal subjects. They used a 60 inch cyclotron which produced 2 MeV deutrons directed to strike a thick target of beryllium $\left[^9\text{Be (d, n) } ^{10}\text{B}\right]$. This produced neutrons between 4 and 12 MeV in the forward direction.

Cohn et al, 1973, reported a special facility for total body N.A.A. using 14 ^{238}Pu/Be (α, n) sources, each of 50 Ci. ^{238}Pu/Be sources give a wide neutron energy spectrum (1 - 11 MeV) with a mean energy of about 4.2 MeV.

Boddy, Holloway and Ellott, 1973, made a special facility for total body N.A.A., where two small generators were used to produce 14 MeV neutrons (section 1.2.4.1.3).

In all the previously mentioned facilities a bilateral exposure is performed to maximise the uniformity of the thermal neutrons fluence through the body of the irradiated subject.

In Table 1.2 are quoted values of reproducibility, dose, total time of irradiation and counting, accuracy and other information about whole body N.A.A. taken from different publications in the field.

1.2.4.1.1 Reproducibility and accuracy

To determine serial changes in body calcium is necessary to be able to repeat the complete measurement with little variability. The accuracy means that of estimating total body calcium (in grammes) from the counted radioactivity. The lowest value of reproducibility quoted in Table 1.2 is that of Cohn et al, 1973, which is $\pm$ 1%. This was calculated from five repeated measurements of a phantom. Reproducibilities of $\pm$ 2% and $\pm$ 8% are quoted by Palmer et al, 1968, as estimated figures. Nelp et al, 1970, 1972, found that the maximum value of reproducibility excluding statistical error was 1.6% from measurements on three cadavers and the statistical error was 1.2%.

The accuracy of measuring the absolute body calcium is bound to be less than the reproducibility since the former measurement requires uniform flux throughout the body, that the counting of the induced activity be independent of both absorption by the body and the counting geometry and lastly the correction of the radioactivity measurement for the nuclear reaction which interferes with it. However, measuring absolute body calcium can have little direct diagnostic value in the absence of knowledge of what total body calcium ought to be for a patient of that age, sex,size and shape. Since one of the major applications of this technique to disease problems will be in observing serial changes in skeletal mass, a given patient can be compared with himself (Palmer et al, 1968). These measurements will be valid so long as the patient does not lose or gain a large amount of weight between measurements.

1.2.4.1.2   Patient dose

The most important practical consideration in neutron activation analysis is safety. The dose in N.A.A. is mainly due to neutrons and secondly due to γ-rays produced from the (n, γ) reaction in the human tissues. The irradiation will include the different parts of the body and will affect the different body tissues. These tissues differ in their sensitivity to radiation.

The whole body dose quoted for in-vivo measurements range from 0.277 r.e.m. to 2 r.e.m. (see Table 1.2). The I.C.R.P. value for maximum permissible whole body dose for members of the public

.../

(excluding medical procedures) is 0.5 r.e.m. per year. Although work
in medical fields does sometimes exceed this dose limitation, it is
necessary not to increase it much higher than the limited value in
order to reduce the radiation hazard. This could be one of the
reasons why in most whole body N.A.A centres no more than two measure-
ments are performed on individual patients per year. A lower dose
is achieved with a suitable neutron source and a high sensitivity
monitor which means higher cost.

1.2.4.1.3   Cost and ease of measurements

Accelerators of various types are the main sources used for
whole body N.A.A. (section 1.2.4.1). These accelerators are mostly
made for other research purposes like physical research and are
generally very expensive. The other sort of sources used are
(α, n) sources and fission neutrons (Cf - 252). Cohn et al, 1973,
used 14 ^{234}Pu/Be sources and the estimated cost of these sources
alone, in Britain, is £28,000 (Cohn et al, 1973). The least
expensive facility built for whole body is that of Boddy, Holloway
and Elliot, 1973. Two generators are used, one above and one below
the patient, to give a simultaneous bilateral irradiation as the
patient passed between them. The monitor system constructed from
two sodium iodide detectors, again one above and one below the
patient. The total capital cost of this facility is about £42,000.
Generally, with the whole body N.A.A. a special irradiation equipment
is used which requires skilled attention and high maintenance cost.

.../

1.2.4.1.4 Patient amenity

In most centres of whole body N.A.A. accelerators are used. In the earliest studies with a modest neutron source, sufficient uniform flux was obtained by curving the subject in an arc of one meter radius (Anderson et al, 1964). This geometry was acceptable for bilateral irradiation of healthy individuals but may prove unacceptable for patients with bone disorders (Boddy, Wilson and Alexander, 1970). The most expensive clinical studies have avoided this problem by measuring relative changes in body calcium in the same subject using a bilateral irradiation with the subject lying on his side (Boddy et al, 1972, Cohn et al, 1973).

The times of irradiation and counting depend on both the neutron source and the counter. In general, with high neutron flux, five minutes irradiation is needed to get sufficient activity. The counting time takes about fifteen minutes, roughly twice the half life of ^{49}Ca (Table 1.2), which makes the total time twenty minutes. This fairly long time does cause some distress to the patient, especially if the patient has to be isolated during measurements which is usually the case in whole body N.A.A. Distress could be minimised if a special facility is made taking this point into account (Boddy et al, 1972, Boddy, Holloway and Elliot, 1973).

1.2.4.2 Partial body neutron activation analysis

This technique involves irradiation of part of the body like a hand or a foot with an acceptable dose. Induced activity is measured subsequently by external counting.

Partial body N.A.A. has some advantages over whole body
N.A.A. in measuring calcium which include low capital cost, ease
of measurement, low patient dose and less distress to the patient.
Also, partial body N.A.A. would be more suitable in skeletal
diseases when the soft tissue is calcified (British Authors, 1959)
and whole body N.A.A. may not reflect calcium changes in the skeleton.
This could be done by activating the part of the body which has the
lowest percentages of soft tissue, like the hand.

In most work done on partial body N.A.A., human and animal
dead bones were used (Boddy, Glaras and Robertson, 1975, Appleby
et al, 1972, Boddy, Al-Hashimi and Boyle, 1968). Catto, McIntosh
and Macleod, 1973, irradiated anatomical hands and in-vivo hands.
The workers used 2 5 Ci ^{241}Am/Be source (of approximately 4.6 MeV
mean neutron energy) positioned with a perspex tube in a water tank
to provide the neutron flux. The fast neutrons were slowed down by
water moderation and the hand bones which gripped the tube were
exposed to the neutron flux.

Successive partial body N.A.A. of a limb does give the varia-
tion in calcium in the limb concerned which usually includes a fair
part of the skeleton but relation between measured calcium in the
limb and total body calcium is not accurately known.

In Table 1.3 are quoted values of reproducibility, dose, cost
and other information about in-vitro partial body N.A.A.

.../

1.2.4.2.1   Reproducibility and accuracy

For a given monitor system, the sensitivity of the measure-
ment depends upon the radiation dose which is delivered to the
patient. The best value of reproducibility quoted in Table 1.3
is that of Appleby et al, 1972. With a neutron dose of 15 r.e.m
to the bones of the forearm, the coefficient of variation in the
counts (reproducibility of counts) was 1.1%. The reproducibility
figure increased to 5% when the neutron dose decreased to 1.5 r.e.m.
The authors mentioned that the overall accuracy of the method will
depend upon experimental errors which include inaccuracies in fore-
arm positioning during both irradiation and counting, size and
shape of the forearm, definition of irradiation and counting volumes
and neutron flux distribution.

Catto, McIntosh and Macleod, 1973, did activation studies on
nine anatomical hands and the mean reproducibility was 5%. The
authors said that the reproducibility should be less than 5% for
a patient for the reason that the patient could grasp the source
firmly in the same position in each irradiation. In old people,
who are the group most affected by metabolic bone diseases, it is
expected that it will not be easy for a patient to hold still for
the long time of irradiation or counting (16.6 and 33.6 minutes
respectively). The larger error in counts with partial body N.A.A.
is due to the statistical error.

Catto, McIntosh and Macleod, 1973, measured the accuracy of
absolute calcium estimation by partial body N.A.A. Five anatomical
hands were activated, separately, and then the calcium content was

measured chemically. The variation in calcium estimation from counted radioactivity was found to be within ±10%.

1.2.4.2.2   Patient dose

The neutron dose needed to provide sufficient activity depends on both the neutron source and the monitor system. Catto, McIntosh and Macleod, 1973, reported a hand dose of 5 r.e.m. Higher neutron dose is reported by Appleby et al, 1972, with better reproducibility (section 1.5.2.1). The I.C.R.P. quoted value for the maximum permissible dose for hands, feet, forearms and ankle for a member of the public is 7.5 r.e.m. (Coggle, J, 1971), and for occupational worker is 75 r.e.m. $_\wedge$*per annum* (Boddy and Glaras, 1973). In partial body N.A.A. it will not be easy to give complete shielding to the rest of the body from neutrons and γ-rays and the body will be subjected to a certain extent to radiation. The dose in partial body, even though higher than that for whole body N.A.A., is restricted mainly to a small region of the body and it does not include sensitive organs which might allow more measurements per year.

1.2.4.2.3   Cost and ease of measurement

The cost of the neutron sources used for partial body N.A.A. depends on the sort of sources used. α- n sources of reasonable activities could be the cheapest and they need less shielding. Catto, McIntosh and Macleod, 1973 used 25 Ci ^{241}Am/Be source (Table 1.3) which has a half life of 458 years. To give an idea of the cost of

the source alone a 10 Ci ^{241}Am/Be (2.2×10^6 ns^{-1} yield per Ci)

is worth about £1,000. Boddy, Robenson and Glaros, 1974, used

two 0.107 Ci spontaneous fission sources ^{252}Cf (4.3×10^9 ns^{-1}

yield per Ci). The total cost of the two sources is about £6,000

and the principal disadvantage of ^{252}Cf is its short half life

(2.65 years) (Boddy, Robenson and Glaras, 1974).

The monitor system cost depends mainly on the size and number

of detectors used which in turn depends on size and region activated.

For hand or foot activation, which seem the easy parts of the body

for doing measurement, two large detectors of NaI (Tl) for example

are needed. Generally, in partial body N.A.A. simpler facility is

needed and measurements are easier to perform compared with whole

body N.A.A.

1.2.4.2.4   Patient amenity

With less total calcium weight, a higher neutron dose is

required to get satisfactory counts in a prescribed counting time.

Higher neutron dose could be achieved either by a stronger source

or by longer irradiation (not to exceed about three times the half

life). From Table 1.3 the shortest total time of irradiation and

counting achieved with a good accuracy was by using a reactor.

Boddy, Al-Hashimi and Boyle, 1968, using a reactor at a power of

20 kW reported five minutes irradiation and ten minutes counting.

Appleby et al, 1973, reported a longer total irradiation and counting

times ($>$ 30 minutes). Generally with in-vivo partial body N.A.A.

the total measurement time is longer than the time needed for in-vivo

...∕

whole body N.A.A. but still with good shielding, it could be safe for staff to attend the patient and this would decrease patients' distress.

1.2.4.3 Summary

Neutron activation analysis has the following advantages:

1) the specific measurement of the body calcium with high reproducibility. The reproducibility is lower in partial body N.A.A.,

2) the simultaneous measurement of other body elements of interest is possible.

The disadvantages of N.A.A. are:

1) high radiation dose to the patient which may not permit frequent measurement to follow closely the course of treatment, and also it may not allow the measurement of some categories of patients, like children or pregnant women,

2) long time of performance with complexity of measurement which can cause distress to patients,

3) high equipment cost and the
necessity for skilled maintenance.
This is relatively less in partial
body N.A.A.,

4) in cases of soft tissue calcifica-
tion it will not be suitable to
use whole body N.A.A. for measuring
skeletal calcium, therefore other
techniques have to be used. Partial
body N.A.A. may be more suitable to
use in these cases.

1.2.5   Other techniques

Different techniques have been used in measuring bone mineral
content. Bone biopsy is among the early methods used. In this method
a small part of certain bones is cut off and analysed chemically to
find the percentage of calcium.

Tracer isotopes have been used in the study of human skeletal
metabolism by estimating the exchangeable mass of an element (calcium)
during the life of the isotope.

Jurish, J, 1970, used an acoustic technique in-vivo to
estimate the elastic response of bone by measurements of ulnar
resonance. This was done by recording the response of the bone at
the distal end to sinusoidal vibration applied at the olecranon
process, as a function of driving frequency. The product of resonant
frequency and length of the ulna is proportional to the speed of

sound in this bone which in turn is proportional to the square root of Young's modulus for a given density. From the correlation of the breaking strength of bone with its Young's modulus it was maintained that estimating Young's modulus of bone in-vivo could be used clinically to evaluate bone quality.

Clark and Van Dyk, 1973, have described a method to determine the electron density in bones using both transmitted and scattered beams of gamma rays.

Osbas, E, 1975, using neutron activation has applied a new method to estimate calcium by making use of the ^{40}Ca $(n, \alpha)^{37}An$ reaction. The radioactive argon formed in the bone diffuses into the blood and passes into the lungs and is exhaled. The exhaled gases are collected and argon is obtained by chemical separation. The calcium content is estimated from counting the radioactivity of the argon. This technique has the advantage of requiring lower dose than that needed in the ^{48}Ca $(n, \delta)^{49}Ca$ reaction. The technique has been applied with animals and the possibility of applying it to patients was studied.

1.2.6   Conclusions

Whole body N.A.A. technique provides a unique measurement of total body calcium with high reproducibility and good accuracy. However, the procedure requires special facilities for neutron exposure and total body counting which are expensive and require skilled staff to run. In partial body N.A.A. simpler facilities are required which are less expensive and easier to use, but the reproducibility and accuracy are lower.

The high patient dose in N.A.A. does not permit frequent measurements to follow closely the course of treatment and it can be unsafe to use with some categories of patients, like children and pregnant women. Also N.A.A. required a relatively long time of performance with complexity of measurement which can cause distress to patients.

Bone densitometry using monochromatic or polychromatic photon sources (as is the case in the Aston technique) provides relatively rapid, simple, cheap apparatus and a very low dose restricted to a very small region. The measurement reproducibility is also high. Therefore, it allows frequent measurements on patients with no restrictions on some categories of patients.

Bone densitometry using photon sources is more suitable to use with patients having soft tissue calcification by measuring bone mineral content in areas of minimum overlaying soft tissue.

It has been questioned whether the mass of a small piece of bone reflects total skeletal mass, and whether one bone mass reflects the mass of another bone. A number of investigators have shown from in-vitro measurements on post mortem bones that there are good correlations between the mineral content in the sites of different bones (radius, ulna, humerus and metacarpel). Also good correlations were found between bone mineral content in bone sites and the skeletal total mineral content (West, 1973, Chesnut et al, 1973, Smith et al, 1974). Other investigators have carried out in-vivo measurements at different sites of different bones to follow closely the variation in mineral content in women during lactation and in cases of bone disorders (Sorenson, Cameron and Wisconsin, 1967,

.../

Atkinson, 1970, Sorenson and Cameron, 1970). They reported variations in mineral content in these cases which indicated that bone densiometer measurements reflect the (expected) changes in total mineral content. It remains to find the exact correlation of the changes in mineral content in the bone sites and total body calcium to standardise the scanning technique. Work is being conducted with the Aston technique to measure mineral content of patients who are already having total body calcium measurements every six months.

The Aston technique has the merit over bone mineral content measurement using monochromatic sources, namely, a better spatial resolution which provides the structure in the medulla of the ulna with no distortion to the observed profile.

Table 1.1 Some information on bone densitometry using monochromatic sources taken from different references

Reference	Repro-ducibility ±%	Dose m r.e.m.	Photon Source	Scanning Time (min)	Slit dimension mm	Bones Used
Smith, Johnston and Pao-Lo Yo, 1972	2.6	-	^{125}I	-	3 diam	Radius
West and Reed, 1970	2.4	100	^{241}Am	3	5 x 15	Femur
Reed, West and Atkinson, 1970	5.0	-	^{241}Am ^{137}Cs	6	2 x 10	Femur
Evens et al, 1969	2.0	-	^{125}I	-	3 diam	Radius
Mazes, 1968	~2.0	-	^{125}I	2.4 mm/sec speed	3 diam	Ulna Radius Humerus Femur
Sorenson, Cameron and Wisconsin, 1967	2.2	500	^{125}I	0.25	3 diam	Radius
Cameron and Sorenson, 1963	3.0	150	^{125}I ^{241}Am	~3.5	3 diam	Radius

Table 1.2 Some information on whole body N.A.A. taken from different references

Reference	Repro- ducibility ±%	Accuracy ±%	Dose r.e.m.	Neutron source Ci	Total irrad. and count time (min)	Other information (all bilateral irradiation)
Cohn et al, 1973	1	-	0.277	50 ^{238}Pu/Be 14	20	phantom
Boddy, Holloway and Elliot, 1973	2	-	4	2 Generators	40	phantom
Nelp et al, 1970, 1972	2	5	2	Cyclotron	14	in-vivo
Palmer et al, 1968	2	8	1	Cyclotron + Generator	27.5	cadavers
Chamberlain et al, 1968	3.7	-	-	Cyclotron	22	cadavers
Cohn and Dombrowski, 1968	4	-	0.6	Generator	20	in-vivo

Table 1.3 Some information on partial body N.A.A. taken from different references

Reference	Repro-ducibility ± %	Accuracy ± %	Dose r.e.m.	Neutron source Ci	Total irrad. and count. time (min)	Other information
Boddy, Robertson and Glaros, 1974	2.2	-	1.63	0.107 $2 \times {}^{252}\text{Cf}$	-	Six measurements on the tibia
Catto, McIntosh and Macleod, 1973	5.0	10	5.0	25 ${}^{241}\text{Am/Be}$	49.9	Anatomical hands and in-vivo
Appleby et al, 1972	1.1 4.9 only statistical	-	15.0 1.5	Generator	32.0	Phantoms of the distal ends of ulna and radius
Boddy, Al-Hashimi and Boyle, 1968	1.6	4	18.0	Reactor	15.0	Standards and sections of animals' bones

CHAPTER TWO

Improvements made on the Scanning Machine

2.1   Introduction

The discussion in this chapter is about the different improvements carried out on the Aston scanning machine. A general description of the scanner is given in section 2.2. The improvements are twofold: work done to overcome weak points in the machine and additions of extra parts which were found to be important, partly from clinical experience.

Subjecting the scanning machine to experimental trials for a sufficient time was necessary and useful in order to discover the weak points which could not easily be found otherwise. Similarly, after a length of experience on the machine, one would be familiar with the possible breakdowns which the machine is most prone to.

2.2   The Aston scanning machine

This section describes the scanning machine as it was at the beginning of the project. The description is largely taken from the paper of Archer-Hall et al, 1973.

The technique which has been developed at Aston University uses a clinical X-ray set. The apparatus is made to slot into the diaphragm box of the X-ray tube (using a brass flange) so that X-rays fell first on a lead plate having two holes. Beneath one of these there is a detector which serves to monitor the X-rays. The second is a collimating slit which permits a beam 2 x 10 mm to pass down through a perspex water bath containing the limb. The depth over the part of the limb being scanned is kept constant by a depth fixer (a waterproof perspex box) placed over the limb.

.../

Fixing frames (fig. 2.18) are designed to hold the patient's arm in the bath. A spring-loaded clamp is applied to the radial styloid so that the ulnar styloid is pressed against a fixed perspex block padded with firm rubber. The patient's elbow is held between two further blocks which are adjustable in position to enable the ulna to be aligned parallel to a second slit underneath. Three straps are made to hold the thumb, fourth finger and the limb between the elbow and the wrist.

The transmitted beam passes through a slit 0.25 x 9.5 mm to a second detector. The detectors are small $C_SI(Tl)$ coupled with photodiodes whose output is so great that a d.c. current rather than a series of pulses is observed.

During successive half cycles, variations of the mains results in considerable variations of the X-ray output (section 1.2.1) and hence of the detector outputs. The monitor detector is used to compensate for these variations as follows. The photocurrents S_1 and S_2 from the monitor and the second detector respectively are simultaneously integrated with respect to time from the start of each half cycle of the mains supply until a time t_1 when the integral of S_1 reaches a pre-set value of $\overline{W}$.

$$\overline{W} = \int_0^{t_1} S_1 \, dt \qquad\qquad 2.1$$

The higher X-ray output from the tube, the shorter is t_1. When $\overline{W}$ is reached, electronic switching causes the integration of the second current S_2 to stop and the value of its integral is held and fed out to give a y-deflection on an oscilloscope screen. At the

end of each half cycle both integrators are reset to zero and the
procedure repeated. Thus as the limb is moved through the X-ray
beam (in a scan) a value G is found, 100 times a second such that

$$G = \int_0^{t_1} S_2 dt \qquad\qquad 2.2$$

The integration of signal current S_1 and S_2 is carried out by
feeding them into high quality small capacitors. The instantaneous
voltages across the capacitors are measured by amplifiers of unity
voltage gain with very high input impedence. Voltage gain is provided
on each channel by integrated circuit amplifiers with large negative
feedback. The output of the monitor channel goes to a discriminator
which operates a Schmitt trigger when the preset level has been
reached. The output of the channel dealing with S_2 goes to a unity
gain stage which holds its instantaneous value, when its input is
disconnected. A block diagram of the electronics is shown in figure
2.1.

The optimum working conditions of the tube voltage, current
and the mean point of cut-off in the cycle have been studied. It
was found that the conditions which give the best discrimination
between bone and water and, at the same time give satisfactory
compensation for mains variation, were 90 keV and 50 mA beam current
with an 80° (80 x $\dfrac{1}{100 \times 180}$ sec) mean termination of the
integration (Archer Hall et al, 1973).

The photographed trace of the limb scan gives a graph of $-G$
on a linear scale against displacement. Therefore, an increase in
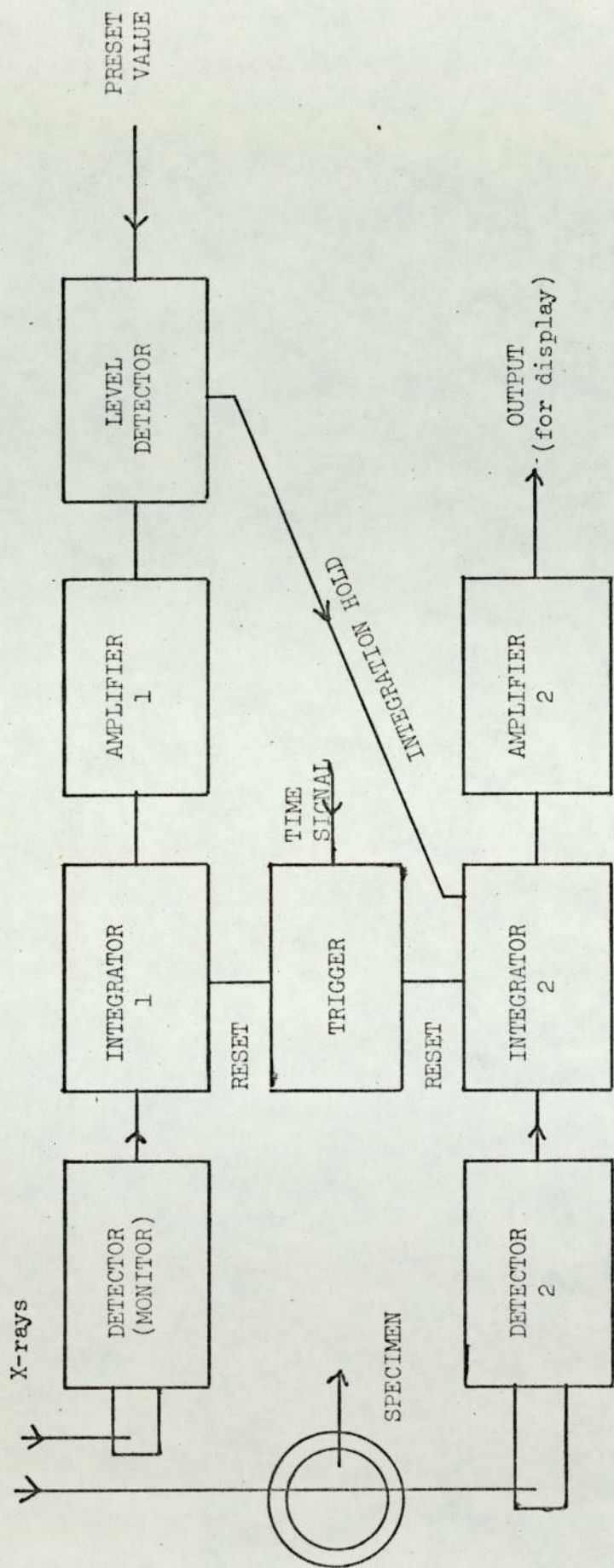the x-axis indicates an increase of bone mineral (fig. 2.13).

Fig. 2.1   A block diagram of electronics

Because of the difficulty of calculating directly the amount of
bone mineral from G values (section 4.1), a calibration scale of
G has been provided by an ivory stepwedge. This was later sub-
stituted by an artificial bone stepwedge (section 3.1.11)

Changes in mains voltages have some effect on G since they
alter the spectrum of the output photons. If the absorption paths
of the test and reference beams are of identical composition there
will be no variation in G from these changes. Thus to minimise the
error in G a 4.8 mm slab of artificial bone is included in the X-ray
path to the monitor detector. The complete monitor reference path
consists of a perspex box containing a depth of 4.5 cm of salts
solution (section 3.2) and the artificial bone block above it (see
fig. 2.16).

A general view of the apparatus is shown in figure 2.2.

2.3 The new solid state rectifiers

The H-T supply of the diagnostic X-ray tube used with the
scanning machine was full wave rectified with four valve diodes, but
because of a fault in one of the diodes, the four were substituted
by new solid state rectifiers. The correction afforded by the
densitometer switching technique is obviously related to the fluctua-
tions of the X-ray output intensity over the half cycles. Since
voltage fluctuations cause approximately twice the fractional change
in the total X-ray output, it was decided to investigate the intensity
wave forms produced by the diagnostic set with the new rectifiers and
compare it with the waveforms taken when the valve diodes were used.

Fig. 2.2   A general view of the scanning machine
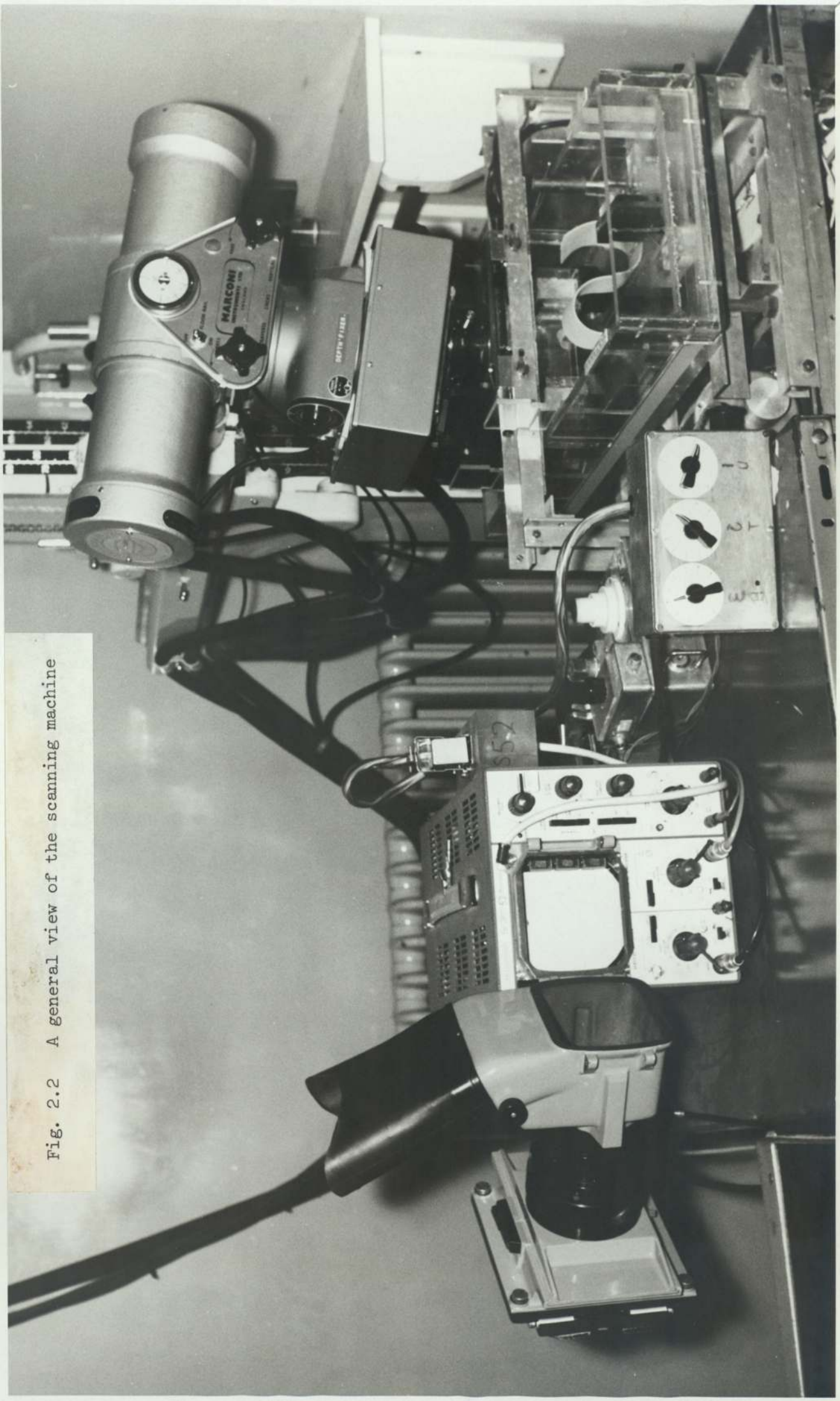
The X-ray output intensity was measured using a CsI(Tl) scintillation crystal which was coupled to a vacuum photodiode by a light guide. Current from the photodiode was fed into a source follower and amplifier. The wave form of the output voltage represents the wave form of the X-ray energy and this voltage may be viewed on an oscilloscope (Edwards, J, 1973). Figure 2.3 shows several voltage waveforms given by the set with the solid state rectifiers. The camera was left open for 1/8 second to allow the film to record several successive wave forms. The large wave forms show the instantaneous X-ray output of 90 keV and 50 mA, whilst in the smaller wave forms the X-ray current was 25 mA. In figure 2.3 there is no noticeable difference in the wave forms of the half cycles of equal current over short periods, i.e. they are superimposed, and this was typically the case in all other photographs. Figure 2.4 shows a typical photograph of the instantaneous X-ray intensity wave forms recorded over several half cycles. This measurement was carried out when the valve diodes were used in the X-ray set. It is clear that there are variations in X-ray intensity over the several successive half cycles.

It was noticed that using valve rectifiers in X-ray sets may introduce extra variations in X-ray output (other than that due to mains fluctuations) caused by a part failure in thermal emission in one or more of the rectifiers. Solid state rectifiers in an X-ray set do not appear to introduce variations in X-ray output on top of the variation of the mains. This is an advantage since it improves the correction of the switching technique.
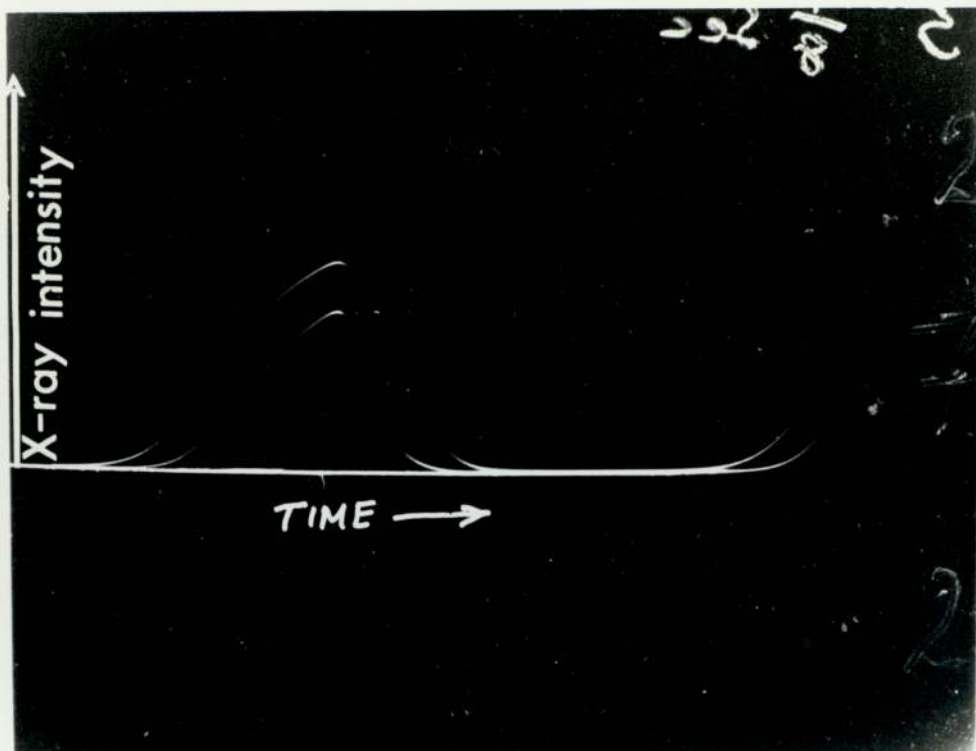
Fig. **2.3**   The instantaneous X-ray intensity wave forms
(taken when solid state rectifiers are used)
Upper wave forms   90 keV, 50 mA
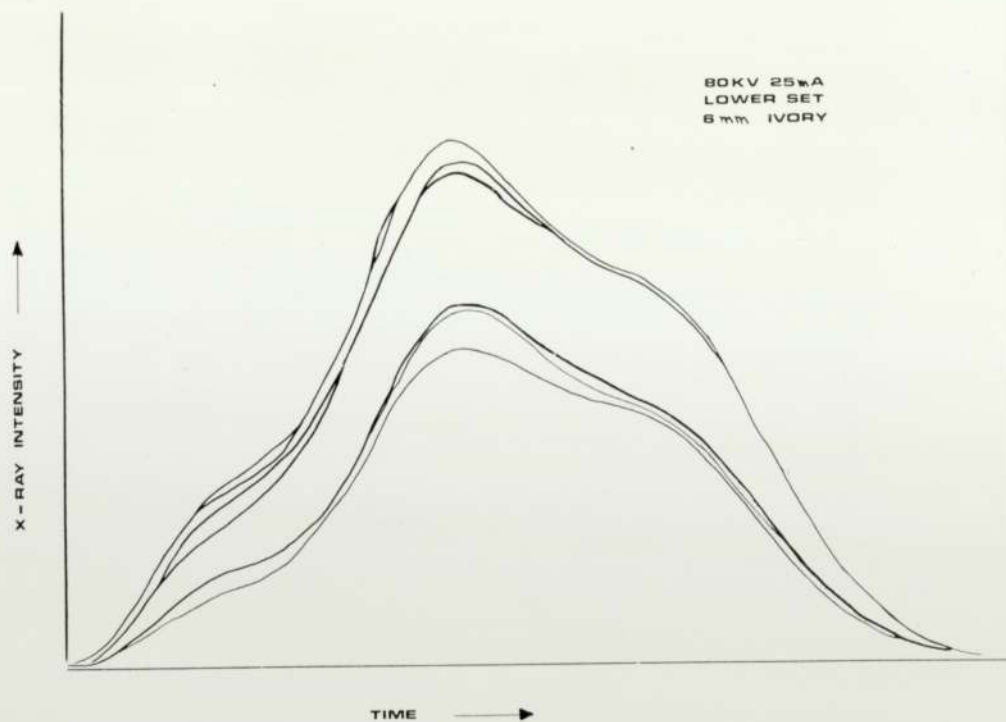Lower wave forms   90 keV, 25 mA

Fig. **2.4**   The instantaneous X-ray intensity wave forms
(taken when valve rectifiers were used)
Upper wave forms   80 keV, 25 mA
Lower wave forms   6 mm ivory absorber

A second difference occurred with the use of these triggered rectifiers: no current is passed and hence no X-rays are produced until the voltage across them reaches 18 keV. This lowers the dosage to patients as the total fraction of low X-ray energy photons is decreased.

2.3.1   The resetting pulse

Each of the two detectors' signals goes to its own integrator and amplifier. The latter two are reset at the end of every half cycle from a rectified pulse, derived from the mains supply. In view of the separate H-T supply with large power transformer needed to drive the X-ray generator, it is important that the resetting pulse be in phase with the minimum anode voltage of the generator. The phase shift circuit used when the valve diodes were in operation was capable of being changed within $\pm$ 45° (Edwards, J, 1973).

It was found that with the new solid state rectifiers there was a higher phase shift of about 120° between the mains voltage and the X-ray output and therefore a new phase shift circuit was required. The new circuit of the phase shift is illustrated in figure 2.5. The wave form at BB is out of phase by 90° with that at AA and the phase shift is capable of being increased up to 140°.

2.3.2   The total X-ray output

Using the solid state rectifiers, it was found that the integration time increased significantly, which must be due to a decrease in the total X-ray energy reaching the monitor. This causes the monitor

.../

Mains
240 V
a.c.

Transformer

40 V

L

R_1

R_2

C_1

C_2

Output to a full
wave rectification

L = 6H

C_1 = 2.5 μF, C_2 = 2μF

R_1 = 10k ohms (potentiometer)
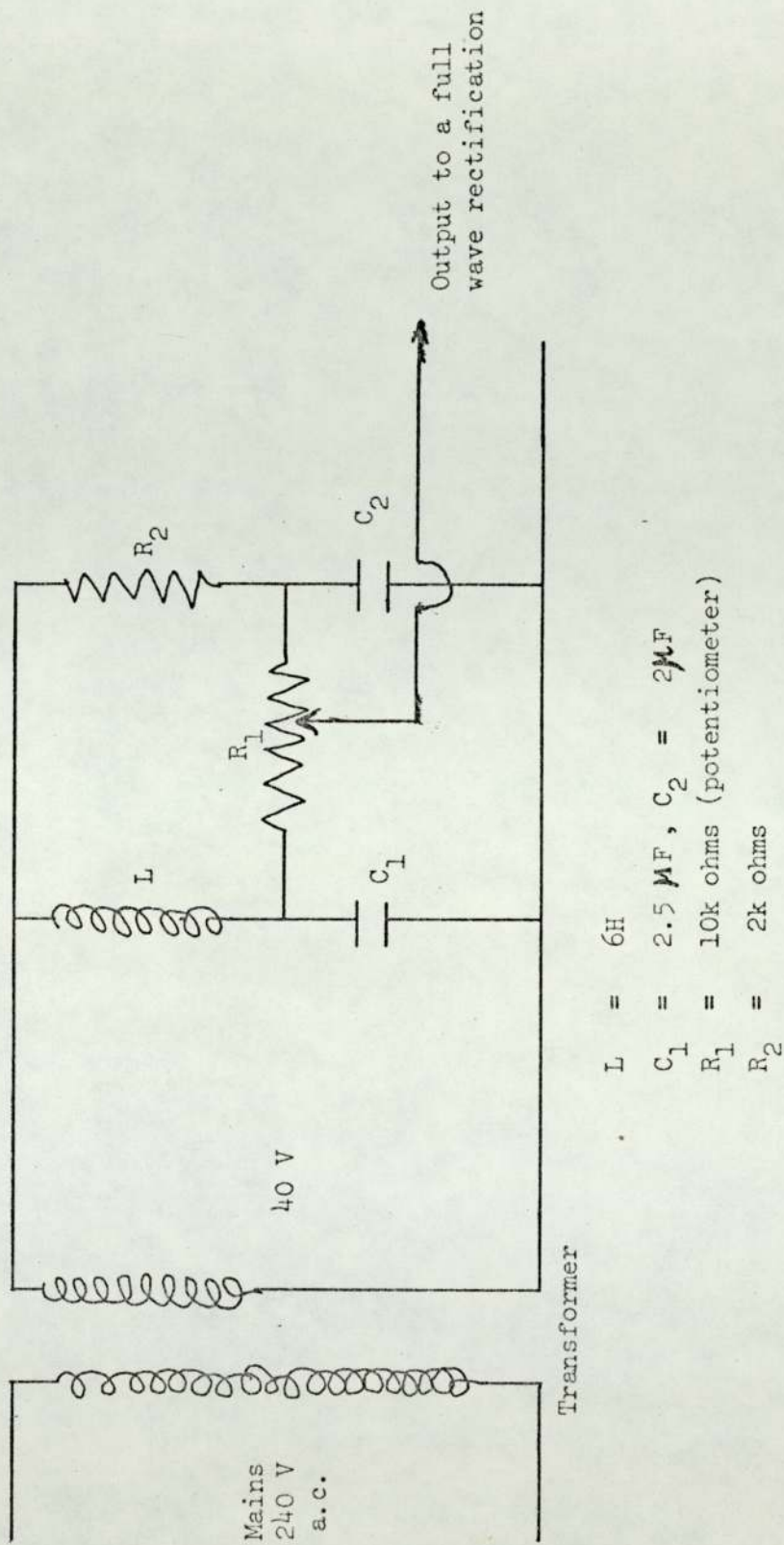
R_2 = 2k ohms

Fig. 2.5   The new phase shift circuit

detector to integrate for a longer time in order that the rising signal from the monitor amplifier reaches the preset value and then terminates the integration in the detector (section 2.2). The areas under the curves of the instantaneous X-ray intensity in the two sorts of rectifiers (figs. 2.3 and 2.4) represent the total X-ray energy produced per half cycle. They cannot be compared directly because the height of the X-ray tube from the measuring instrument (section 2.3), in the case of the valve rectifiers, was not known and because of the difference in peak voltages. However, it is shown in figure 2.3 that the production of X-rays does not start until the voltage reaches about 18 keV. On the other hand, the X-ray production starts from a very low voltage in the case of the valve rectifiers (fig.2.4).

To compensate for the decrease in total X-ray output the pre-set voltage was decreased which, in effect, decreased the total monitor signal voltage the amplifier should reach before terminating the integration in the detector (section 2.2).

The optimum working conditions of the X-ray tube with the valve rectifiers were 90 keV and 50 mA and the mean integration time was $\frac{1}{225}$ second , i.e. 80° (section 2.2). With the solid state rectifiers, since the fluctuations in X-ray output are less it was expected that the integration time could be increased beyond 80° without effecting the compensation for mains variation.

.../

2.4   The new slit

2.4.1   The need for a new slit

In some of the traces a periodic spot splitting was noticed.
This was clearer in the position where the anode was perpendicular
in direction to the slit of the detector, i.e. in the case of left
limb scanning. Figures 2.6 and 2.7 show traces of a dural plate
stationary above the detector slit (without using the water bath)
and with a similar one fixed above the slit of the monitor detector
(in place of the water cell). This was done in order to get similar
X-ray spectra received by the two detectors which increased the
accuracy of the compensation mechanism for variations in the X-ray
output (section 2.2). In figure 2.7 the scan was taken with the
axis of the anode parallel to the slit of the detector and, in
figure 2.6 the scan was taken after rotating the scanning machine 90°
with respect to the X-ray tube. It is clear that the trace of
figure 2.7 suffered less spot splitting than the trace of figure 2.6.

It was thought that the spot splitting was due to anode wobble
during rotation which affected the total X-rays reaching the detector.
The spot splitting would be more significant in the left limb scanning
if the wobble was mostly in the form of axial anode movement. Mis-
alignment of the X-ray tube with the detector s lit was found to
increase the spot splitting. The monitor detector is less affected
by anode wobble because its slit is wider (18 x 10 mm). Investigation
of the spot splitting is merited because the fluctuations limit the
accuracy with which a scan may be made.
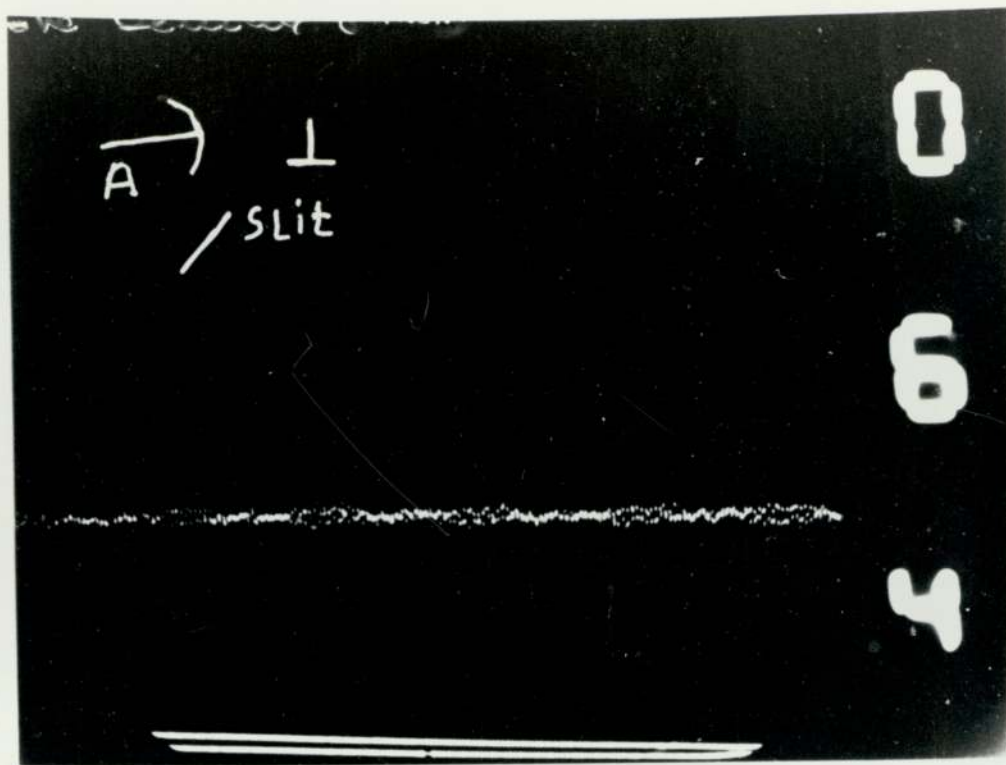
Fig. 2.6   A trace showing spot splitting (anode axis
             perpendicular to the detector slit)
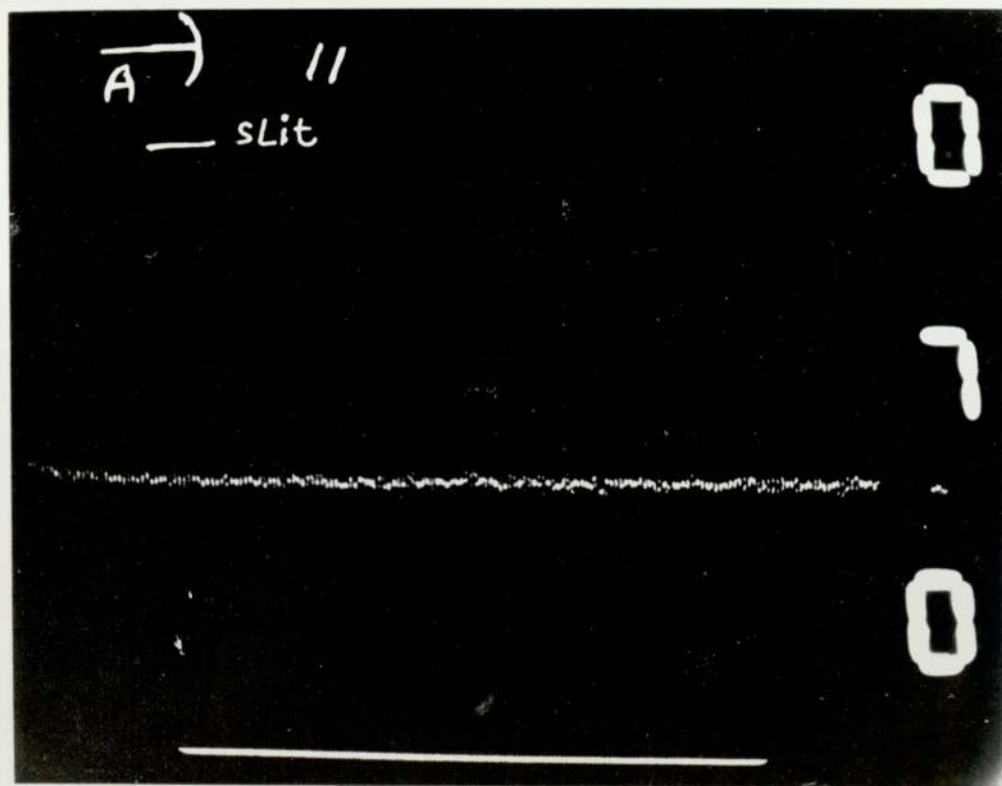
Fig. 2.7   A trace showing spot splitting (anode axis
             parallel to the detector slit)

The effect of axial anode movement on total X-ray energy reaching the detector depends on a number of factors (see fig. 2.8) among which is the thickness of the slab forming the slit.

    If   O is the normal anode position,

$\bar{x}$ is the possible movement of anode from the normal position on either side estimated to be $\pm$ 1 mm,

d is the distance from the anode to the detector slit $\simeq$ 500 mm,

$\bar{t}$ is the thickness of the slab forming the slit = 2 mm,

$\bar{b}$ is the slit width = 0.25 mm,

$\bar{I}_o$ is the X-ray intensity reaching the detector when the anode is vertically above the slit,

$\bar{I}$ is the X-ray intensity reaching the detector at any possible position of the anode,

    then   in position O : $\bar{I}$ = $\bar{I}_o$ the anode is vertically above the detector slit.

In position 1 :

$$\frac{\bar{x}}{d} = \frac{\bar{y}}{\bar{t}}$$ where $\bar{y}$ is the decrease in the width of the detector slit apparent to the anode,

    or $$\bar{y} = \frac{\bar{x}\bar{t}}{d} \qquad\qquad 2.3$$

$$\bar{I} = \bar{I}_o \bar{K} \frac{\bar{b} - \bar{y}}{\bar{b}} \qquad\qquad 2.4$$

$\bar{K}$ is a constant which is nearly 1 for small anode movement.

-l   0 $\bar{x}$ l

O : the normal anode position
l, -l, is two possible
positions of the anode during
its movement

X-ray beam

d

$\bar{b} - \bar{y}$

$\bar{y}$

slit width ($\bar{b}$)

$\bar{t}$

The slab forming the slit
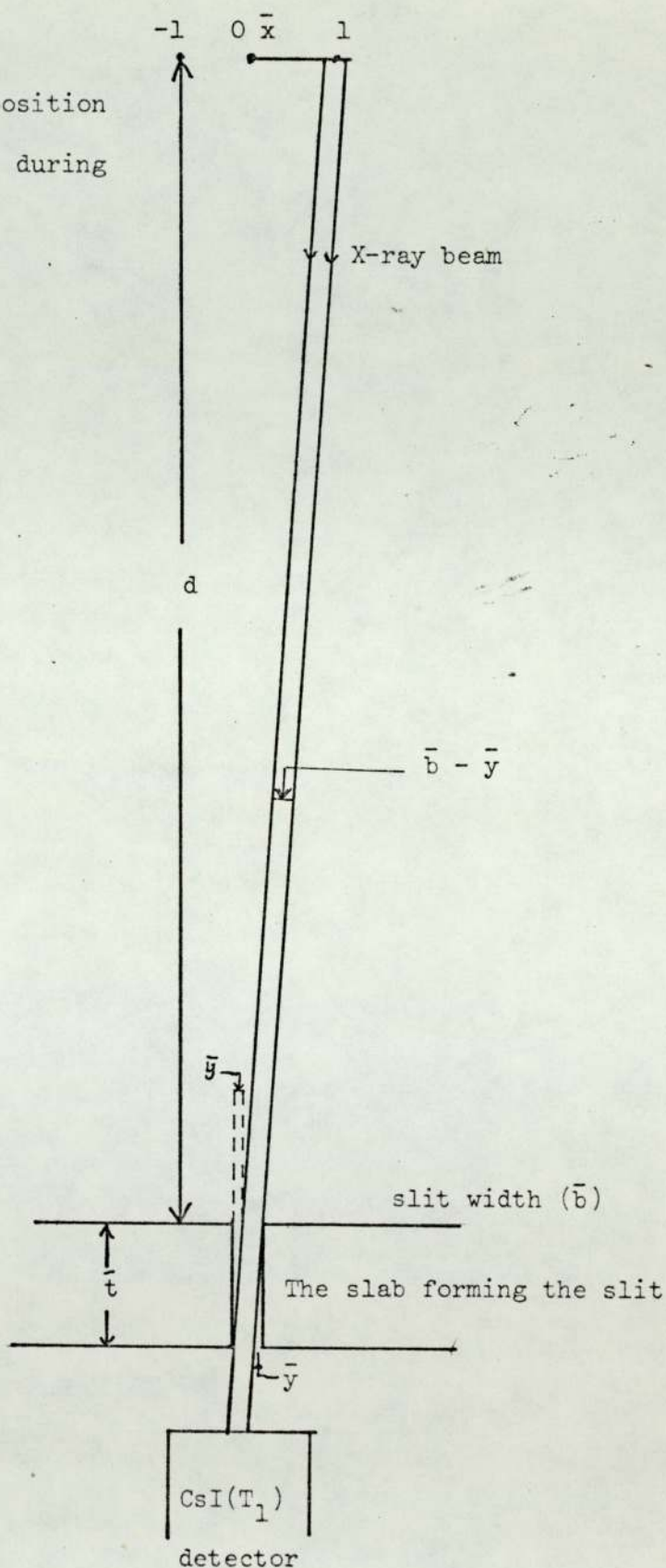
$\bar{y}$

CsI(T_1)

detector

Fig. 2.8   The effect of axial anode movement on the X-rays reaching
the detector

By substituting $\bar{y}$ from equation 2.3 in equation 2.4

$$\bar{I} \;=\; \bar{I}_o \, \bar{K} \, \frac{\bar{b} - \dfrac{h \, \bar{x}}{d}}{\bar{b}}$$

$$\bar{I} \;=\; \bar{I}_o \, \bar{K} \left[\, 1 \;-\; \frac{\bar{b}\bar{x}}{d\bar{b}} \,\right] \qquad\qquad 2.5$$

For a 1 mm displacement:

$$1 \;-\; \frac{\bar{t}\bar{x}}{d\bar{b}} \;=\; 1 \;-\; 0.016 \;=\; 0.984 \qquad\qquad 2.6$$

It is desirable that $\frac{\bar{t}\bar{x}}{d\bar{b}}$ be as small as possible. Decreasing the slab thickness $(\bar{t})$ will decrease the effect of anode wobble on total X-rays reaching the detector or could alternatively be used to increase the resolution of the machine by decreasing the slit width without causing extra spot splitting. This is possible only if the total X-ray energy reaching the detector is adequate.

In order to decrease the thickness of the walls forming the slit and at the same time keep its X-ray attenuation high ($I^*/I_o^* < 10^{-3}$), materials of high linear attenuation coefficients in the energy region 30 - 85 keV are required. A combination of uranium and another material was theoretically proved to give greater attenuation over the energy range than a single material of the same total thickness. Tungsten which has its k-edge at 68 keV was chosen to be used with uranium whose k-edge is at 113 keV. Lead, platinum and gold were considered as alternatives to tungsten but, as is seen in figure 2.9, the overall attenuation coefficients of uranium and tungsten $(\mu_u + \mu_w)$ at the kw-edge does not drop as low as k-energies of the other elements.
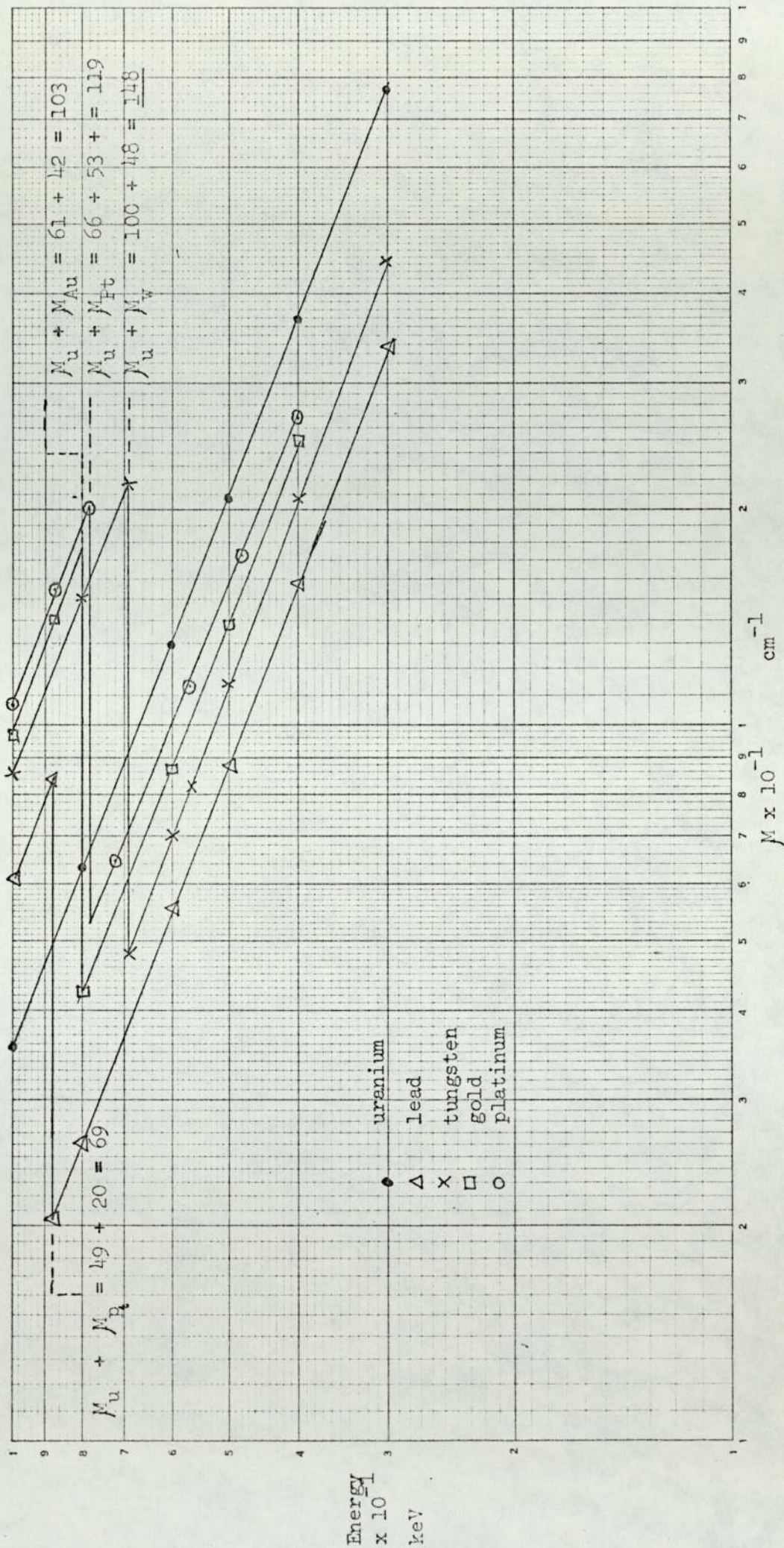
.../

Fig. 2.9   Linear attenuation coefficients of U, Pb, W, Au and Pt (54, 64)

The optimum thicknesses of (U) and (W) for high attenuation of X-rays, over a range of energies mainly important at higher keV ～ 60 - 85, where the attenuation coefficients are relatively low, were calculated using the attenuation equation for collimated monochromatic photons

$$I^* = I_o^* e^{-(M_u t_u + M_w t_w)} \qquad 2.7$$

where I_o^* is the X-ray intensity for zero thickness,

I^* is the X ray intensity transmitted through t_u and t_w, the thicknesses of uranium and tungsten,

and M_u, M_w are the linear attenuation coefficients of uranium and tungsten respectively,

let $x^* = M_u t_u + M_w t_w \qquad 2.8$

By choosing a certain total thickness ($\bar{t} = t_u + t_w$) and then working out x values for the different X-ray energies and different thickness combinations of U and W, a ratio of approximately $\frac{tu}{tw} = 2.3$ was found to give the highest absorption in the energy region (60 - 85) keV.

In order to achieve an attenuation of 10^{-3}, x has to be equal to or higher than seven. A total thickness of 1 mm with 0.3 mm of tungsten and 0.7 mm of uranium gave attenuations higher than 10^{-3} at the different energies (Table 2.2).

2.4.2   The construction of the new slit

The uranium slab was made from a 3 mm diameter rod by hand-

.../

filing [1] in water, in order to prevent the uranium dust being

inhaled. It was also unsafe to machine uranium in the workshop

for the same reason. The uranium slab was made 0.7 mm thick, 2 mm

wide and 60 mm long, then it was cut laterally into two equal halves.

A tungsten slab 0.15 mm thick was used with the uranium. Each

uranium slab was sandwiched between two similar slabs of tungsten

and cemented together with araldite (AV 100 and hardener HV 100).

The sandwiching was done in order to avoid the uranium being exposed

to air which would oxidise it. A small lead alloy box (lead antimony

14%) open on top and bottom was made and the two sandwiched slabs

cemented to it (fig. 2.10). A gap of 0.25 mm between the two slabs

was ensured by fixing a feeler gauge of this thickness in between

and clamping them together. The surface of all the slabs were

covered with a thin film of araldite to prevent uranium oxidisation.

The slit was also filled with araldite for the same reason and an

equal thickness (1 mm) of polymerized araldite slab was fixed above

the slit of the monitor detector in order to get equal attenuation.

above the two detectors. The old slit in the lid of the detector

box was enlarged to 2 mm wide then the lead box (with the cemented

U-W slabs) was soldered to the lid from underneath, with the U-W

slabs in contact with the slit vertically on the lid in the position of

the old one. A low melting alloy (Serrolow alloy 117) was used in

soldering to prevent any possibility of changing the shape of the

small lead box and the detector box which could happen when using
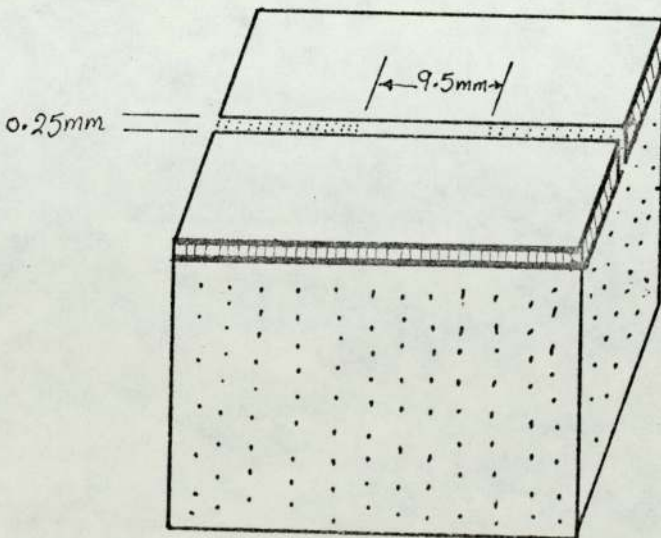
ordinary solder.

---

[1] Uranium is a very hard material and it was found that hand-filing
was a time-consuming procedure.

Fig. 2.10   The new U-W slit
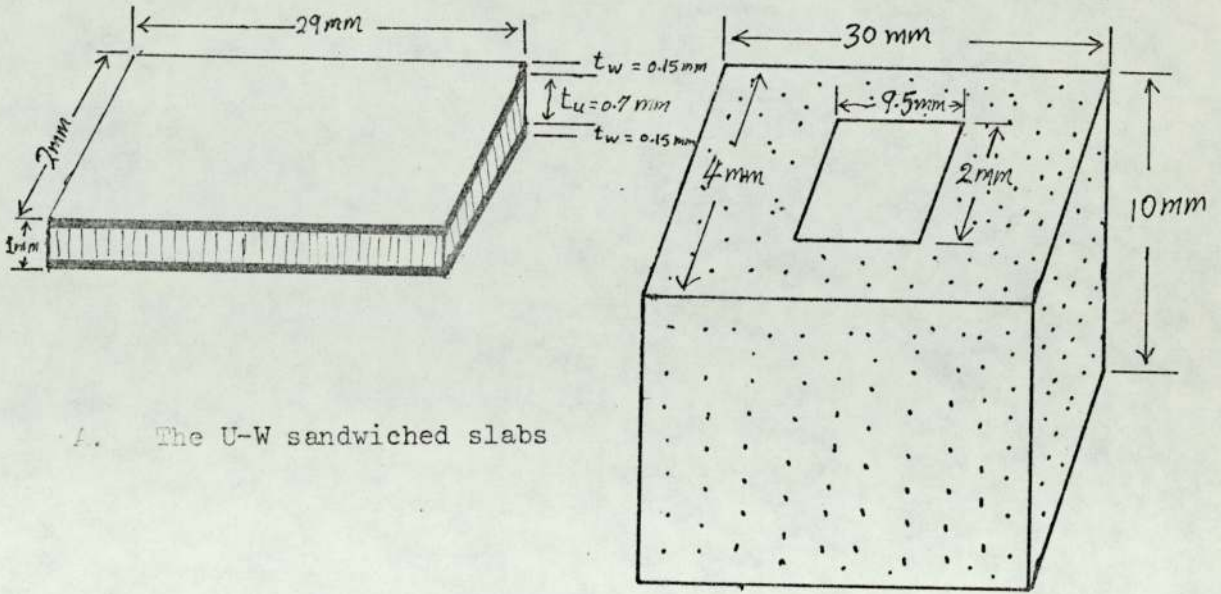
A.   The U-W sandwiched slabs

B. _ The lead alloy box

C.   The two sandwiched U-W slabs cemented
on top of the lead alloy box

2.4.3   The effect of fixing the new slit

After replacing the detector box in position, a number of traces were taken of the ivory stepwedge with both the right and the left fixing frames (figures 2.11 and 2.12). As shown in these figures, there is a shrinkage in the heights of the traces with a clear periodical spot splitting. The drop in X-ray signal was most probably due to a decrease in the slit width, i.e. the first slit width being more than the nominal value.

There are two ways of increasing the total X-ray signal to compensate: either by increasing the integration time or by increasing the amplifier gain of the detector. Due to the restricted possible increase in integration time, the amplifier gain was increased by decreasing the feedback in the second amplifier. The integration time control was then used to give a small adjustment in signal height to regain the previous standard height.

Periodic spot splitting was still apparent in some of the traces inspite of the modifications made to the slit. It was therefore necessary to think of another method to decrease the spot splitting. Decreasing the slit width may have produced some benefit since it is now known that the slit is accurately 0.25 mm wide and 9.5 mm long (earlier the slit width was most probably wider than the nominal value) but it was not obvious that this improvement was worth the effort made.
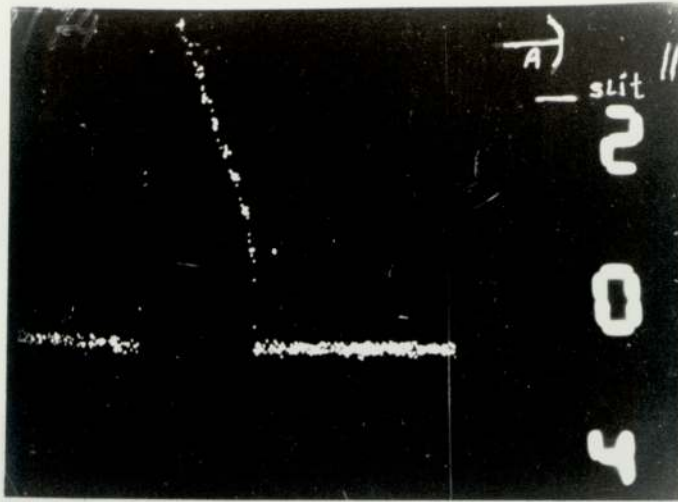
.../

Fig. 2.11   A trace showing spot splitting and
            shrinkage (anode axis perpendicular
                to the detector slit)
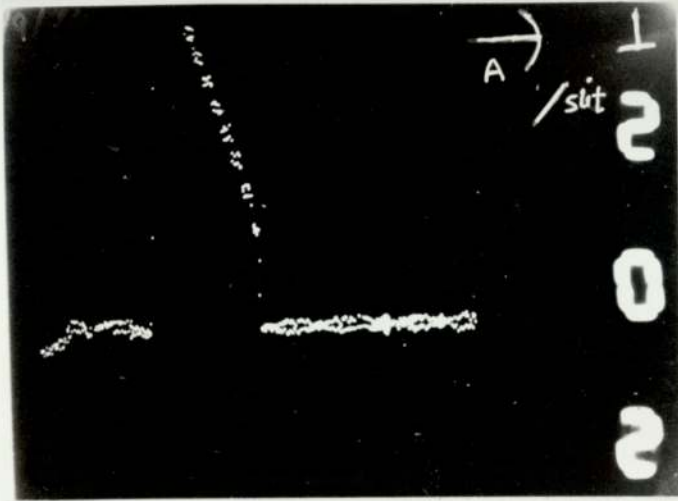
Fit. 2.12   A trace showing spot splitting and
            shrinkage (anode axis parallel to
                the detector slit)
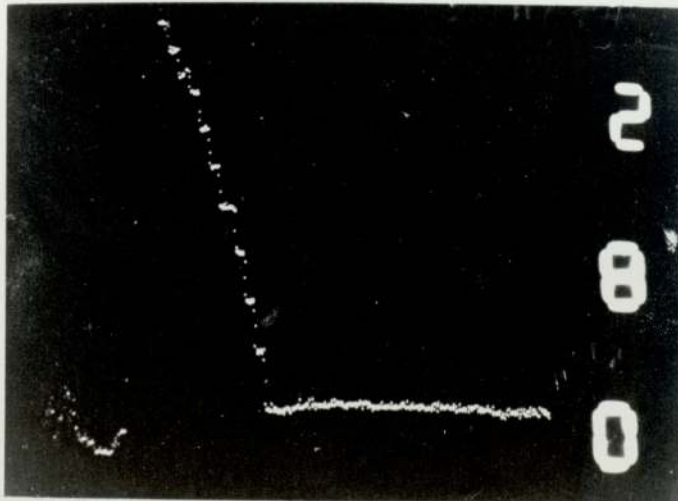
Fig. 2.13   A trace taken with the X-ray tube
                in a tilted position

2.5   The tilted frame of the X-ray tube

The spot splitting which appeared on some of the traces even after fixing the new slit (section 2.4) was still thought to be due to wobble in the anode of the X-ray tube and that decreasing the slit wall thickness from 2 mm to 1 mm was insufficient to remove this effect.

To decrease the spot splitting, the possibility of using the X-ray tube in a tilted position was studied.   In this case the gravitational force would work to pull the anode down which would tend to take up the slack on the bearing.

The X-ray output was measured at different tilt angles using a CsI(Tl) crystal with a photomultiplier and an amplifier.   An increase in signal voltage of about 3% was noticed in the first 5° inclination and there was no more increase until 9° when the X-ray beam coming vertically was cut-off by the diaphragm walls of the X-ray tube head.   The effect of using a tilted X-ray tube was also examined experimentally by removing the X-ray tube head from the brass flange which is fixed to the top of the scanning machine and, fixing the tube at 8° to the horizontal above the brass flange and aligned with the two detector slits.   A scan was taken of the ivory stepwedge and it was clear that this trace suffered very little spot splitting (see fig. 2.13).   Compare this trace with those of figures 2.11 and 2.12 where the X-ray tube was fixed horizontally.

Two of the three top dural blocks which were mounted in either side of the monitor detector to support the brass flange (Edwards, J, 1973) were removed and replaced by a new frame in which the brass flange is fixed at 8° with respect to the horizontal. Figures 2.14 and 2.15 show side and vertical views of the tilted frame. The brass plate (18 x 7.6 cm) is bolted to the fixed dural blocks (see fig. 2.2). The rest of the frame with the brass flange, which is fixed to the X-ray tube head, is joined to the brass plate with four latches. The tilted frame with the latches ensured a simple and reproducible positioning of the X-ray tube with respect to the two detectors. The frame is provided with four side screws (see figs. 2.14 and 2.15) which allowed about 5 mm sideways movement of the X-ray tube relative to the scanning machine. These screws enable an easy alignment of the X-ray tube with the two detectors.

The water cell constructed to provide a bath of water over the monitor was replaced with another cell which was accommodated in the tilted frame (see fig. 2.16).

Using the X-ray tube tilted has improved the traces by decreasing spot splitting. However, slight spot splitting in some traces has appeared less often, which was thought to be due to side wobbles of the anode unaffected by tilting the tube.

2.6   The numerating system

For record purposes it is clear that some sort of permanent identification system on the traces, for instance numbers, is desirable. This could be done either after scanning and developing

.../
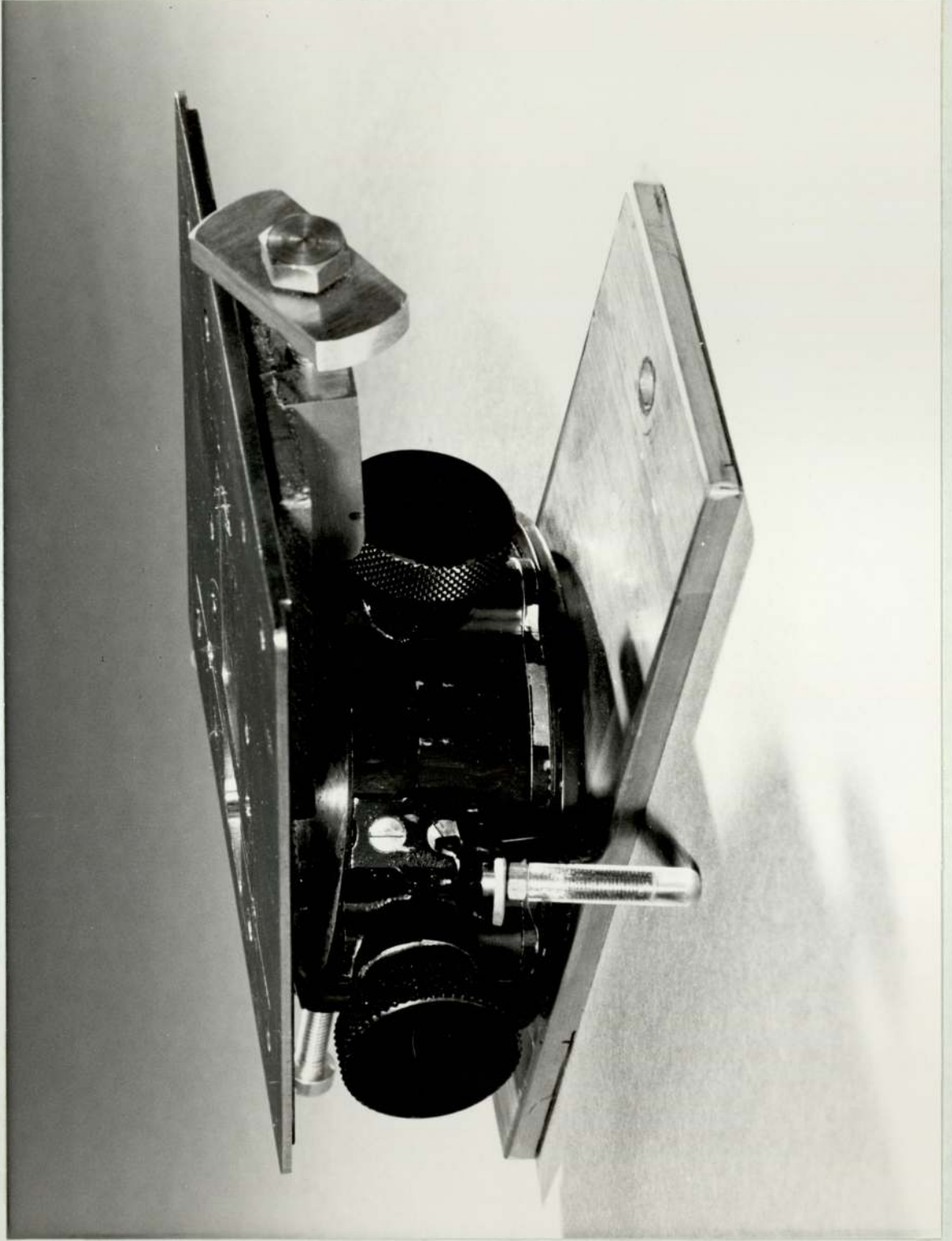
Fig. 2.14 A side view of the tilted frame
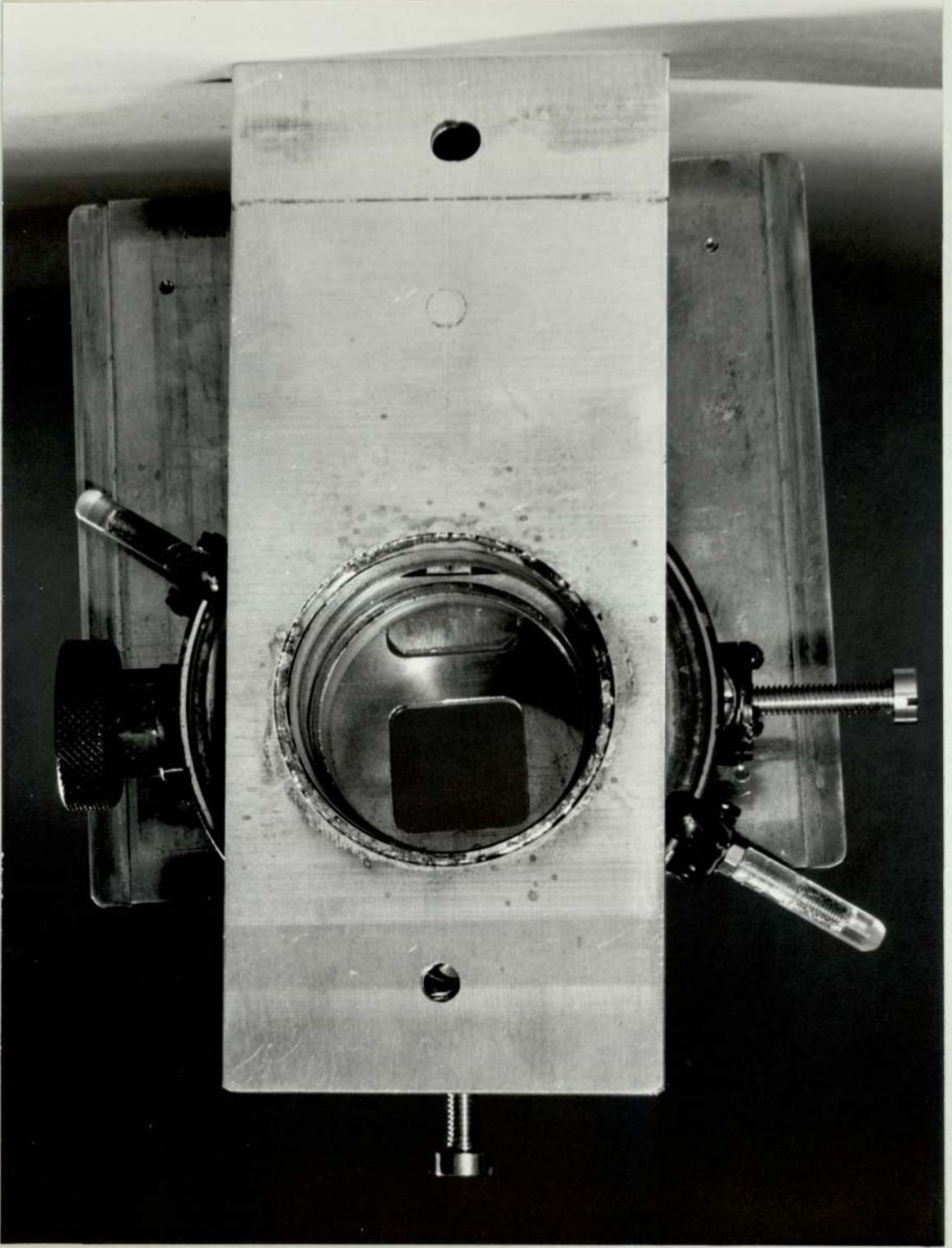
Fig. 2.15   A vertical view of the tilted frame
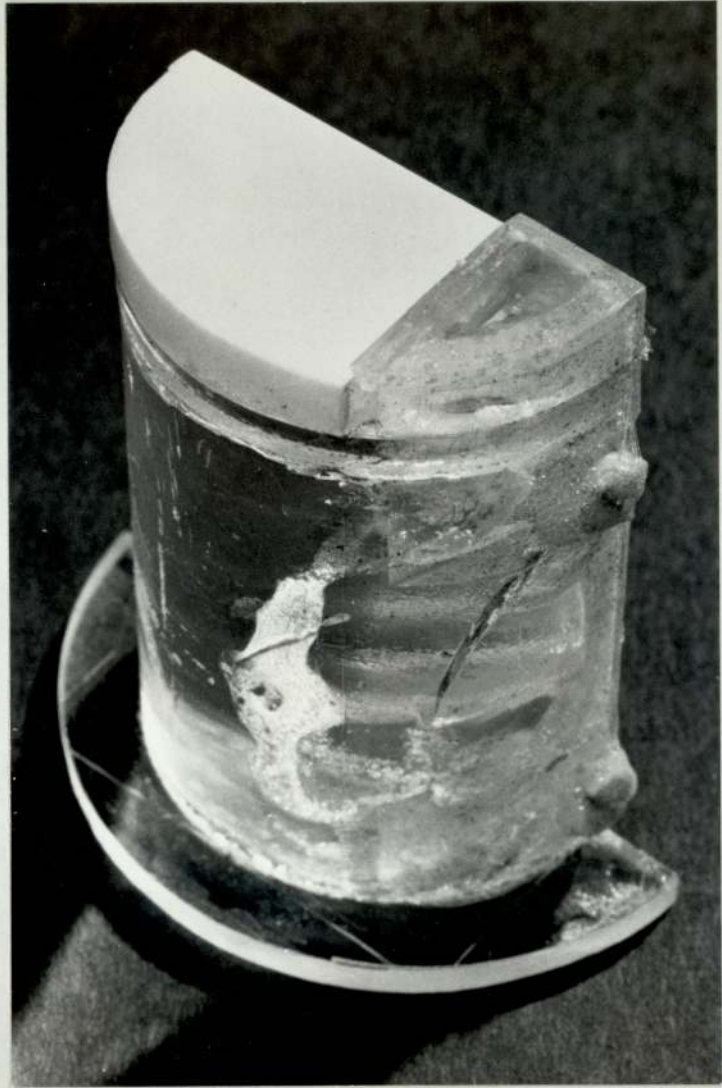
Fig. 2.16   The water cell with the artificial bone
slab (4.8 mm) on top

the film using, for example, a fibre-tip pen or the numeration

could be done during the scanning procedure using numeral lamps

giving developable images on the films. The latter saves extra

effort and the numbers appear clearer, more reliably and more

tidily; therefore, this way was chosen.

Three Japanese number lamps with tungsten filaments (menitron

3015F) were used. Each lamp was 22.5 mm long, 12 mm wide and 5.5 mm

in height and consisted of eight straight tungsten filaments connected

in parallel to a common point. Each lamp was provided with a separate

socket where wires to the different filaments could be soldered and

any damaged lamp could easily be replaced with a similar one. Three

ten ways switches were used in connecting the case leads of the

filaments in the lamps to the power supply with one switch for each

lamp. Using the three lamps, numbers from 000 to 999 could be

displayed.

The recommended d.c. supply to the filaments was 5 volts and

the quoted resistance of each filament was 220 ohms. These filaments

were run on a lower voltage supply of about 4.5 volts in order to

preserve them as long as possible. A transformer (240 to 6.3 volts)

was used to supply the lamps after full wave rectification and

stabilisation. The circuit diagram of the electronics is shown in

figure 2.17. All the electronic components and the three switches

were fixed in an aluminium box (12 x 18.5   x 8 cm height). Three

holes were drilled in the lid of the box to be used for the switches.

The three sockets of the numerating lamps were cemented with bostik

to the inner side of the oscilloscope screen frame on top of each

other. To ensure that the displayed numbers will be photographed
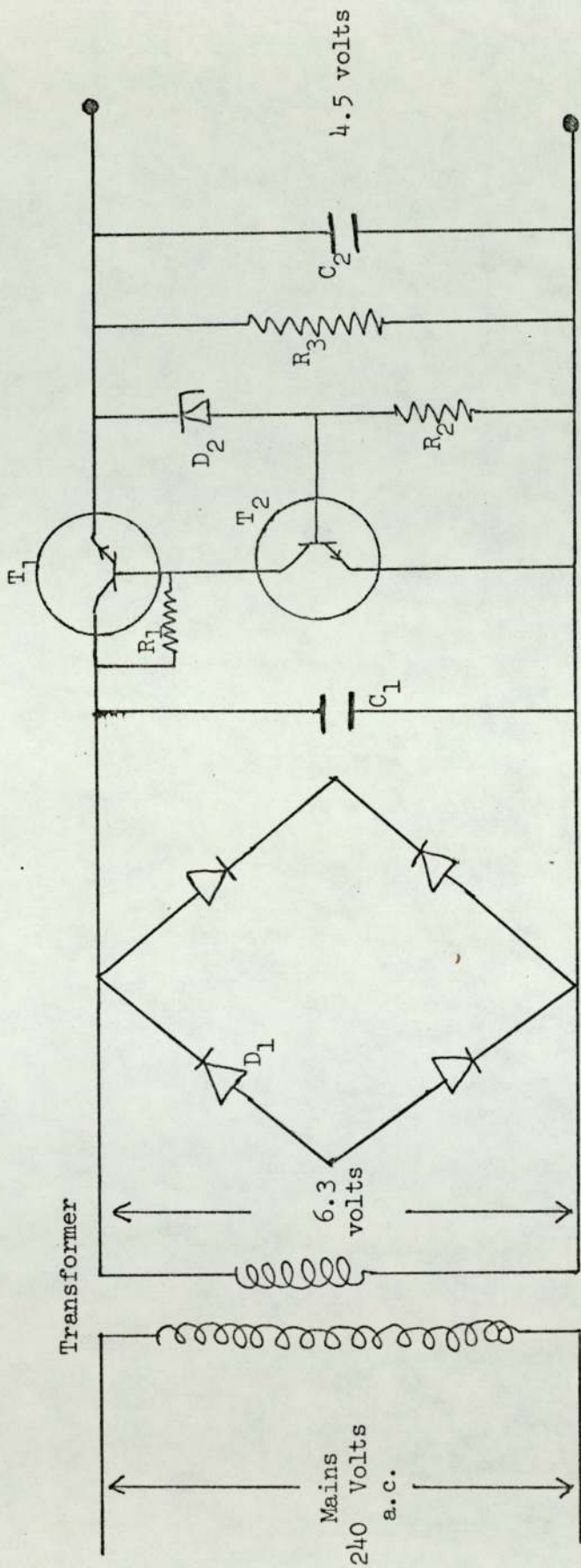
Fig. 2.17   The circuit diagram of the numerating lamps' supply

in the X-ray film the two end lamps were fixed at about 10 mm
from the screen corners. Thin flexible wires were used in
connecting the pins of the lamp cases (eight wires for each lamp)
to a socket which was fixed to the side of the oscilloscope. An
equal number of wires connected the stabiliser to the plug. In
this way, it is possible to separate the supply box from the lamps.
The camera cable release and the numeration switch were linked to
the on/off motor switch so that only the on/off switch and the
'Prep' knob of the X-ray tube needed to be operated.

An exposure time of about 5 seconds was required to get
sufficient exposure of the X-ray film. The main reason for this
high exposure time is the low sensitivity of the X-ray films to
the yellow light. Figure 2.13 shows traces of the artificial bone
step wedge with the numbers apparent. The photographed numbers do
not interfere with the scan.

2.7   The elbow fixer

In doing repeated scans of patients, a difficulty has arisen
in repositioning the limb accurately. The method adopted to re-
position the limb was to feel the ulnar styloid by hand with a view
to fixing the limb so that the ulnar styloid is in the middle of the
rubber padded perspex block. The difficulty arose from identifying
the middle of the ulnar styloid and positioning it in the middle of
the rubber padded perspex block. Earlier, (Edwards, J, 1973)

.../

repeated scans were done by taking a note of the position of the

third finger after fixing the limb. This scheme was found

experimentally imprecise.[69]

To solve this problem another scheme was required to determine

accurately the position of the limb. The elbow was found suitable

for this purpose because of the little soft tissue covering it.

Two perspex elbow fixers were made one for the right limb, i.e.

to be used with the right fixing frame, and the second for the

left limb (fig. 2.18). After fixing the patient's limb in the

predetermined position, the elbow fixer was pushed till it butted

against the olecranon. Two scales were fixed on the top of the

sides of the water baths to provide a reading to the elbow position

as shown in figure 2.18. Two extra extensions of perspex blocks

3 cm and 4 cm of length were made to allow extra latitude of the

elbow fixer in the case of short limbs.

Whenever a scan is taken to patient, the elbow position is

recorded in a book together with other relevant information.

2.8   The standing platform

To allow subjects to stand comfortably during limb positioning

and scanning they should be at a certain height with respect to the

water bath, so that the elbow is levelled with the floor of the bath.

In the case of mature subjects of normal height($\sim$ 160 cm) no standing

platform is needed. A very tall person needs to bend down slightly

during positioning and scanning procedures; on the other hand for
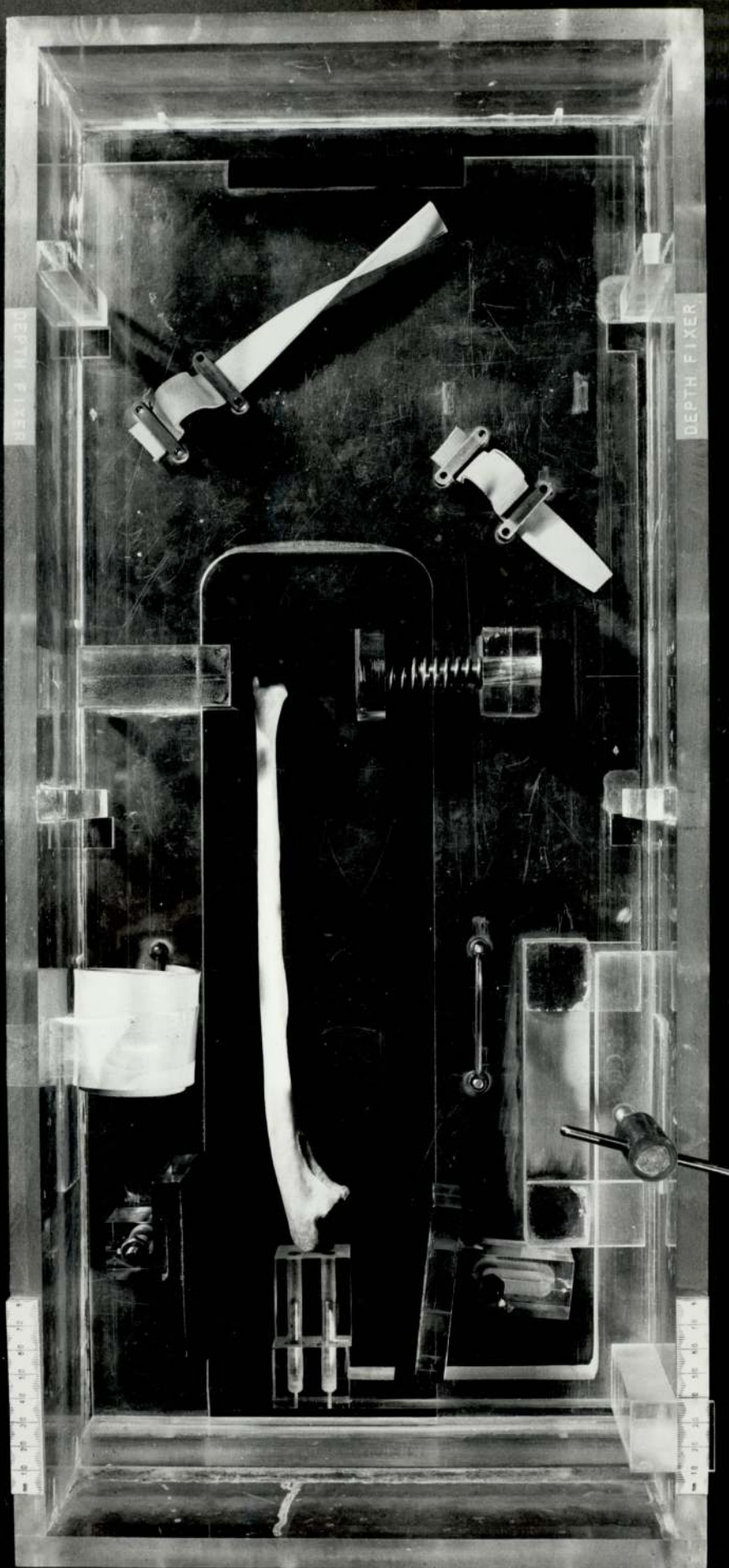
Fig. 2.18   The right arm fixing frame and elbow fixer
in the perspex bath.

patients of short height or for teenagers, a standing platform of variable height is required.

A wooden plate 35.7 x 45.9 cm and 2.5 cm thick was made for this purpose together with extra wooden plates (7.5 x 34 cm) for increasing the height from 2.5 cm to 15 cm in 2.5 cm steps. The plate height required is determined before immersing the limb in the water bath by estimating the difference in heights between the bottom of the water bath and the elbow of the patient.

The ideal thing would be to use an adjustable platform, either pneumatic or hydroulic, easily operated by foot pressure. However, the wooden plates were used as these would be much cheaper.

2.9   The painting of the detectors housings

Inside each lead-roofed dural detector box was housed the photodiode, the crystal with its housing and the electronic integrator. The small crystal was held in a perspex container. Inside the container was milled a central rectangular cavity for the crystal. The outer curved surface of the crystal housing was aluminised by evaporation in vacuo with the aim that it will reflect back some of the light emitted away from the photocathode in a scintillation event (Edwards, J, 1973).

During the opening of the two detector boxes it was noticed that some of the evaporated aluminium on the crystal housing had come off. Therefore, it was decided to remove the rest of the

aluminium and do a new aluminium evaporation. Before doing so,

an experiment was carried out to test the significance of this coating

on the total photodiode current. In this experiment a photodiode,

similar to the one used with the detector, was used together with

CsI(Tl) detector and a perspex container. The circuit is illustrated

in figure 2.19. The X-ray tube current was 10 mA and the voltage

was 50 k Vp. A brushing cellulose aluminium was used in painting

the outer curved of the crystal house. The photodiode current was

measured with the crystal house unpainted then it was measured

again after painting.

Upon comparing the photodiode currents with and without the

painting, it was found that there was no significant difference.

This indicated that there was no advantage in coating the crystal

housings and therefore the idea was abandoned.
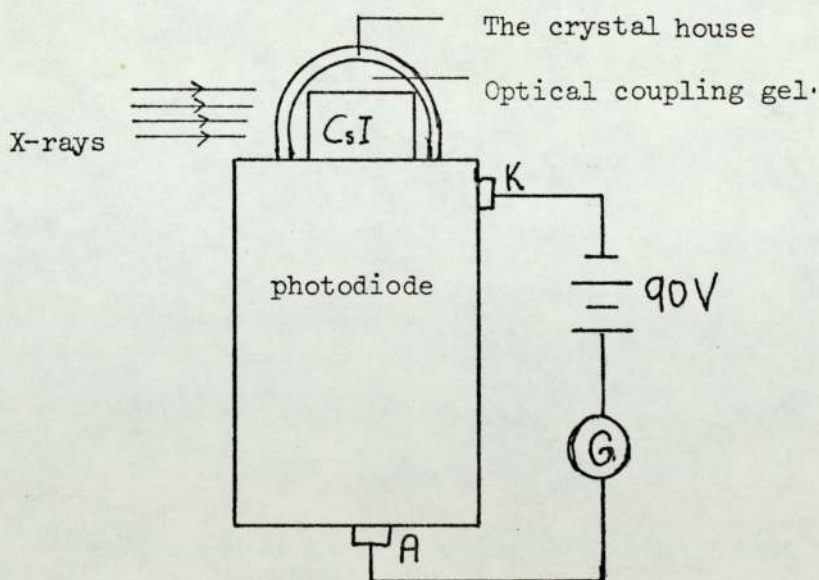
Fig. 2.19   A circuit diagram of the apparatus measuring the
photodiode current

2.10 The external interference

In some of the traces regions of erratic behaviour can be clearly seen, which presumably is caused by external interference. Figures 2.20 are typical traces showing this interference. The interference can be observed on the oscilloscope with a scan time of $\frac{1}{100}$ second, in the absence of X-rays to the detectors.

An investigation was done to see whether the interference was mains borne or radiated . As a result of the investigation (which is mentioned in the following paragraphs) it was found that the interference was almost entirely due to radiation.

As a first step a hand-drill was switched on and brought near the boxes of the two detectors and the box of the amplifiers. Also a strong magnet was moved rapidly by hand near the boxes and in both cases no significant interference was noticed. It was thought at this stage that the interference was probably coming through the mains supply and a filtration of some sort would be beneficial. The filters tried were inductance and capacitance systems designed as low pass filter, 50 cps tuned filter and common mode rejection filter. In all cases they were ineffective.

The other method tried to stop any interference coming through the mains was to provide a separate electric supply using two synchronous motors. The shafts of the two motors were coupled with complete electric insulation as shown in figure 2.21. One was used as a motor and the second was used as a generator supplying the electronic equipment. The supply was used for a few minutes during

Figs. 2.20   Traces showing the effect of
              interference on output signals
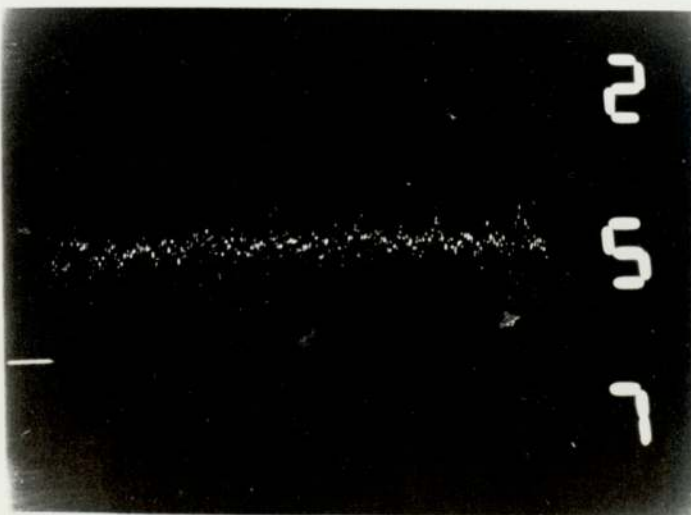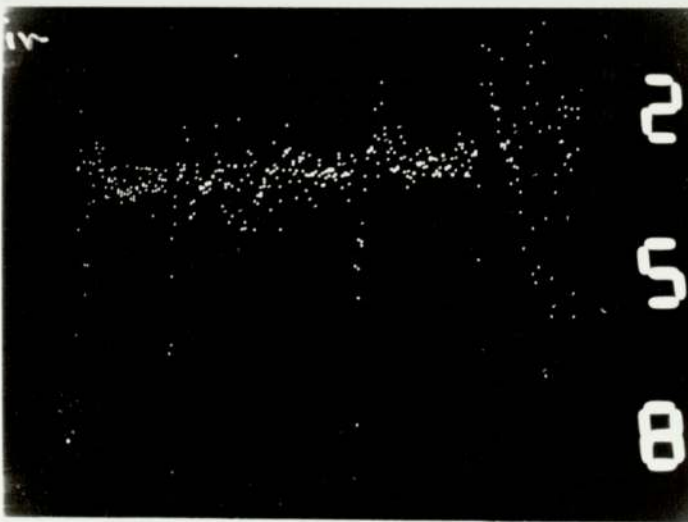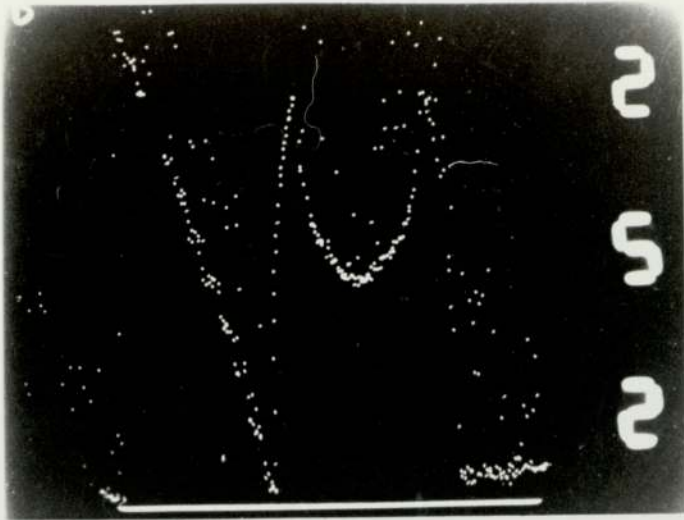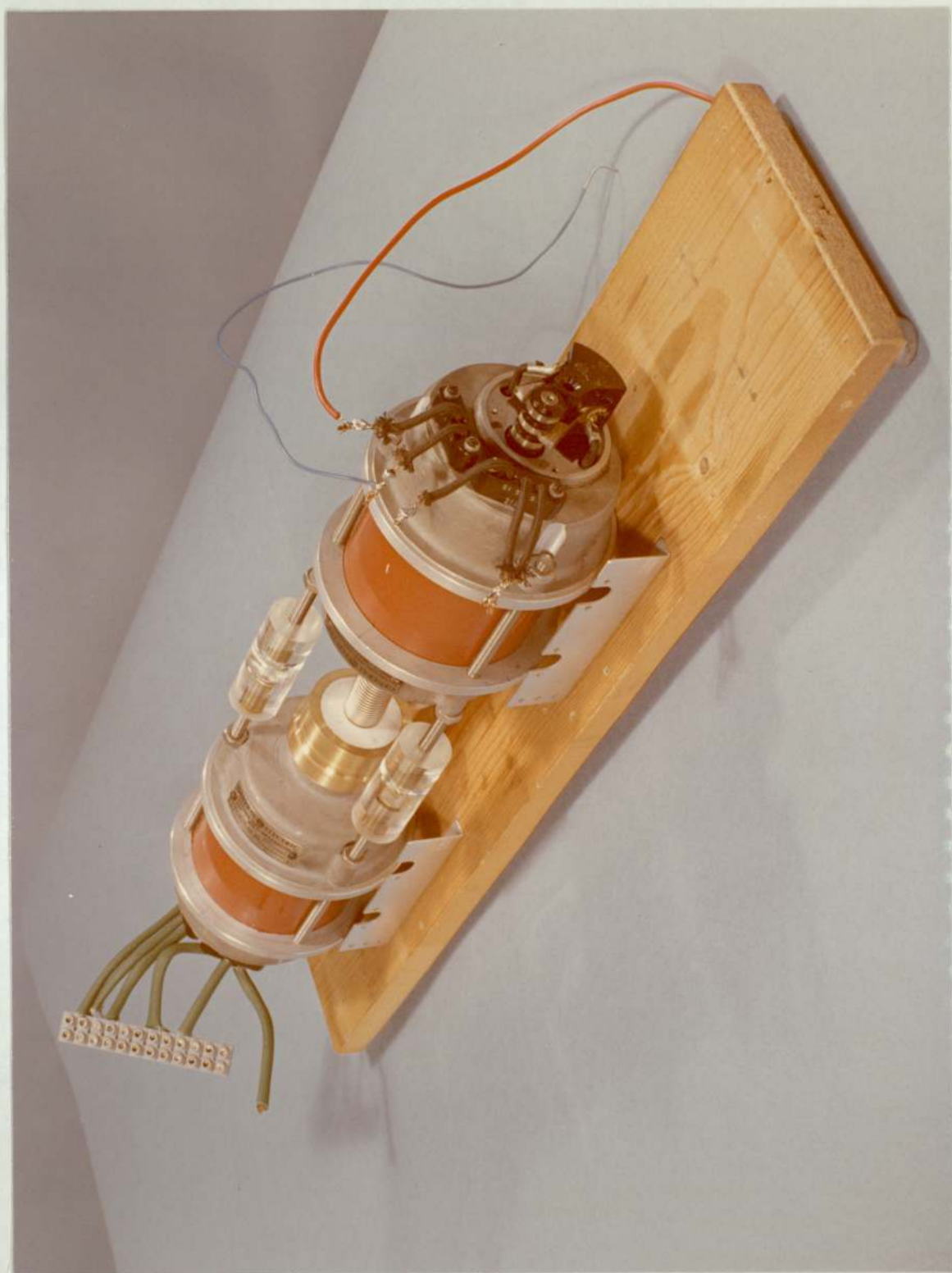
Fig. 2.21   The two coupled synchronous motors

the presence of interference and it was found that the latter was still present. This showed that the interference was not coming directly from the mains. It was most probably radiated from the mains, i.e. the mains was working as a transmitting aerial.

To verify this, a coil supplied from a signal generator was used to produce alternating magnetic fields. The alternating magnetic fields caused an induced voltage, which appeared in the output signal starting from 100 H_Z and increasing slightly in amplitude with increase in frequency. The effect was produced when the coil was brought near the boxes of the detectors and amplifiers and near the cables carrying the signals to the amplifiers. It was at maximum when the coil was above the detector box and also high when it was above the monitor detector box.

Once it had been recognised that the interference was almost entirely the result of electromagnetic radiation, it was decided that it would be necessary:

a)   to re-arrange the wiring, i.e. cables between the parts of the electronic system and

b)   to provide the detector boxes with as effective electromagnetic screens as possible, as a signal introduced into these will be subjected to the full amplifier gain.

.../

The boxes of the detectors were screened as described in the following sections. The cables of the supplies and the signals were shortened and were arranged so that they run parallel in bundles with the earth wires. The d.c. power pack was also arranged in such a way so as to decrease the length of the wire supplies.

To ensure maximum attenuation of external radiation inter-ference the whole equipment needed a suitable screening. This in turn required the redesign of the equipment which was considered not desirable for the long time it is expected to take. Therefore, a design was made for screening of the two detector boxes using the following theory.

2.10.1 The screening of the detectors' boxes

2.10.1.1 The calculation

It was thought that the magnetic radiation was emitted from mains cables at a distance from the equipment. To estimate the required screening to the boxes, the radiation was considered as a plane wave. The penetration current in screening material can then be worked out and the thickness to cause 60 db attenuation (10^{-3}) for the lowest frequency, i.e. 100 H_Z calculated.

The equation of the conduction current in the screening [74] is

$$\frac{\partial^2 I_Z}{\partial x^2} = \sigma \bar{M} \frac{\partial I_Z}{\partial t} \qquad\qquad 2.9$$

.../

Where $\bar{M}$ is the magnetic permeability (in H/m) of the screening material,

σ is the electric conductivity (in mhos/m) of the screening material

and I_Z is the current at depth x.

If $I_Z = I_{Zo}$ at $x = 0$ then

$$I_Z = e^{j\bar{w}t} \, e^{-\alpha^2 x} \qquad 2.10$$

Where $\alpha^2 = j\,\sigma\bar{M}\,\bar{w}$ from equation 2.9

$\alpha = \sqrt{j\,\sigma\bar{M}\,\bar{w}}$

Since $\sqrt{j} = \dfrac{1+j}{\sqrt{2}}$ and $\bar{w} = 2\pi\bar{f}$

then $\alpha = (1+j)\sqrt{\pi\bar{f}\,\bar{M}\,\sigma}$

$= \dfrac{1+j}{\delta}$

Where $\delta = \dfrac{1}{\sqrt{\pi\bar{f}\bar{M}\sigma}}$ meters

A complete solution of equation 2.9 is

$$I_Z = C_1\, e^{-\frac{1+j}{\delta}x} + C_2\, e^{\frac{1+j}{\delta}x}$$

$$2.11$$

The solution $C_2\, e^{\frac{1+j}{\delta}x}$ is not acceptable since the current will increase to infinity at $x = \infty$

Therefore $I_Z = C_1\, e^{-\frac{1+j}{\sigma}x}$ \qquad 2.12

.../

air   screening material

$\bar{M}, \sigma$

I_z

y

δ X

B_y

$x=o$

z
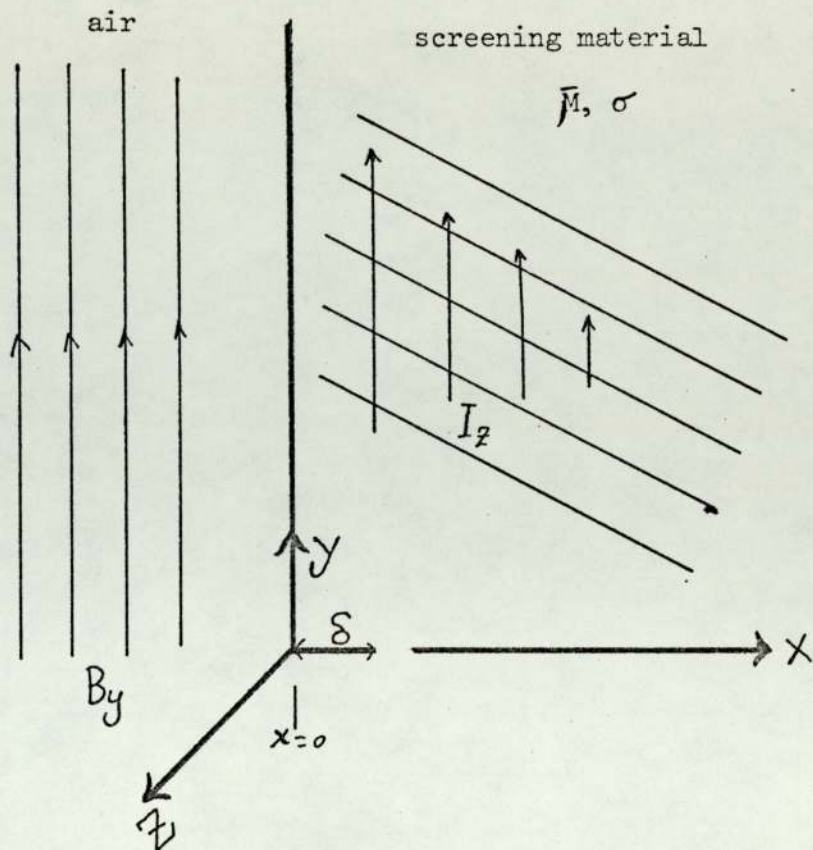
Fig. 2.22   The penetration of a plane magnetic field into a
conductor

It was considered desirable to get 60 db attenuation or better,

then $\frac{x}{\delta} \geqslant 7$. It must now be decided if the required product of $\bar{M}\sigma$

implied, could be achieved forafrequency of 100 H_z, and for a

reasonable screen thickness i.e. about 1 mm. Copper or mumetal

alone could not meet this requirement. It was considered however

that it could be met by alternating layers of the two metals. For

very thin layers, the permeability will be about half that of μ-metal

and the conductivity will be about half that of copper.

...../

$$\bar{M} \ (H/m) \qquad\qquad \sigma \ (mh_os/m)$$

Copper[74] $\sim$ 2.61 x 10^{-6} $\qquad \sim$ 5.8 x 10^{7}

Mumetal[54] $\sim$ 8π x 10^{-3} $\qquad \sim$ 1.82 x 10^{6}

A possible construction was theoretically found to give an attenuation of 112 db for 10^{2} H_Z frequency and it will increase with increase in frequency. The experimental attenuation in the screening is expected to be less than the calculated value because of the approximation made in assuming plane magnetic fields, and a small number of sheets of copper and mumetal. A total thickness of 1.14 mm was used.

2.10.1.2   The method of screening

It was more convenient to screen the boxes from inside with the minimum total thickness in order to provide sufficient space for the electronic components. A dummy was made to fit the inside of the boxes with some allowance for the extra thicknesses of the copper and mumetal layers to be wound round it. The copper sheet, which was annealed for easy bending, was 0.005 in thick and was wide enough to be cut to the required width. The mumetal available was 0.004 in thick and only 1 in wide. It was first wound round the dummy where seven separate windings were required to make one layer for the second box and four for the monitor box. A paint solder was consistently used to join the strips. The copper sheet was soldered at one end to the wound mumetal and then was wound round it and soldered at the other end.

Five layers of each metal were wound round each other making the total thickness 0.045 in (1.14 mm). An end cap of mumetal and copper layers was also made for both boxes. A reamer was used to make the slits in the screening of both boxes. Changes were carried out on the electronic frames of the two detectors with some rearrangement in order to be accommodated in the screening boxes without making short circuits. Figure 2.23 shows the second detector box in the dismantled state and the dummy of wood and perspex and figure 2.24 shows the box partly assembled. Similar figures for the monitor box are shown in figures 2.25 and 2.26.

Care was taken in handling the mumetal so as to cause as little work hardening, with consequent loss in permeability, as possible. The magnetic permeability of sample loops of mumetal, after bending round the dummy, was compared with that of unworked material on a crossed coil differential permeability bridge constructed for the purpose. It was shown that the permeability of the formed strips could be maintained at over 90% of its initial value with smooth bending.

2.10.1.3   The effect of screening the boxes

The interference has not been observed since making screening for the two boxes and re-arranging the cables. The magnetic fields produced by the coil mentioned earlier (section 2.10) was used to find the response of the output signal to external interference after screening. The coupled voltage signals decreased by at

Fig. 2.23   The second detector box in the dismantled state and the dummy
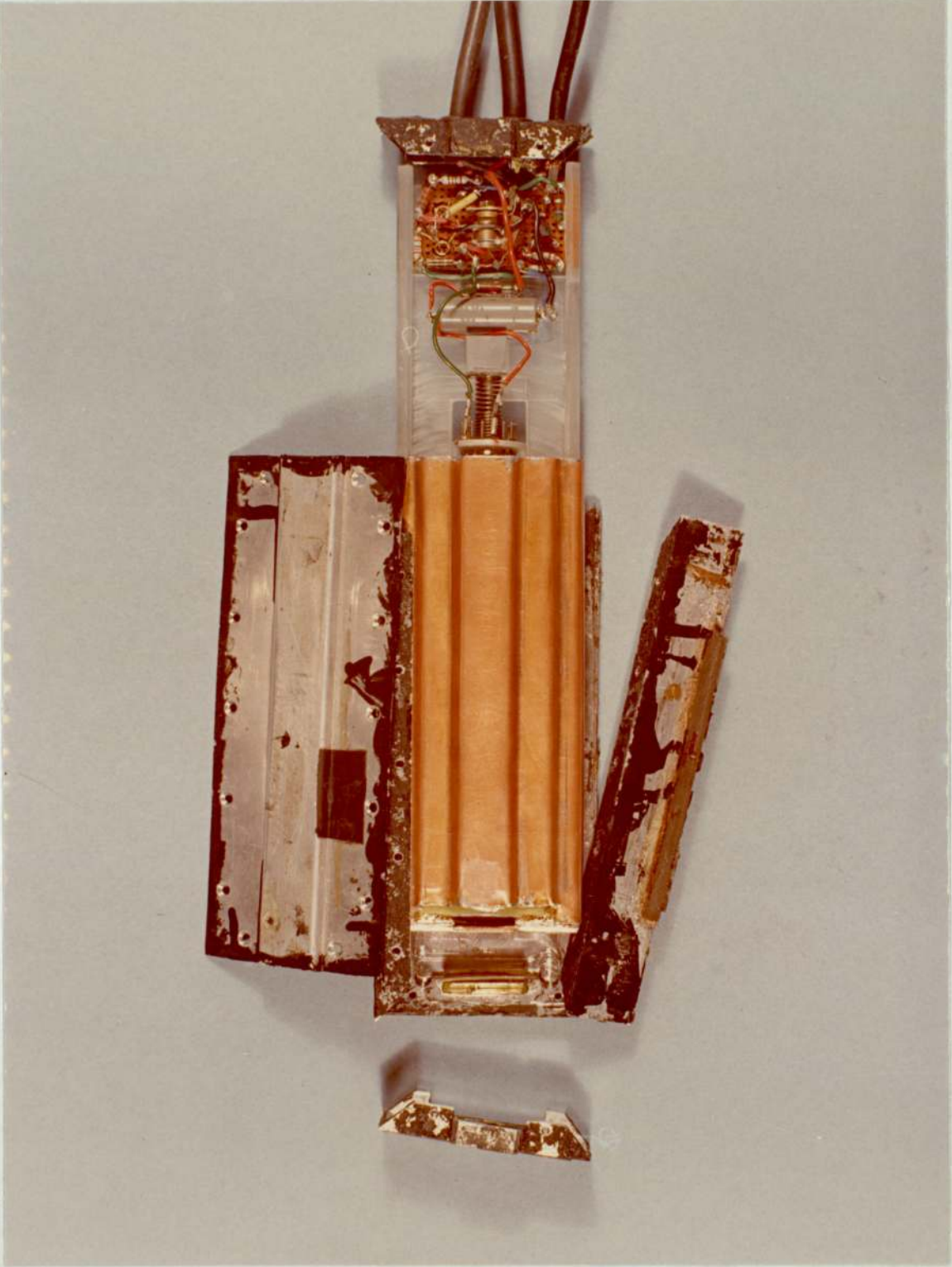
Fig. 2.24   The second detector box partly assembled
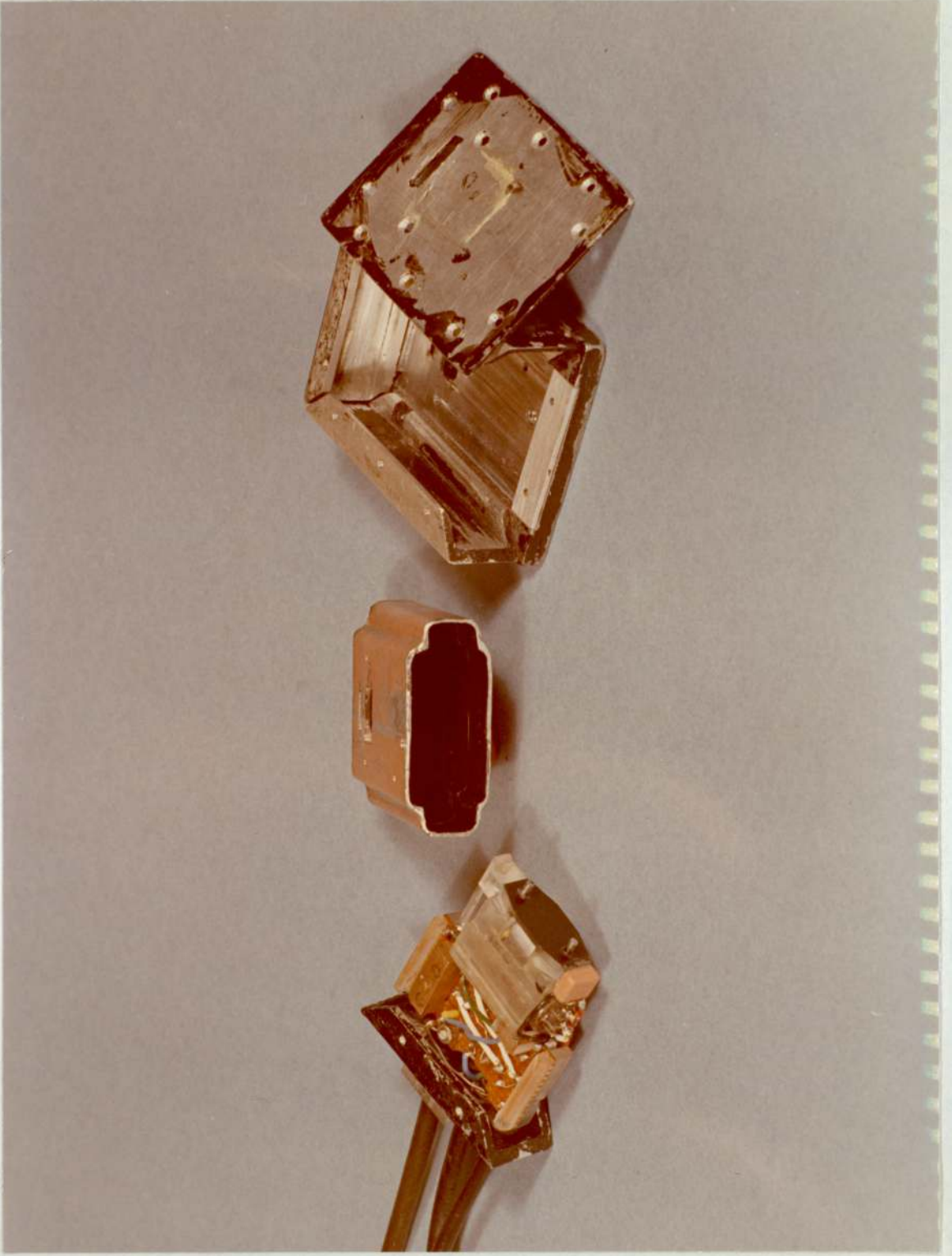
Fig. 2.25   The monitor detector box in the dismantled state
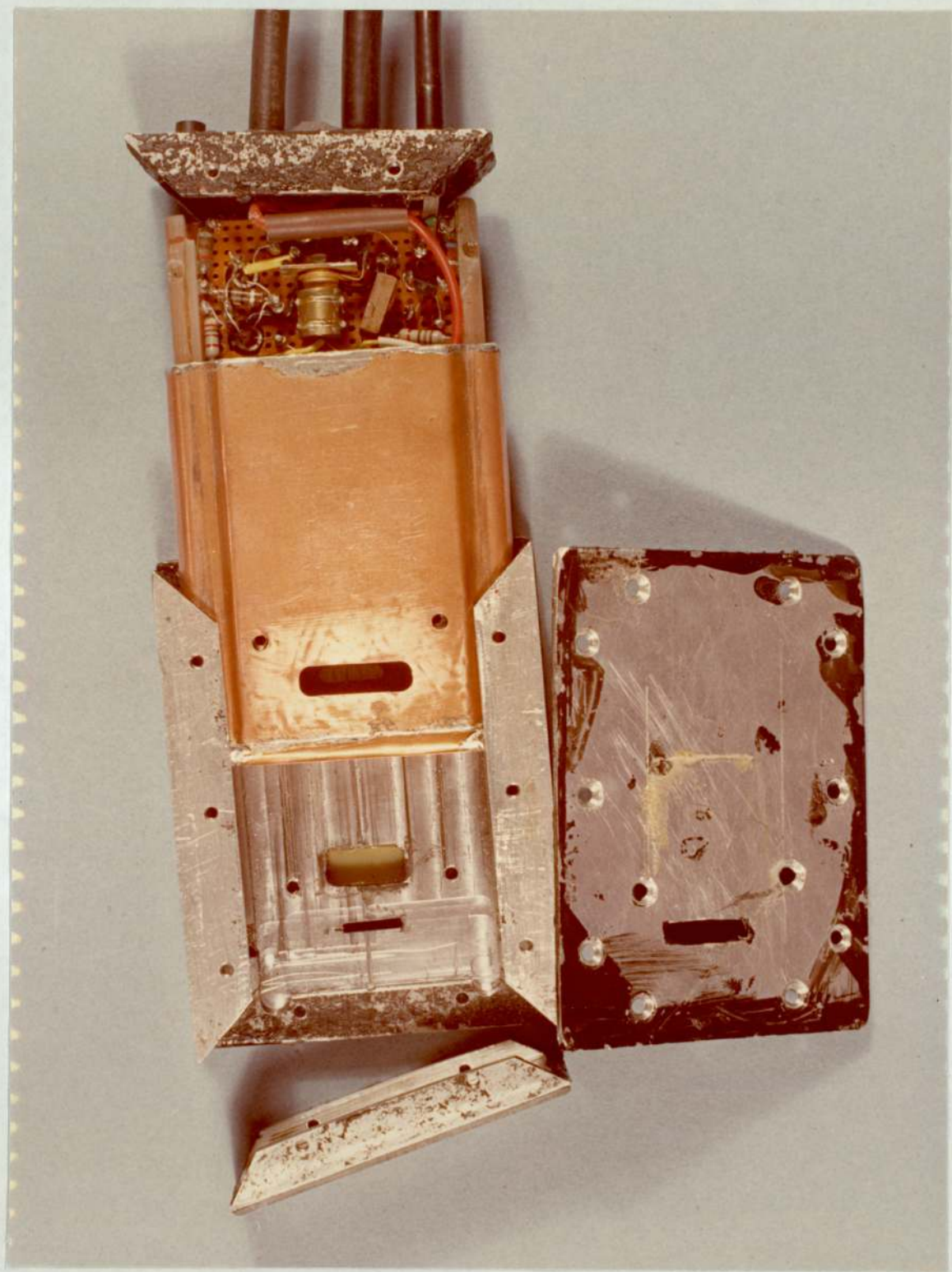
Fig. 2.26   The monitor detector box partly assembled

least 70 times when the coil was held above the second detector box.
Some of the interference must be coming through the unscreened part
of the equipment.

It was considered that the modification has proved satisfactory.

2.11   The new reference line

The reference voltage line is a horizontal line on the trace
which ensures the correct orientation when examining the photograph
negative and defines a d.c. voltage above the base line of the second
amplifier.   The reference line was set at about 16 volts and adjust-
ment of the line was provided by a potentiometer (Edwards, J, 1973).

In traces showing straight lines of signal voltages, representing
attenuations in uniform materials, it is apparent that these lines are
not parallel to the reference lines as shown in the typical step
wedge trace of figure 2.27.   The voltage line of the second amplifier
always showed a linear decrease in the scanning direction which appeared
to be independent of the signal value.

The declination, which is about 2 degrees (varies from $\sim 1.6^\circ$ to
$\sim 2.5^\circ$) could be due to a decrease in the signal reaching the second
amplifier, a d.c. drift in the machine or it could be due to variation
with time of the scale of the oscilloscope.   It was checked that the
declination is not due to a fault in the scale of the oscilloscope.
To check the possibility that the decrease in output signal is merely
due to an increase in filtration, caused for instance, by a tilt on
the depth fixer, several scans were taken of a stationary 'dural'
slab (fixed above the detector slit with the perspex bath removed).

.../

All the traces showed this declination which excluded the latter cause. The declination in output signal of the second amplifier could possibly be due to an unidentified d.c. shift in the machine.[69] Because of this, there was no advantage in using the reference line to ensure the orientation of the trace before solving the declination problem and therefore it was abandoned.

In a scan, the second amplifier records one signal spot, on the oscilloscope, every 0.01 seconds. The mean number of signal spots shown in traces of the step wedge between the end of the base line and the line representing the first scanned step number 11, as shown in figure 2.27, were counted and it was found equal to four. The total movement of the trolley during this time is 0.4 mm, which is represented by about twice this distance in the trace. So the top line of the first step scanned is advanced 1 mm in the x-axis from the end of the base line, before the wedge, (see fig. 2.27) and a line at right angles is drawn as an extension to the base line before the wedge, to be the new base and reference line.

A discrepancy of about 1% could occur in the transformed scan areas of patients' traces (section 4.3) because of the variation in the angle of declination.

2.12 The horizontal scale calibration

To obtain a scan of the ulna, the perspex bath for the limb is driven by a synchronous motor which is connected to a $\frac{15}{1}$ worm box so as to make $\frac{10}{3}$ revolutions each second. The worm box is connected to

Fig. 2.27   A trace of a step wedge showing a base line
            with the reference voltage line
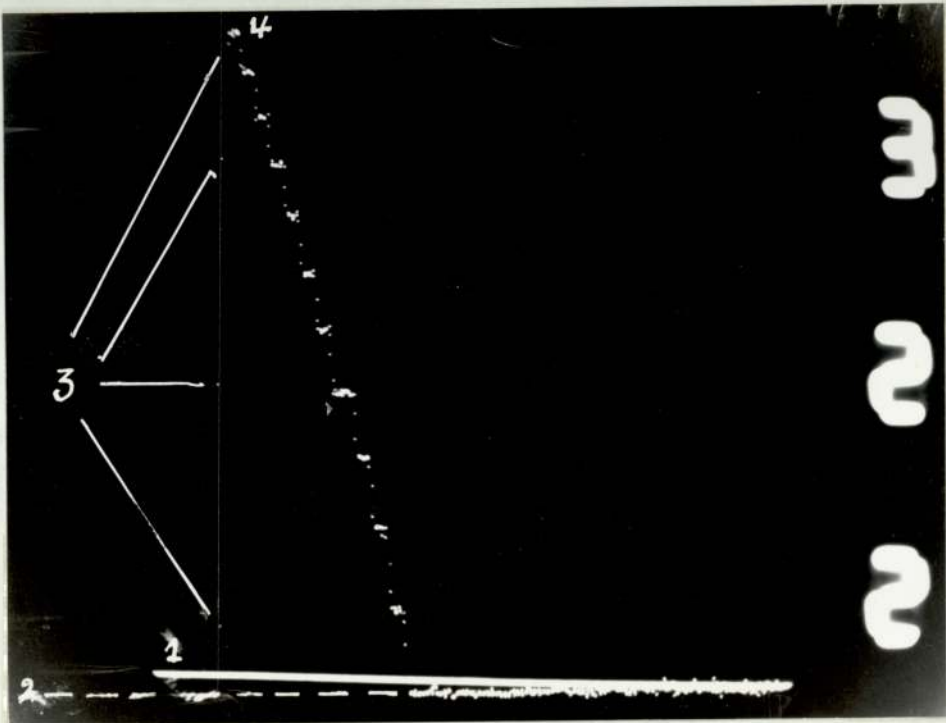
1   reference voltage line

2   new reference and base line

3   signal spots

4   line representing 1st step scanned

a driving shaft which has a square thread of 3 mm pitch making the speed of the trolley 10 mm/sec.

A potentiometer is used to record the horizontal movement of the bath on the oscilloscope. It was made of constantan wire 0.009 in (0.228 mm) diameter wound round a true perspex rod of 25.4 mm diameter and supplied from a stabilised power pack. The potentiometer is fixed underneath the water bath in the movement direction of the trolley. A rotating roller is fixed to the cross member of the travelling bath (with an insulated block) so as to move with the water bath and to make contact with the top of the potentiometer where the enamel is removed. The roller is connected to the oscilloscope.

The calibration of the oscilloscope can be done by measuring the voltage across the potentiometer and then setting the scale of the oscilloscope so that each 1 cm movement of the roller on the potentiometer is represented by 2 cm movement on the oscilloscope. To check the calibration of the scale, a dural slab exactly 24 mm wide was scanned and the width, in the trace, measured. It was checked that the measured width was within the expected resolution of 0.23 mm, i.e. 0.11 mm of actual width.

Table 2.1

The linear attenuation coefficients of uranium and tungsten at different energies

Element	Atomic No.	E_k keV	Density g/cm^3	μ cm^{-1}				
				60 keV	69 keV	70 keV	80 keV	85 keV
U	92	115.6	18.7	130	90	87.5	61	53.5
W	74	69.0	19.3	70	48	210.0	150	128.0

Table 2.2

'x*' values for a total thickness of 1 mm at different thickness combinations of U and W

Energy keV	Thickness mm				
	tu = 0.5 tw = 0.5	tu = 0.6 tw = 0.4	tu = 0.7 tw = 0.3	tu = 0.8 tw = 0.2	tu = 0.9 tw = 0.1
60	10.0	10.6	11.2	11.4	12.4
69	6.9	7.32	7.74	8.16	8.58
70	14.88	12.85	12.42	11.2	9.98
80	10.55	9.66	8.77	7.88	6.99
85	9.08	8.33	7.53	6.84	6.10

CHAPTER THREE

The Artificial Materials

68

3.1   The artificial bone

3.1.1   Introduction

The skeleton has great significance as an active organ with a
large metabolic turnover and ceaseless chemical and physiological
activity throughout life. Many disturbances are first reflected in
the skeleton.

Contrary to the belief of many clinical radiologists the
visual grading of the bone density has been shown by Kellgren and
Bier, 1956, and other investigators to be unreliable (Virtama P, 1957).

In the last three decades several radiographical methods have
been developed to show early in-vivo changes in the mineral content
of bones. The early methods used simultaneous pictures of a bone of
unknown mineral content with a material of known content for
comparison and this method is still used.

Various materials have been used to make the standard which is
usually in the form of a step wedge, a wedge or a tube. Among the
materials used are ivory (Stein I, 1937, Bywaters E, 1948, sections of
human or animal bones (Henry G, 1950), powdered bone (Sorenson, Witt
and Cameron, 1966), pure or alloyed aluminium (Engstorm and Wein,
1949, Richards A, 1953) copper and pure calcium salts.

Bone standards are also used in some bone densitometry
techniques using monochromatic sources and a detector. With these
systems, a bone standard is used not only for calibration purposes
but to help detect system errors like spectral changes in the source

.../

due to filtration or contamination, changes in the amplifier gain
of the analyser or errors in the count time (Witt and Cameron, 1969).

In bone densitometry using polychromatic X-rays from an X-ray
tube, a suitable bone standard is necessary to estimate bone mineral
content since to solve the transmission equations in this case one
needs to know the μ values of bone and soft tissue for the whole
energy spectrum together with photon intensities at these energies.
It is even more difficult to solve these equations in the Aston
technique due to the correction the scanning machine makes for
fluctuations in the mains supply (section 2.2).

It is also desirable to have some absolute reference standard
in order to calibrate and intercompare results from different
scanning systems and from different laboratories.

In neutron activation analysis the problem of choosing the
material for a calcium standard is simple. A known weight of calcium
salt is used as a standard in order to estimate bone calcium (Boddy,
Al-Hashimi and Boyle, 1968).

In the following sections, real and artificial bone materials
will be discussed in more detail.

3.1.2   Composition of bone

A bone is foremost a variety of connective tissues. Its
material could be divided into two main parts. The organic part
of a bone comprises over half of its weight and about two thirds of
its volume. It is composed of cells, the collagen fibres and the

.../

cement substance. Ninety five percent of the organic fraction is collagen (Fourman and Royer, 1968). Inorganic constituents are complex, the main constituent being a double salt of calcium phosphate and calcium carbonate (Virtama P, 1957). Calcium hydroxide is also reported present in bones (Jackson W, 1967). Apart from calcium phosphate and carbonate, a bone contains sodium, potassium, magnesium and sulphur in low percentages (Virtama P, 1957).

A bone is divided into two types - compact and cancellous or spongy. A cancellous bone exposes a large area to the body fluids and shares in metabolic exchange to a greater extent than a compact bone (Fourman and Royer, 1968). A cancellous bone is less mineralised than a compact bone (Progress in MS. of B.M.M. 1968).

Most bones are composed of two parts; the outside solid part, namely, the cortex and the inside which is the marrow.

A table of the compact bone elemental composition, published by the National Bureau of Standards, 1964, is shown in Table 3.3. The values given in the literature for the calcium content of various bones vary considerably. For example, D'An and Lax, 1949, give 14.5% for femur and 15.2% for ribs. Greygy, 1955, gives 11% for long bones and ribs (National Bureau of Standards, 1964).

The absorption of X-rays by a bone in the energy range 30 - 90 keV is mainly due to calcium, then oxygen, carbon and phosphorus, in that order. The fractional contribution of the different bone constituents to the mass absorption of bone is shown in Table 3.1.

Because of the variation in bone composition, bone standards are made mostly to represent the cortical part of the bone.

.../

3.1.3   Bone standards

There are a number of conditions which should be satisfied in making a bone standard. A bone standard should preferably have the same linear and mass attenuation coefficients as the compact bone in the energy range of interest (Witt and Cameron, 1968). This implies that the physical density and chemical composition are similar to that of the compact bone. The standard should be stable physically and chemically at room temperature, simple to produce from commercially available materials and easy to fabricate into phantoms. It should be able to withstand normal handling and shipment. Obviously, if the standard is to be immersed in a solution during usage, it should not contain any element or compound which dissolves in the solution.

The first standard used with the scanning machine was ivory in the shape of a step wedge. Ivory was chosen as an easily machinable material, having constituents nearly similar to that of the bone, but it was realised that ivory is not ideal as a calibration standard because it is slightly water absorbent and possesses a grain structure which can just be resolved by the apparatus (Archer-Hall et al, 1973). At the same time the composition of ivory is not exactly constant, and therefore it would be suitable only for serial tests.

Some investigators have used aluminium or aluminium alloys as standards because its atomic number (Z = 13) is close to the effective atomic number[1] of bone (Z = 12). Aluminium has other advantages; it is machinable and readily available. However, its density is

[1] Mayneord, 1937, gave a formula for the effective atomic number of a compound (Z) where the mass absorption of the compound is a linear function of Z for a given wavelength (Spiers, 1946)

substantially different from that of the bone ($P_{Al} = 2.7$ g/cm^3, $P_{bone} = (1.6 - 2.05)$ g/cm^3, Long C, 1961).

Other materials like bone and bone ash were used, but less often. Bone was mainly used in bone radiography and not in bone densitometry, where accurate mineral estimation is required, because of the difficulty of machining the desired shape and also due to the difficulty in knowing accurately the distribution of mineral in the bone section. Furthermore, if bone is used it should be kept and used in water solution so as to prevent dehydration. Bone ash alone cannot simulate a real bone except through mixing with other materials to substitute for the protein part. Sorenson, Witt and Cameron, 1966, have tried mixing bone ash with plastic in their efforts to make a bone standard and difficulty in obtaining homogeneous mixture was reported (Witt and Cameron, 1968).

In the standards mentioned the condition of similar chemical composition to that of the real bone is not satisfied except when using a bone.

The lack of a suitable bone standard showed the need for making a homogeneous calibration material whose elemental composition is similar to that of the compact bone and is precisely known. In this case, it will be possible to express the y-deflection of the signal in terms of milligrams of mineral per unit area (mostly calcium and phosphorus) for each X-ray scan instead of using an arbitrary scale of millimeters of ivory.

The following sections discuss the attempts carried out to make an artificial bone standard.

3.1.4   The earlier trials

Attempts were made to make an artificial bone by mixing known percentages by weight of insoluble powder together with a known percentage of araldite epoxy resin which is a powder at room temperature (section 3.1.5).   The powders were mixed in proportion so as to give percentages of each element equal to those of the real compact bone, especially the heavy ones.   All the powders were mixed thoroughly then compressed under 10 tons/in^2 pressure in a steel cylinder.   A thin sheet of polytetra fluoro ethylene 'P.T.F.E.' liner was fixed to the inside surface of the steel container in order to prevent the araldite sticking to the metal surface.   The compressed mixture was then heated in an oven, at approximately 130°C, to allow the araldite to melt and polymerise.   The polymerised araldite provided the binding for the mixture.

As a first simple homogeneity check to the artificial bone specimens, the scanning machine was used to scan a rectangular piece of uniform thickness from different faces (section 3.1.10).

All the specimens made by the first approach were inhomogeneous (see fig. 3.1).   It was recognised that the cause of the inhomogeneity was the settlement of heavy particles to the base of the container when the araldite melted leaving light particles on top.

Because of the failure to get homogeneous specimens by simply heating the compressed powder, it was argued that to overcome this problem, the mixture needed to be mixed during the melting of the araldite.

.../
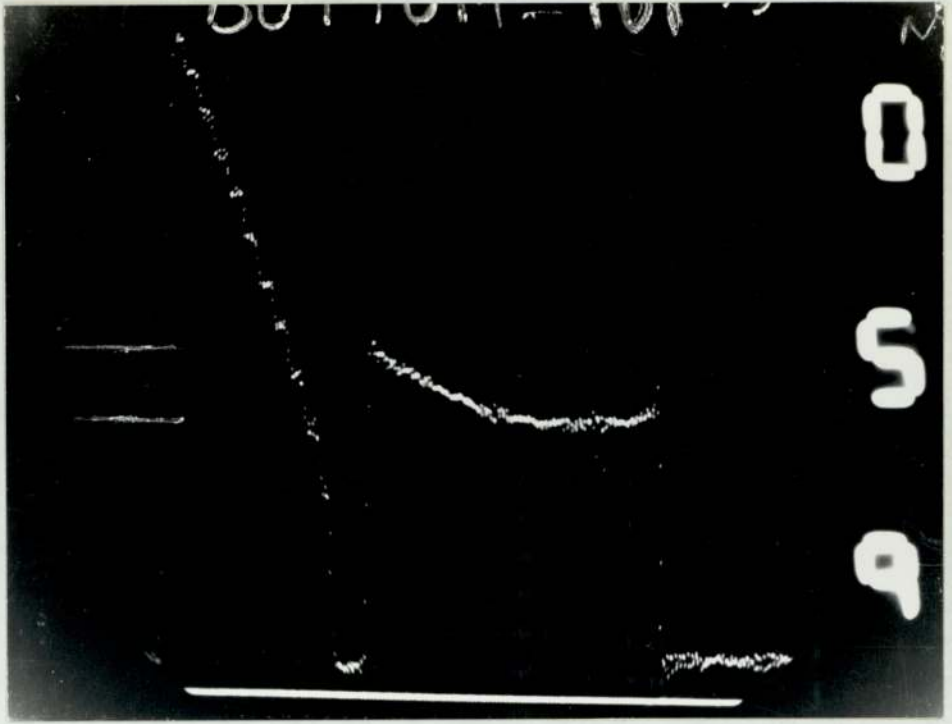
Fig. 3.1   A trace of a uniform thickness of artificial bone specimen
showing inhomogeneity

powder $m_2 = V\rho_2$

araldite $m_1 = V\rho_1$

$\rho_2 \simeq 3\rho_1$
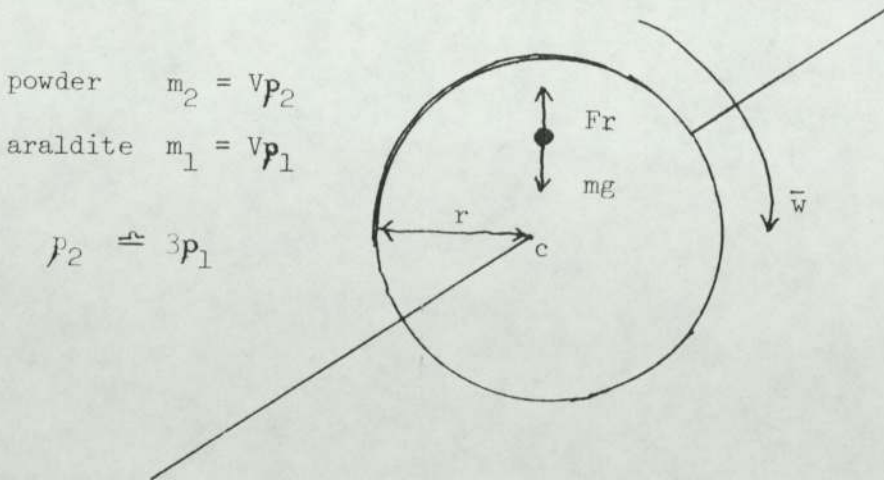
Fig. 3.2   A diagram showing the forces acting on a solid particle
in the molten resin (in the rotating cylinder)

Experiments were tried to heat the steel cylinder containing the powder using a flexible heater round the cylinder and to mix the powder when the araldite started melting (Tm_1 80 - 100°C). The mixing of the powder was performed using a stainless steel rod (3.8 mm diameter) which was connected to a variable speed motor. Mixing was stopped when the araldite started polymerising leaving the heater on to speed up the reaction.

It was observed that the specimens contained a large number of air bubbles and some powder did not get sufficient araldite to bind. Better mixing might solve the second problem. The air bubbles were believed to have been trapped during the mixing process.

Other experiments were tried to heat and mix powder under low pressure to overcome the air bubbles problem. A special apparatus was made to mix the powder in the vacuum chamber of a coating unit from outside using the rotating jig of the machine. A selection of gears was used to give the desired speed. The gears were fixed on a steel plate with the last gear connected to the mixer shaft. The mains supply to the coating unit filament was used to supply the flexible heater surrounding the powder container. When the pressure started dropping, a fair amount of the powder flew out from the container due to air in between the fine powder particles. Because the powder particles differ in density, lighter ones were more liable to fly out than heavy ones and hence the percentage composition could have changed.

A perspex lid with a hole in the middle (to allow for the mixture shaft to pass through) was used to prevent the powder from

flying out but powder still came out from the small gap allowed in the mixer hole when the pressure was decreased.

Attempts were made to heat and mix the powder till the araldite melted then the mixture was subjected to low pressure with continuous heating and mixing. A glass beaker was used instead of the steel cylinder to avoid the problem of keeping the P.T.F.E. liner in place during the mixing process. The glass beaker was put in a large copper beaker which was annealed to accommodate the glass beaker with good contact. An external metal beaker allowed safe fixing and uniform temperature outside the glass beaker. To increase the heat conductivity between the two beakers, a suitable fluid was used to fill the gap between them.

With all the modifications made, it appeared that it was not easy to overcome the problem of temperature gradient where the araldite near the glass wall started melting while the rest was not hot enough to melt. Accordingly, the araldite near the edge started polymerising earlier causing difficulty in mixing and resulting in an inhomogeneous specimen. The other problem faced was that which arose from the high viscosity of the araldite together with its small quantity. Accordingly, it was extremely difficult to get all the powder wetted with araldite.

Because of the unsuccessful experiments with powdered araldite (A.T.1) to make a suitable standard specimen, it was thought that using a liquid araldite might give more encouraging results. With liquid araldite there would not be a time limit on mixing since the polymerisation of the araldite would not start until the hardener was added. This might allow a chance of better mixing.

The first araldite found, having satisfactory properties, was araldite 778 with its hardener HY 951. The powder was first mixed with the araldite by adding small quantities at a time then stirring with a stainless steel rod which was connected to a variable speed motor. In this way, it was possible to get a satisfactory mixture of powder with araldite. A reaction was noticed of the hardener (HY 951) with the sulphur, where a gas was produced and the liquid hardener was observed to change colour.

In all experiments done with araldite MY 778 (with hardener HY 951)[1] and other liquid araldites like AY 105 (with hardener HY 951) the problem of inhomogeneity was still present. This was because in these araldites the polymerisation reaction is fairly slow ($\sim$ 20 minutes) which allowed some of the heavy particles to settle to the bottom of the container after the mixing stopped.

After the unsuccessful trials with a number of different liquid araldites, powder araldite A.T.1 was considered again with new ideas to solve the problem of inhomogeneity. The first idea was to decrese the quantity of the araldite and to substitute this decrease by another suitable powder to make up the right element percentages. By so doing, the amount of molten material would be less which in turn would restrict the movement of the powder particles.

The specimens made with 20% less araldite were brittle so it was not possible to machine them. The brittleness was due to insufficient araldite to stick the powder firmly together.

---

[1] A new mixture of the constituent powders was made without the addition of sulphur in order to prevent the reaction of the latter with the hardener (HY 951).

The other idea which was tried to overcome the gravitational force was to rotate the specimen while it was heated in the oven. Using this technique, it was possible to make homogeneous and machinable artificial bone specimens having an elemental composition similar to that of the real compact bone.

3.1.5   The artificial bone materials

Table 3.2 shows the important properties of the materials used to make the artificial bone standard. The most important points which should be considered in choosing the substances for making a bone standard are water solubility, reaction with other constituents and melting temperature.

Each material should be insoluble or have negligible solubility in warm or cold water since the bone standard will be used while immersed in water (section 2.2). The other requirement is that the constituent should not react with any of the other constituents because this produces different compounds which may have unsatisfactory properties. The composition may also change if a gas is produced in the reaction.

It is preferable that the constituents have melting temperatures higher than the curing temperature of the araldite. If a constituent has a melting temperature less than the araldite's curing temperature then it will melt when the compressed mixture is heated and thus increase the liquid percentage in the heated specimen. This will, presumably, make it more difficult to prevent heavy particles from settling.

All the selected constituents satisfied these conditions except sulphur which has a melting point of 112.8°C. (The araldite A.T.1 was polymerised at approximately 130°C). The sulphur was not, in fact, added in preparing the later artificial bone specimens because a powder mixture (free from sulphur) was already available. The sulphur percentage in a bone is very small (see Table 3.3) and its fractional contribution to the mass attenuation of the bone is less than 0.5%, (see Table 3.1). Moreover, the sulphur can be added to the mixture without difficulty although giving the specimen a brownish colour instead of ivory white.

Table 3.3 shows the elemental composition of real compact bone (National Bureau of Standards, 1964). The artificial bone constituents were calculated to approximate to these percentages. The calcium and phosphorus ratios were found from the two compounds; calcium orthophosphate and calcium hydroxide. The right percentages of nitrogen and carbon came from the melamine and araldite. The elemental compositions of melamine and araldite A.T.1 are shown in Table 3.4. Magnesium oxide was used instead of magnesium and a fine powder of sulphur could have been used.

Table 3.5 shows the composition by weight of artificial bone specimens which have been prepared. Specimens of slightly different compositions could be made by this method to represent different bones.

Oxygen and hydrogen are the two elements where accurate percentages have not been achieved. The percentages deficiency of hydrogen and oxygen in the specimens made are 3% and 12.85%

respectively with a corresponding increase in the percentages of the other compounds by a factor of about 1.31% (Table 3.5).

3.1.6 The development of the technique

In this section, a brief account is given of the development of the method adopted to make the artificial bone standard.

For better mixing of the different powders and the araldite, a mixer was used which was provided with three different speeds and an adjustable angle of rotation. A large amount of the powders (total weight about 350 g to make a number of specimens) were mixed together for about thirty minutes using the different mixer speeds and angles of rotation.

A small amount of the mixed powder (approximately 40 g) was used in each experiment to make one specimen. It was put in a steel tube. The tube was of 4.15 cm diameter inside and had P.T.F.E. liner made from solid rod by drilling a hole in it of diameter 3.8 cm. The outside diameter of the P.T.F.E. was made to be a tight fit inside the steel tube and was pushed into it. Two duraluminium ('dural') cylindrical discs 3.8 cm in diameter were used in compressing the powder in the tube. Circular sheets of P.T.F.E. were stuck to the surfaces of the discs in contact with the powder. The P.T.F.E. prevented the araldite from sticking to the inside surfaces of the steel tube and the dural discs in order to be able to use them again, since it is not easy to remove the araldite once it stuck to the metal surface.

.../

Powder compression was performed with an L-30 press. Ten tons per square inch was found to be the highest suitable pressure. Higher pressure caused the specimen to crack after releasing the pressure.

Homogeneity checks on the specimen, after compression (section 3. 1.10) proved that it was not homogeneous and therefore hand mixing was tried after using the automatic mixer. Hand mixing and grinding was done using a pestle and mortar. It was done little by little first, then the whole quantity was mixed together. The time taken for this mixing was nearly fifteen minutes. Specimen homogeneity examinations were carried out after compression. The result was positive leading to the conclusion that hand mixing and grinding was necessary to get homogeneous mixtures.

In order to get a solid machinable specimen, the compressed powder was heated in an oven at approximately 130°C (after it had been taken from the container) for a few hours (6 - 7) to let the araldite polymerise. It was observed that the specimens split partially after heating. Compression during heating might prevent specimens from cracking by obstructing free expansion. A G-clamp was used for this purpose. It prevented the specimen from cracking in the middle but there were some cracks near the edges. This indicated that the specimen needed to be compressed all round during the heating process to prevent the occurrence of cracks.

To solve the problem the specimen was left in the tube (after the compression) and was compressed, as before, using a G-clamp on the ends of the dural discs. All the specimens made by this method were free from cracks but they were not homogeneous because of

.../

settlement of the heavy particles. The simplest way to overcome
this difficulty was to try rotating the specimen in the oven. The
rotation speed whereby a homogeneous specimen could be obtained
was roughly estimated (section 3.1.7). This speed was about 1.7
rev/min.

A simple frame was made to rotate the specimen in the oven
from outside by drilling a hole in the door of the oven and passing
a shaft through it (section 3.1.8).

A set of springs were used to keep the specimen compressed
during the baking process instead of the G-clamp. The compression
of the specimen during the heating process served two purposes;
first it restricted the movement of the powder particles in the
molten resin and second it increased the density of the specimen
by squeezing the molten resin in between the particles of the solid
powder (section 3.1.8).

3.1.7   The speed calculation

The rotation speed whereby homogeneous specimens would be
obtained was roughly estimated. This estimation of the speed helped
to limit the range of speed which needed to be tried to make a
homogeneous specimen. Accurate speed calculations were difficult to
obtain as they must be based on many approximations.

For simplicity, it was assumed that the powder mixture was
composed of two powders only: the araldite which melts during the
baking process and the calcium orthophosphate $\left[Ca_3(PO_4)_2 \right]$ which

remains unaffected under the baking temperature. Together these two powders constitute about 90% of the total weight of the mixture (see Table 3.2). The density of calcium orthophosphate is about three times that of the araldite.

For reasons of simplicity, the forces acting on the small spherical solid particles of $Ca_3(PO_4)_2$ ('particle') in the molten araldite was calculated. The forces affecting the particle when the specimen is rotating in the oven are the gravitational, the friction and the centrifugal forces. For low rotation speeds the centrifugal force can be ignored. To work out the maximum speed for which the centrifugal force can be neglected, consider the centrifugal force as being less than the gravity force by a factor of 10^4

$$m_2 \bar{w}^2 r \ = \ \frac{(m_2 - m_1)}{10^4} g \qquad\qquad 3.1$$

Where m_2 is the mass of the powder particle in grams

r is the radius of the specimen ($\backsimeq$ 0.02 m)
m_1 is the mass of an equivalent size of araldite in grammes
g is the gravitational force per unit mass, which

is equal to 9.81 m/sec^2 ($\backsimeq$ 10 m/sec^2)

and mg (where $m = m_2 - m_1$) is the net gravitational

force working on the powder particle.

$$m_2 \ = \ P_2 V \ = \ \frac{4}{3} \pi a^3 P_2 \qquad\qquad 3.2$$

Where P_2 is the density of the particle

V is the volume of the particle

and a is the diameter of the particle (and its equivalent

size of araldite, assumed to be 10^{-4} metres).

.../

$$m_1 = P_1 V = \frac{4}{3} \pi a^3 P_1 \qquad 3.3$$

Where P_1 is the density of the araldite.

From equations 3.1, 3.2 and 3.3

$$\bar{w}^2 = \frac{P_2 - P_1}{P_2} \cdot \frac{g}{r \times 10^4} \qquad 3.4$$

Therefore

$$\bar{w}^2 \simeq \frac{1}{30}$$

or $\quad \bar{f} \simeq \dfrac{1}{34}$ rev/sec $= 1.76$ rev/min $\quad 3.5$

Hence for speed rates of about 1.76 rev/min and below, the centrifugal force can be ignored. The two forces left are the gravitational and the friction. The friction force always acts in the direction opposite to the particles' motion. Because the specimen is rotating in the oven, the gravitational force on the particle is changing in direction accordingly.

To calculate, roughly, the possible movement of the particles in the predetermined rotation speed, the equation for motion under rotation vector was applied.

$$m_2 \frac{d^2 \bar{S}}{dt^2} + K^* \frac{d\bar{S}}{dt} = mge^{j\bar{w}t} \qquad 3.6$$

Where $e^{j\bar{w}t}$ represents the variation in the forces' direction,

$\bar{S}$ is the total displacement of the solid particle from the occupied position, before the melting of the araldite,

$\frac{d\bar{S}}{dt}$ is the movement velocity (m/s) of the solid particle in the molten araldite,

...../

$K^* \frac{d\bar{S}}{dt}$ is the friction force on the solid particles

and K^* is the viscosity constant.

Assumed $K^* = 6 \pi \eta a$ 3.7

Where η is the viscosity in $N s m^{-2}$

$\eta \simeq 0.001 \, N s m^{-2}$ (assumed to be the lowest value

of the viscosity of the molten araldite which is equal

to that of water at $20^{\circ}C$)

$P_2 \simeq 3,000 \, Kg/m^3$

$P_1 \simeq 1,000 \, Kg/m^3$

By substituting for the value of K^*, m_2, m and g in equation 3.6

$$3 \times \frac{4}{3} \pi a^3 \frac{d^2\bar{S}}{dt^2} + 6 \pi a \times 10^{-3} \frac{d\bar{S}}{dt} = 2 \times \frac{4}{3} \pi a^3 \times 10 \, e^{j\bar{w}t}$$

or $\quad \frac{d^2\bar{S}}{dt^2} + \frac{3}{2} 10^5 \frac{ds}{dt} = \frac{20}{3} e^{j\bar{w}t}$ 3.8

$$\bar{S} = \frac{\frac{20}{3} e^{j\bar{w}t}}{\bar{w}^2 + \frac{3}{2} 10^5 \bar{w}}$$ 3.9

$$|\bar{S}| = \frac{\frac{20}{3}}{\bar{w} \sqrt{\bar{w}^2 + (\frac{3}{2} \times 10^5)^2}}$$ 3.10

Clearly, if $\bar{w}$ is approximately $\frac{1}{5.5}$ radian/sec, then

$$\bar{w}^2 \ll (\frac{3}{2} \times 10^5)^2$$

Therefore, the motion is viscosity dependent.

$$\bar{S} = \frac{\frac{20}{3} \times 5.5}{\frac{3}{2} \times 10^5}$$

Hence $\quad \bar{S} = 0.24 \times 10^{-3} \, m$

$\bar{S} = 0.24$ mm maximum particle displacement.

These calculations show that the speed value is not so
critical and that the expected solid particle movement in the molten
araldite, in the vicinity of the speed of 1.76 rev/min is negligible.
The viscosity of the araldite in all probability will never be as
low as the assumed figure (η = 0.001 N s m^{-2}).

3.1.8   The rotation frame

A simple frame was made for rotating the compressed specimen
horizontally in the oven using a steel hand angle.   The frame
consisted of a disc as a base and two vertical plates fixed to it
with screws (fig. 3.3).   In each plate there was a hole made for
accommodating the rotation shaft.

The artificial bone specimen was compressed in a steel tube
between two square dural plates (1.3 cm thick and 8.9 cm long) with
six strong springs.   Three holes were made in the ends of the two
plates at equal distances from each other, to allow threaded rods
to pass through.   The three threaded rods with the six springs acted
as a compressor to the specimen.   The compression is affected by
screwing the springs from outside the square plates.

Two circular grooves in the internal sides of the square
plates were made in order to get good hold of each of the two
cylindrical dural blocks.   These two blocks were made to fit
tightly (3.8 cm diameter) to the P.T.F.E. tube which in turn was
fitted tightly to the steel container.   The powder was compressed
in the tube by the two blocks.

.../

Fig. 3.3 A diagram of the artificial bone rotation frame

rotation shaft

dural block

the steel tube

dural plates

spring

base
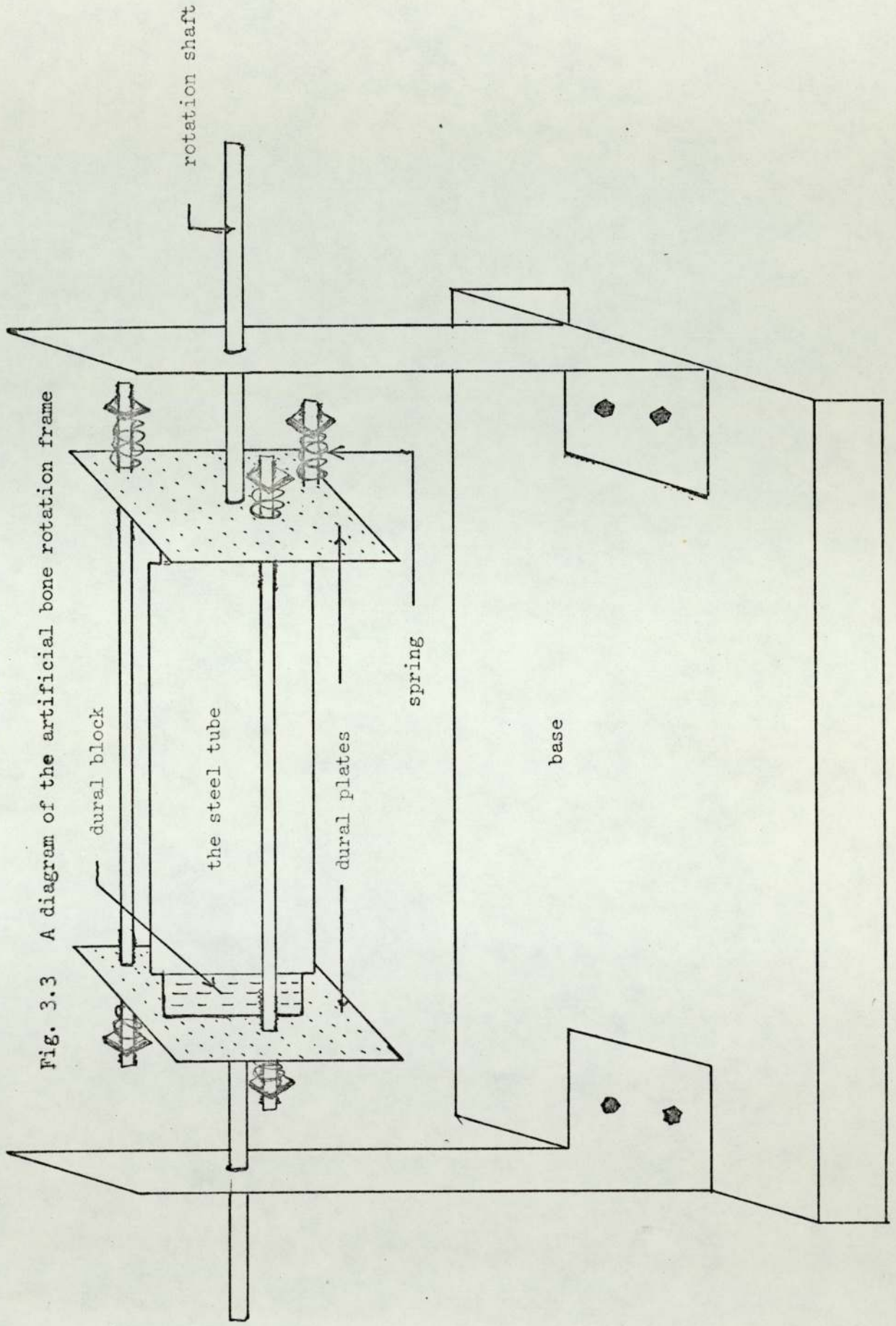
Two steel rods of different lengths, each secured to the middle of one of the square plates from the outside, served as shafts for rotating the tube containing the specimen. The longer rod was made to pass through a specially made hole in the door of the oven to a motor outside. A rubber tube was used in connecting the rod to the motor shaft. The motor was erected vertically on a wooden base with the aid of a separate frame. The motor speed was 300 rev/sec. In order to decrease the speed to the desired rate (1.76 rev/min) a gear box of ratio $\frac{1}{100}$ was connected to it and the motor was supplied from a variac for further reduction of the speed.

Two sets of springs each comprising six identical springs were tried in compressing the specimen during the baking process. Springs of the first set each had a force constant (i.e. $K = \frac{\bar{F}}{X}$) of approximately 160 lb/in^2 and 0.4 in maximum displacement (fig. 3.4). The density of the specimen produced using these springs was 1.63 g/cm^3.

Each spring of the second set had a greater force constant of approximately 435 lb/in^2 and 0.5 in maximum displacement. The second (stronger) springs were applied to try to increase the density of the specimen. An increase of about 7% (from 1.63 g/cm^3 to $\sim$ 1.74 g/cm^3) was achieved. This increase in density is small in comparison with the greater difference between the strengths of the two set springs ($\frac{K_2}{K_1} = 2.72$) used in the two cases. Therefore, it was concluded that even stronger springs were unlikely to cause much further increase in density of the artificial bone specimens.

.../

FIGURE (3-4)

THE RELATIONS OF SPRINGS DISPLACEMENT
TO COMPRESSION FORCES

SPRING 1

K1=159.6 POUNDS/INCH

SPRING 2

K2=434.8 POUNDS/INCH

DISPLACEMENT
X(INCHES)

LOAD F(POUNDS)
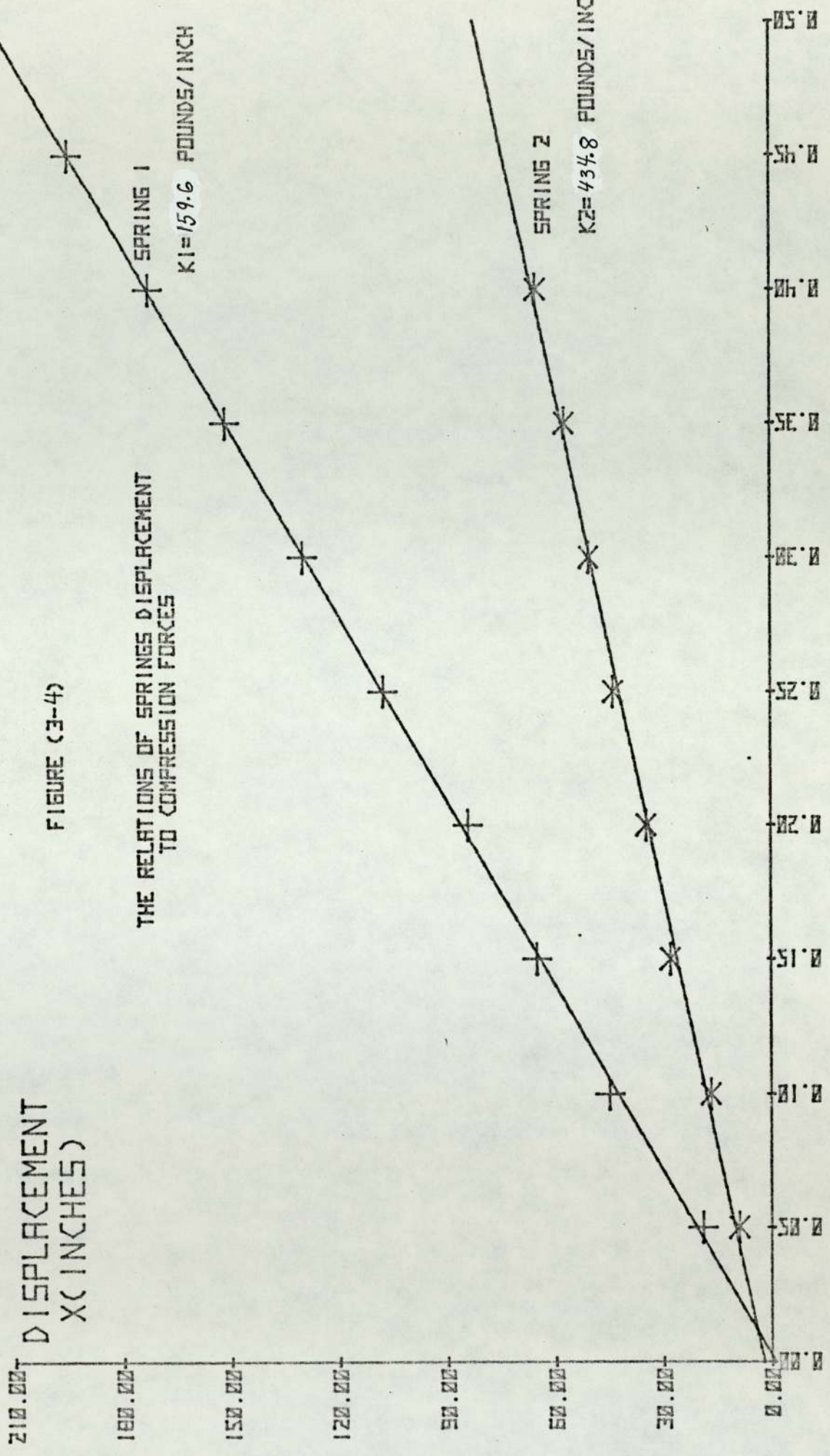
Enough displacement in the springs (0.4 - 0.5 in) was available in order to absorb the specimen shrinkage when the resin melted.

3.1.9   The procedure

The procedure to make artificial bone specimens can be summarised as follows.

1)   Weigh the required quantity of each constituent then mix them together first with an automatic mixer.

2)   Do hand mixing and grinding using a pestle and mortar.

3)   Compress under 10 tons/in^2 pressure in the steel tube.

4)   Fix the tube, containing the powder, in the rotation frame and, insert them in the oven. Begin heating to approximately 130°C and start the rotation (1.76 rev/min) for six to seven hours.

5)   Leave the specimen in the container to cool then remove it from the tube by pushing it down slowly using, for example, a fly press.

6)   Smooth top and bottom surfaces of the specimen then machine to the required shapes.

3.1.10 The properties of the specimen

The composition of the artificial bone ('AB') specimen is shown in Table 3.5. This composition nearly represents a 'dehydrated' bone.

The dimensions of the artificial bone specimens made were 3.8 cm diameter and approximately 2 cm long. The specimen is stable physically and chemically, machinable and does not absorb water. Table 3.7 shows the densities of three artificial bone specimens. The maximum percentage difference in densities is 0.4%.

Two simple homogeneity tests were carried out on the specimens; the first was density measurements. Each specimen was cut into two pieces or more and the density of each piece was measured. Table 3.8 shows the densities of specimen number 2 (Table 3.7) and five cut pieces from it (each was about 2.5 cm^3). The maximum difference in densities is only 0.5%. The slight increase in density of the five pieces compared to the density of the whole specimen is probably due to the presence of more araldite near the edges of the specimen which were not included in the pieces. A value of 1.735 g/cm^3 was taken as the mean density of the AB pieces.

The second homogeneity test done was to scan (using the scanning machine) uniform thicknesses of AB pieces from different faces to check for any differences in X-ray attenuation throughout the pieces and to compare the attenuation at the different thicknesses. Figures 3.5 and 3.6 show scans of an AB piece and an AB tube together with the AB step wedge.
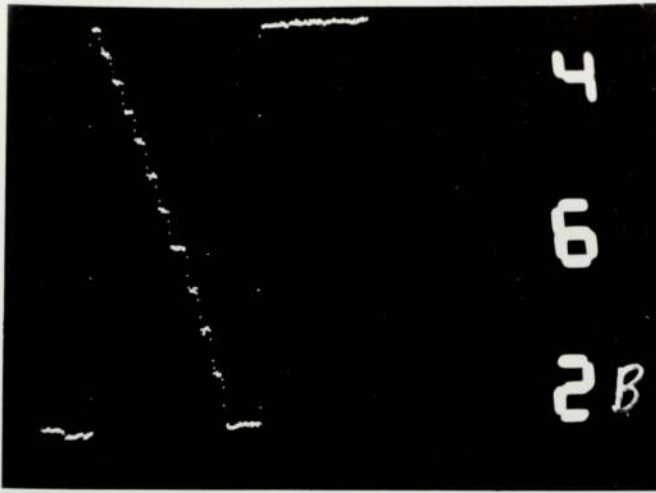
Fig. 3.5   A trace of an artificial bone slab
            (13.19 mm thick) and step wedge
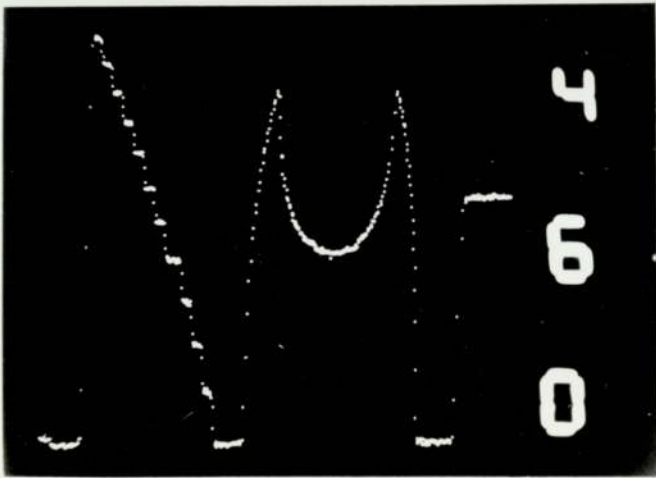
Fig. 3.6   A trace of an artificial bone tube
            (r_1 = 5 mm, r_2 = 7.5 mm) and
            step wedge
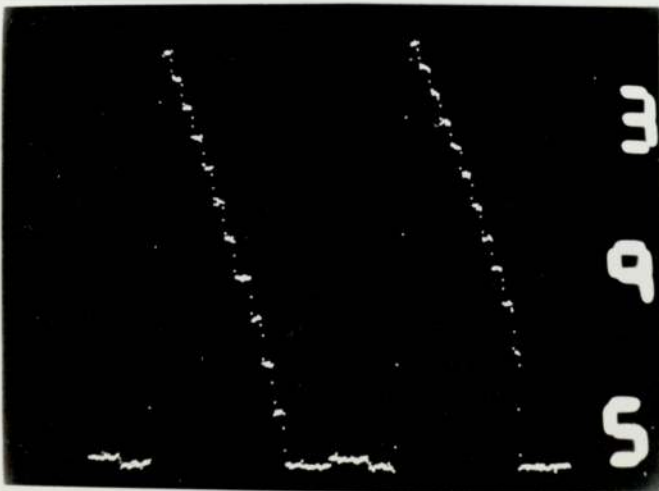
Fig. 3.7   A trace of the artificial bone and the
            ivory step wedges

In order to test more accurately the homogeneity of the latest artificial bone specimens, an attenuation technique was used by comparing the attenuations of well collimated monochromatic photons at different places of a uniform thickness thin AB slab. A slab of 1.02 mm thick was accurately machined and a 22 keV photon source was used. The measured standard deviation of the number of absorbed photons is 1.74% (26 counts in 1502) compared with 5.79% (87 counts) which would be expected from statistics alone. The contribution to the standard deviation from inhomogeneity must, therefore, be very small.

The diameter of the slits used above and below the AB slab was 1.25 mm, so the volume involved in a point measurement is:

$$\pi \left[\frac{1.25}{2} \right]^2 x \quad 1.02 \quad = \quad 1.25 \text{ mm}^3 \qquad 3.11$$

In scanning measurement, the minimum volume of AB involved in a point measurement is

$$9.5 \quad x \quad 0.25 \quad x \quad 1.2 \quad = \quad 2.85 \text{ mm}^3 \qquad 3.12$$

From the above two calculations (equations 3.11 and 3.12), it is clear that the volume of AB involved in a point measurement of the monochromatic source is better than that required in the scanning machine. Measurements of the transmitted photons through narrower slits can be done withastronger source to minimise count statistical error.

3.1.11 The artificial bone step wedge

To provide an absorption calibration of the X-rays which may be easily compared with the ulna traces, two ivory step wedges were

used, one to go with the right frame and the other with the left (Edwards J, 1973).

After successful attempts at making a suitable standard artificial bone specimen , a new step wedge was made to replace the two ivory wedges. The artificial bone standard has a density of 1.735 g/cm^3, which is slightly higher than that of ivory (about 1.69 g/cm^3).

The step wedge has a total width of 19 mm and eleven equal steps. The steps were accurately cut so that each step was 1.2 mm high and 1 mm wide, except for the fourth step which was made 1.5 mm to act as a quick reference to the trace height (see fig. 3.7). The step wedge length was 11. 5 mm with a maximum height of 13.2 mm (fig. 3.8).

A step height of 1.2 mm was chosen in order to have 0.4 mg calcium in each 1 millimeter square column (1.2 mm^3 x 1.735 x 10^{-3}g/mm^3 x 0.192). The step wedge was cemented into a cut made in a strip of 3.2 mm thick perspex which is shown in figure 3.9. Four smaller strips were cemented on to the large strip (each pair to one side of the step wedge) so that the step wedge could be positioned accurately in the scanning bath by slotting one of the two pairs (depending upon whether it is the right or left frame) around the ulnar styloid block. Perpendicularity of the steps to the direction of travel is ensured by pushing the step wedge until its supporting perspex strip butts against the central edge of the hand fixing frame with the low height steps nearer the ulna.

.../

Fig. 3.8   A diagram of the artificial bone step wedge

scale 1 : 10
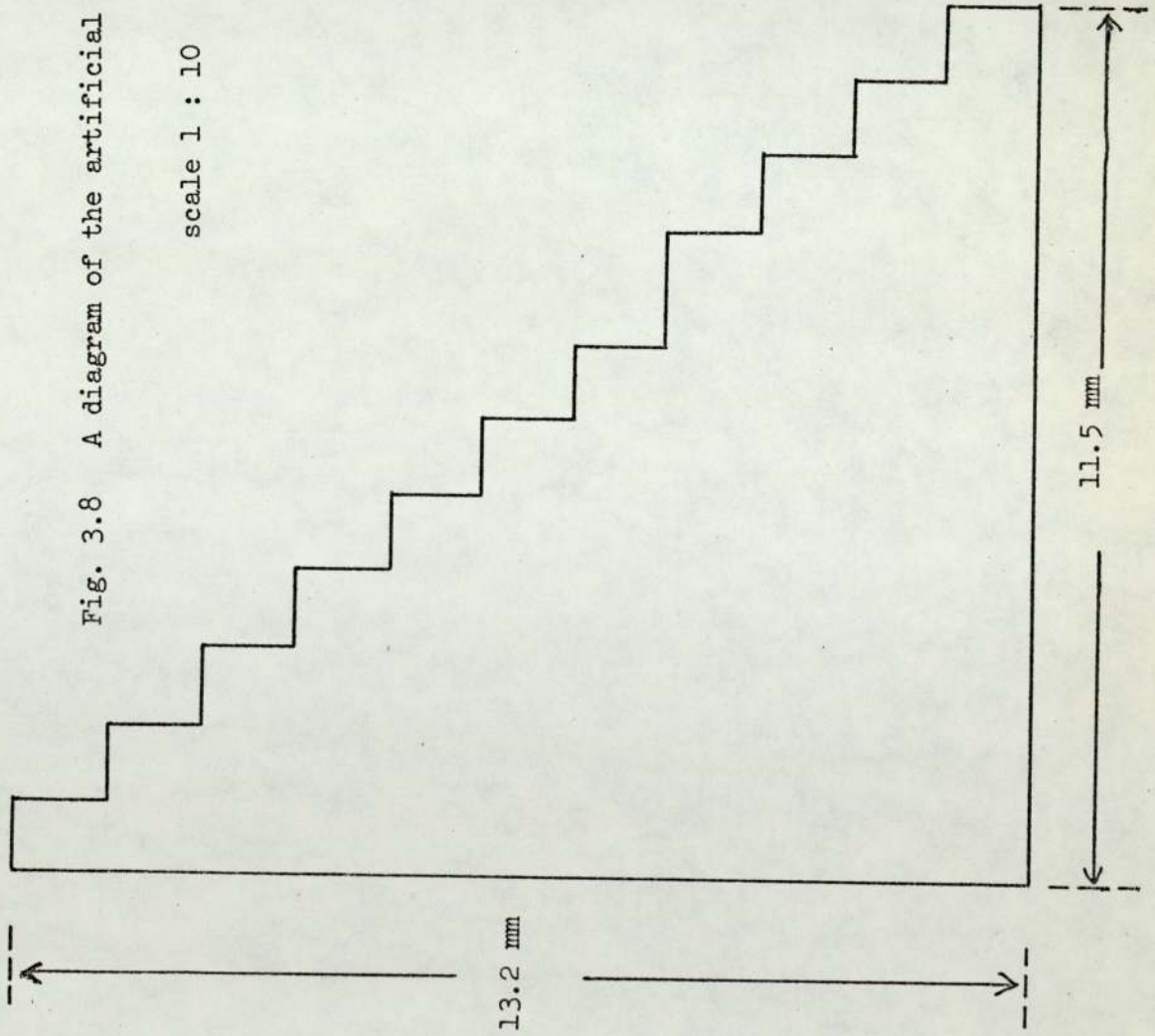
width 19.0 mm
step height 1.2 mm
= 0.4 mgm calcium
in 1 mm square column
per step

11.5 mm

13.2 mm
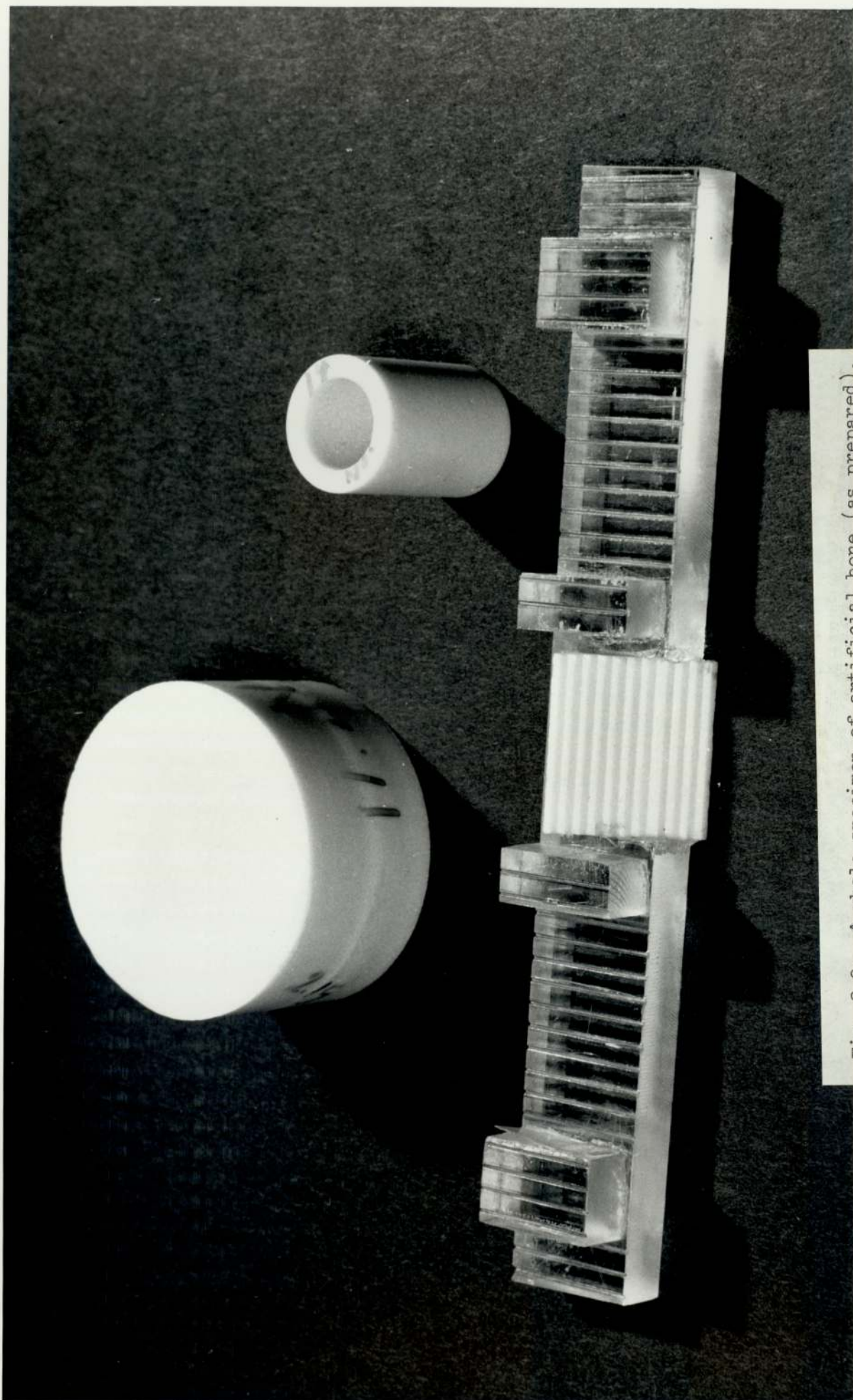
Fig. 3.9 A whole specimen of artificial bone (as prepared), a step wedge and tube machined from this material

3.1.12   The attenuation coefficients of the artificial bone specimen

The mass attenuation coefficients ($M_m = \dfrac{M_1}{P}$) of the AB specimen were calculated, at different energies, by working out the contribution of each constituent to the M_m values, then adding them together (Table 3.9) according to the following equation.

$$M_m = \sum W_i \ M_{mi} \quad \text{in } cm^2/g \qquad\qquad 3.13$$

Where W_i is the weight percentage of the i th element of the AB

and M_{mi} is the mass attenuation coefficient of the i th element.

The M_m values were also measured experimentally at different energies and the results are shown in Table 3.9.

The discrepancy between the calculated and the measured M_m values are apparent (Table 3.9). In consulting the manufacturer of the $Ca_3 (PO_4)_2$ they said that a mean of 6% per weight calcium deficiency in the compound is likely (and a 10% maximum calcium deficiency). A chemical analysis of what is supposed to be $Ca_3(PO_4)_2$ showed 5% calcium deficiency and the accuracy of the analysis was within $\pm$ 5%.

The M_m values of AB specimen with 5% and 10% calcium reduction and equivalent increase in the rest of the constituents, are shown in Table 3.10. The M_m values for the 10% Ca deficiency give best fit with the measured values, within the accuracy of the measured values and the accuracy of the calculated values (Hubell J, 1969).

.../

3.1.13 Comparison with bone standards

Comparison of the attenuation coefficients of bone standards and bone (Hubble J, 1969) is discussed in this section.

Witt and Cameron, 1969, used a saturated solution of di-potassium hydrogen phosphate (1.6 K_2HPO_4 : 1 water) as a bone standard by enclosing it in leak-proof tubes. The density of the solution is 1.72 g/cm^3.

The mass attenuation coefficients of bone, artificial bone (10% Ca deficiency), aluminium and K_2HPO_4 solution are tabulated in Table 3.11 and are shown in figure 3.10. The M_m values of artificial bone are higher than that of bone at low energies (11% at 30 keV) and the differences decrease with increase in energy, matching at 80 and 100 keV. Higher differences are shown between M_m values of bone and each of aluminium and K_2HPO_4 solution.

The linear attenuation coefficients of the standards and bone are shown in figure 3.11. A value of 1.85 g/cm^3 was used as the mean density for healthy young cortical bone (Atkinson, Weatherell and Weidmann, 1962). The aluminium M_1 values differ significantly from that of bone due to its high density (p = 2.7 g/cm^3). The M_1 values of the artificial bone are slightly higher than that of the real compact bone at low energies and decrease more rapidly with increase in energy than the bone M_1 values. K_2HPO_4 solution shows higher M_1 values at all energies.

Fig. 3.10   Mass attenuation coefficients of

- Bone

× Artificial bone (10% Ca deficiency)

○ Aluminium

and ▫ K_2HPO_4 solution

M_m cm^2/g

Energy   keV

Fig. 3.11 Linear attenuation coefficients of

• Bone

× Artificial bone

o Aluminium

and □ K_2HPO_4 solution
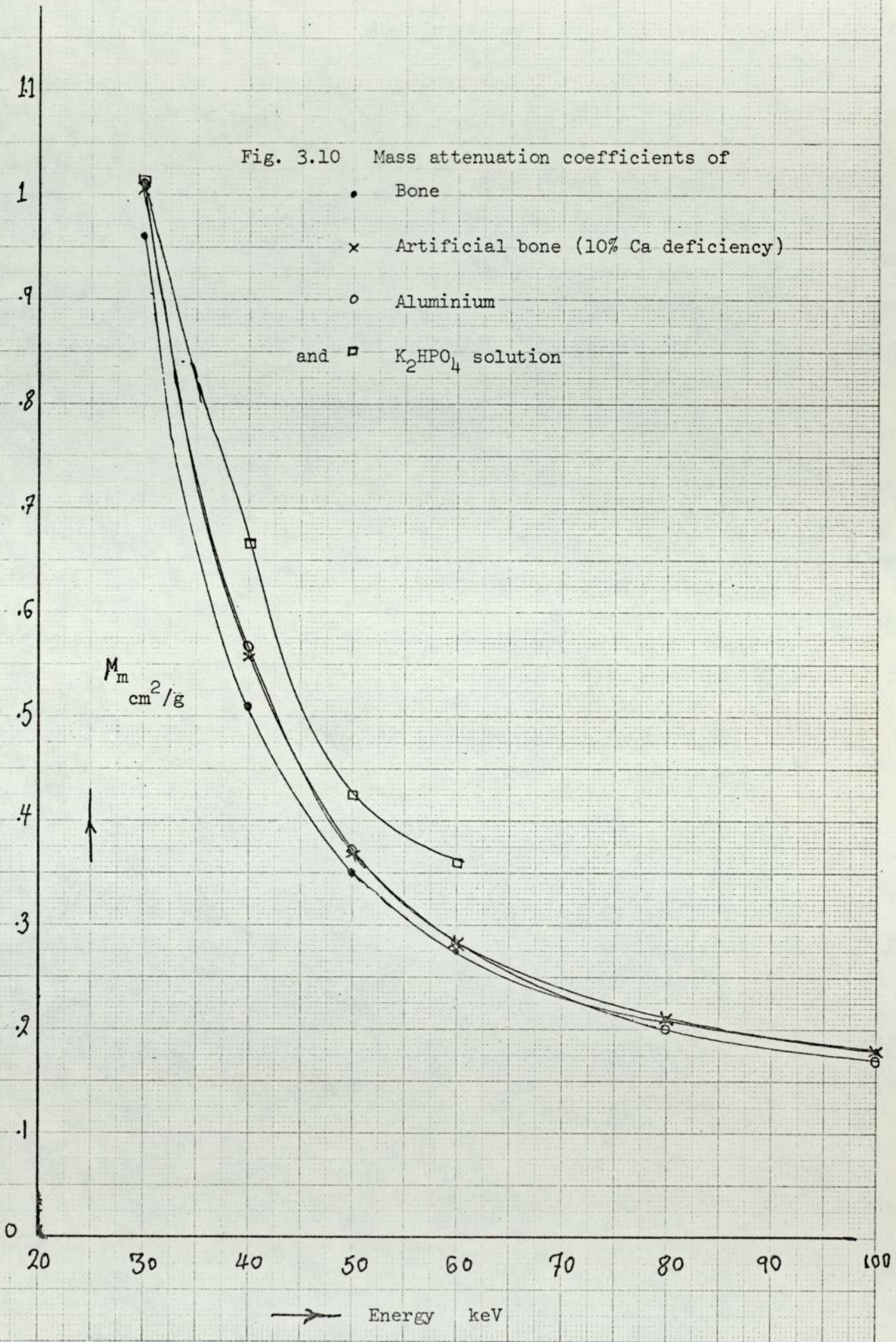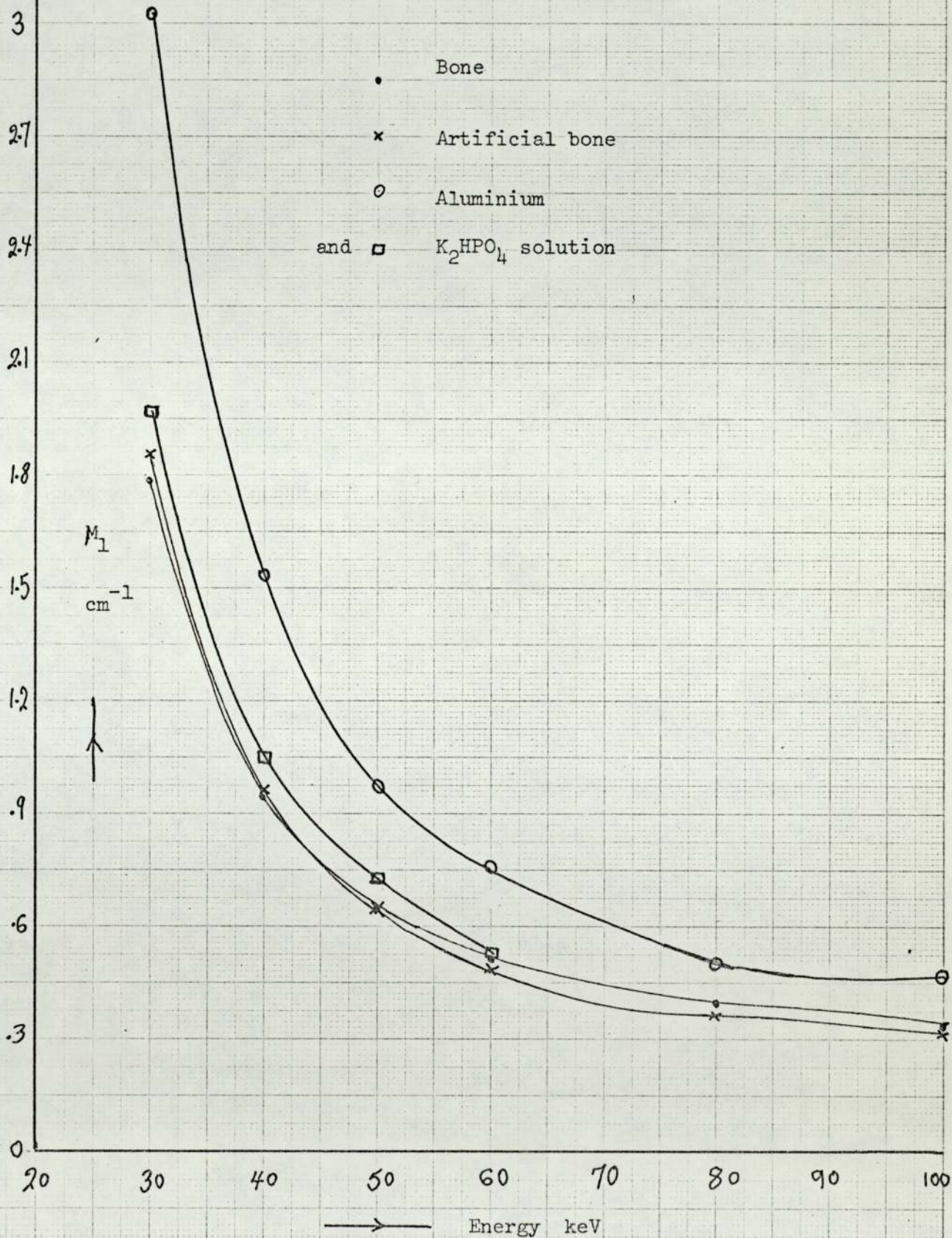
3.2   The soft tissue equivalent solution

Soft tissue is a variable mixture including muscle fibres, fat and water and has the approximate formula $(C_5H_{40}O_{18}N)_n$ (Goodman, 1969).

Soft tissue equivalents are used in bone radiography and in bone densitometry to give equithickness of tissue, overlaying bone so as to decrease errors in measuring mineral content caused by the varying amounts of soft tissue surrounding the bone.

There are several requirements for a soft tissue equivalent which include being non-toxic, inexpensive, easily available and easily cleanable, since limbs, or other parts of the body, are immersed in it.

In initial experiments, to minimise the effect of varying amounts of soft tissue surrounding the ulna, the arm was immersed in a bath of water to a constant depth of 50 mm (Edwards J, 1973). However, it was found when making in-vivo measurements that the average radiographic density of the soft tissue was slightly greater than water. To increase the attenuation coefficients of water, a small percentage of NaCl (1.3%) and KCl (0.7%) were added.

The linear attenuation coefficients of the salts solution has been calculated to be about 9% greater than water at 50 keV. The linear absorption coefficients of the salts solution and water are shown in figure 3.12, and the values are tabulated in Table 3.13.

.../

Fig. 3.12   Linear attenuation coefficients of water and 'NaCl, KCl' aolution

• NaCl, KCl solution

✗ water
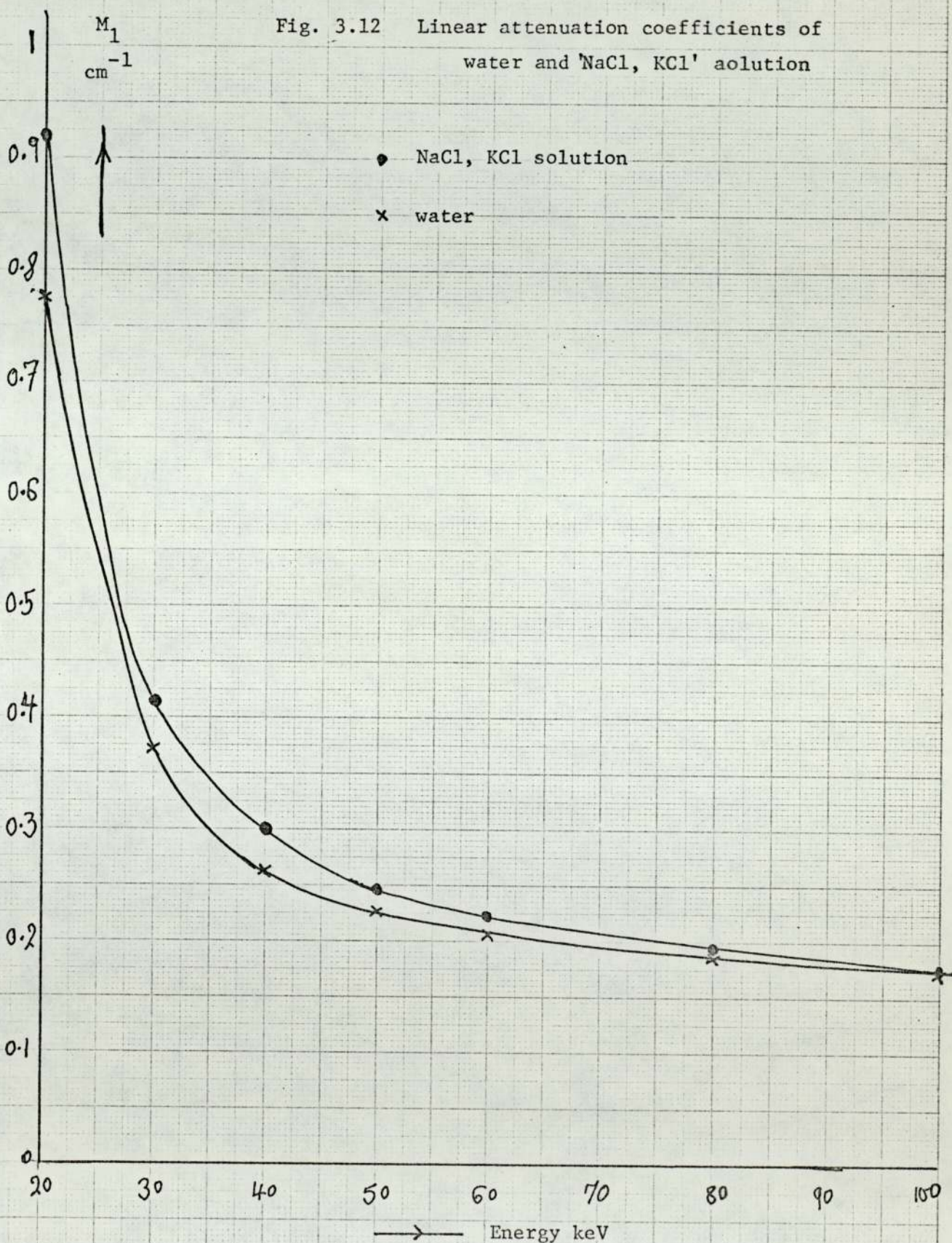
Energy keV

Table 3.1

Percentage fractional contributions of the different bone
constituents[64] to the mass absorption coefficient of bone
at the energy range (30-80)keV

Element	Photon energy keV		
	30	50	80
Ca	63.8	43.6	26.2
P	12.8	10.0	8.1
C	7.7	15.2	22.1
N	0.9	1.6	2.2
Mg	0.2	1.9	0.2
O	11.5	22.8	31.4
H	2.5	6.3	9.8
S	0.5	0.3	0.3

Table 3.2

Properties of the materials used to make the artificial bone standard

Material	Colour	Density g/cm³	Melting Point °C	Weight required g	Solubility in water in 100 parts
$Ca_3(PO_4)_2$	white	3.14	1670	35.05	0.0025
$Ca(OH)_2$	x	2.24	580	2.057	0.185
Melamine	x		360	4.096	0
MgO	x	3.58	2800	0.36	0
S	yellow	S. 2.07 M. 1.96	112.8	0.445	0
Araldite A.T.1	ivory white	1.2-1.3[25]	M.T. 80-100[25]	34.995	0

Table 3.3

Percentage composition by weight of the compact bone[64]

Element	% by weight
Ca	14.7
P	7.0
C	27.8
N	2.7
Mg	0.22
O	41.0
H	6.4
S	0.2

Density[55] (1.6 - 2.05) g/cm^3

Table 3.4

Percentage composition by weight of the araldite A.T.1[25] and the melamine[22]

Element	A.T.1	Melamine
C	75.60	32.81
N	0.25	63.80
H	6.85	3.39
O	17.30	--

Table 3.5

Percentage composition, by weight, of the artificial bone specimens

Element	% by weight	% by weight
Ca	19.2	1.306 x 14.7
P	9.14	1.306 x 7.0
C	36.31	1.306 x 27.8
N	3.53	1.306 x 2.7
Mg	0.29	1.306 x 0.22
O	28.15	1.306 x 21.55
H	3.39	1.306 x 2.59

Density   =   1.735 g/cm^3

Table 3.6

Relation of the displacement of springs to the compression force

Displacement in	Spring 1 load lb	Spring 2 load lb
0.05	9.0	19.1
0.1	16.8	44.9
0.15	28.0	65.1
0.2	34.7	84.1
0.25	43.7	107.6
0.3	50.4	130.0
0.35	57.2	151.4
0.4	65.0	172.6
0.45		194.8

Table 3.7

Densities of three artificial bone specimens

Specimen Number	Density g/cm^3
1	1.733
2	1.733
3	1.727

Table 3.8

Densities of artificial bone pieces cut from AB specimen 2

Piece Number	Density g/cm^3
Whole specimen 2	1.733
A	1.742
B	1.734
C	1.738
D	1.734
E	1.735

Table 3.9

Calculated and measured values of the mass attenuation coefficients

(M_m) of the 'AB' at different energies

Energy keV	M_m Calc. [1] cm^2/g	Energy keV	M_m Meas. cm^2/g
30	1.139	17.44	4.73 ± 0.05
40	0.583	32.06	0.923 ± 0.011
50	0.383	44.23	0.443 ± 0.009
60	0.292	60.00	0.273 ± 0.014
80	0.214		
100	0.187		

[1] Hubbell J, 1969

Table 3.10

Calculated M_m values of AB for 5% and 10%, by weight, calcium deficiency with equivalent increase in weight in the rest of the constituents

Energy keV	M_m 5% Ca deficiency cm^2/g	M_m 10% Ca deficiency cm^2/g
30	1.105	1.07
40	0.569	0.554
50	0.376	0.368
60	0.288	0.283
80	0.212	0.210
100	0.180	0.179

Table 3.11

M_m values of bone, artificial bone (10% Ca deficiency) Al

and K_2HPO_4 solution at different energies

Energy	M_m	cm^2/g		
keV	Bone	AB 10% Ca deficiency	Al	K_2HPO_4 sol.
30	0.962	1.07	1.12	1.144
40	0.512	0.554	0.567	0.667
50	0.349	0.368	0.369	0.425
60	0.274	0.283	0.280	0.309
80	0.209	0.210	0.203	--
100	0.180	0.179	0.171	--

Table 3.12

M_1 values of bone, artificial bone (10% Ca deficiency), Al and K_2HPO_4 solution at different energies

Energy	M_1 cm^{-1}			
keV	Bone	AB 10% Ca deficiency	Al	K_2HPO_4 sol.
30	1.78	1.856	3.02	1.968
40	0.947	0.961	1.53	1.147
50	0.646	0.638	0.996	0.731
60	0.507	0.491	0.756	0.531
80	0.387	0.364	0.548	---
100	0.333	0.311	0.462	---

<u>Table 3.13</u>

<u>Linear attenuation coefficients of water[47] and 2% NaCl,</u>

<u>KCl solution[47, 38]</u>

Energy	M_1 H_2O cm^{-1}	M_1 2% 'NaCl + KCl' solution cm^{-1}
20	0.775	0.921
30	0.370	0.416
40	0.267	0.297
50	0.226	0.247
60	0.206	0.223
80	0.184	0.195
100	0.171	0.175

CHAPTER FOUR

Measurement of the Scan Area

4.1   Measurement of the total mineral content

Established principles of radiation absorption permit
quantitative determination of bone mineral by densitometry. The
theory has been derived earlier in section 1.2.2. For example,
to measure the mineral content of a bone section using a mono-
chromatic source, logarithms of the counts are plotted on a graph
paper and the two smooth curves representing beam attenuation in
soft tissue and in bone are drawn through the plotted points (see
figure 4.1). The area between the two curves, i.e. the scan area
which is proportional to the total mineral content in the site of
the bone scanned (section 1.2.2), can be measured either by repeated
planimeter tracing or using a strip chart planimeter (Fischer and
Porter Company). The measurement can also be done on line and off
line by the use of a computer. The other method which is sometimes
applied to measuring the scan area is to draw the area on a uniform
homogeneous sheet of material which can be cut easily. The weight
of the cut sheet will be directly proportional to total mineral
content.

In the Aston technique and all other techniques using poly-
chromatic X-rays, it is not possible to do a straightforward
integration of the scan area, since to do this one needs to know
the attenuation coefficients of the bone and the soft tissue for
the energy range applied, together with the X-ray intensities at
these energies. This information is not easily obtained. For
this reason a calibration standard in the shape of a step wedge is

...⁄

Fig. 4.1   Relation of monochromatic photon beam attenuation,
            as indicated by the scan area, to bone mineral content

attenuation in soft
                 tissue

bone width

SA   attenuation in
            bone mineral

In count rate
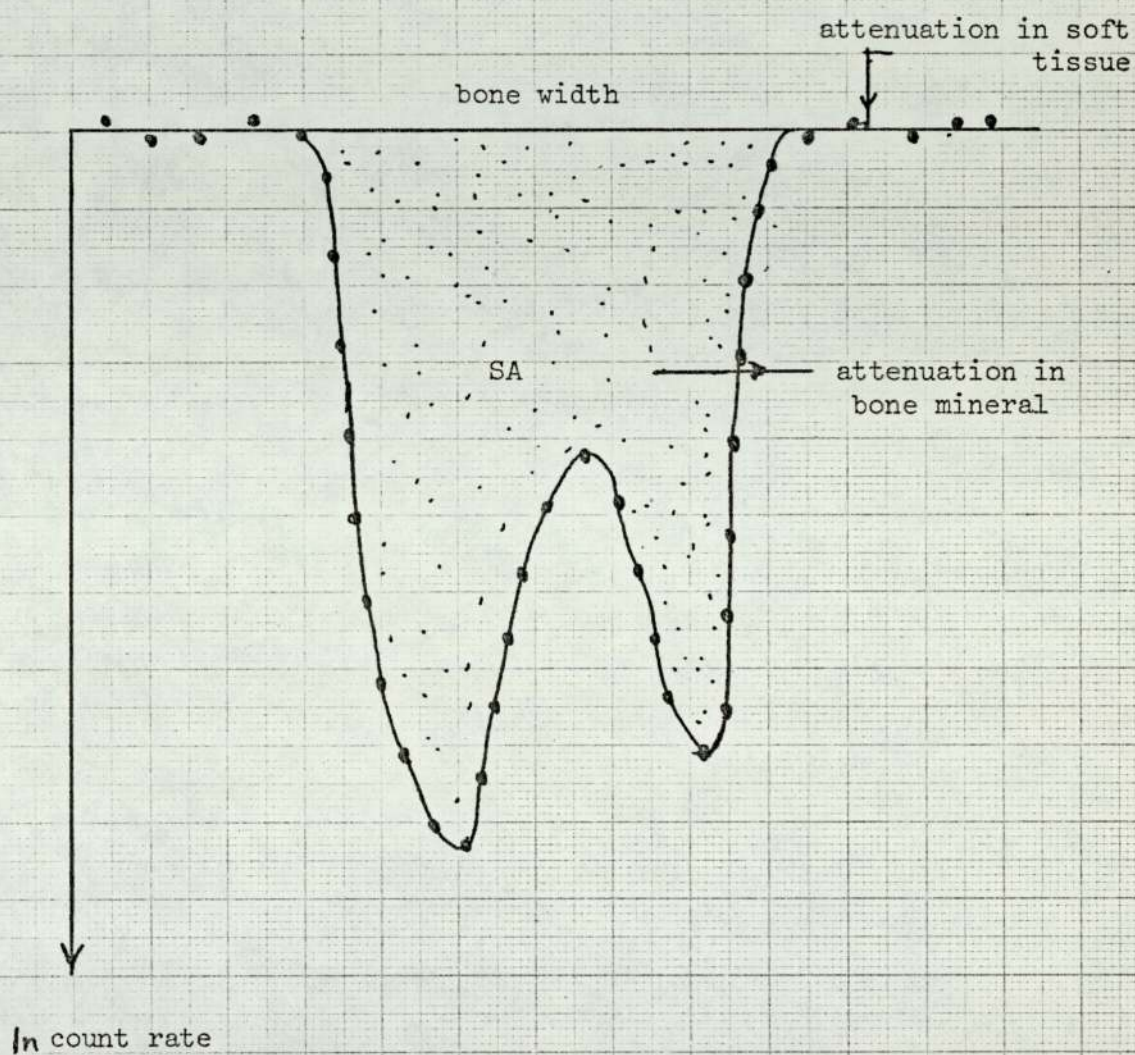
Scan area (SA) ∝ mass/unit length

usually used (see figure 4.2). The step wedge will enable direct measurement of trace height at any position.

Direct measurement of the scan area is only possible when there is a linear relation between the transmitted X-ray signal and absorber content. With the aid of the different signal heights (given the symbol y_n) representing the different steps, one can measure the trace heights at the different positions in terms of the standard steps and plot these points then measure the area. Not only is this method a prolonged one, as it involves measuring the width of the trace for each step (within the range of the trace height), it is also inaccurate because of the limited number of steps in the standard.

The method of interpolating for each spot in the trace in terms of the standard steps is possible but it also involves a prolonged procedure.

4.2   The earlier trials

A number of techniques were tried to find a simple and accurate method of changing the non-linear relation of the signal height and absorber content (given the name 'the signal function' $y_{(n)}$) to a linear relation.

The idea of the first method was to achieve the linearity correction by inserting a suitable electronic circuit between the output and the signal lead of the oscilloscope. The action of this circuit was to convert the non-linearity in the signal function to linear form. This was tried on an empirical basis.

.../
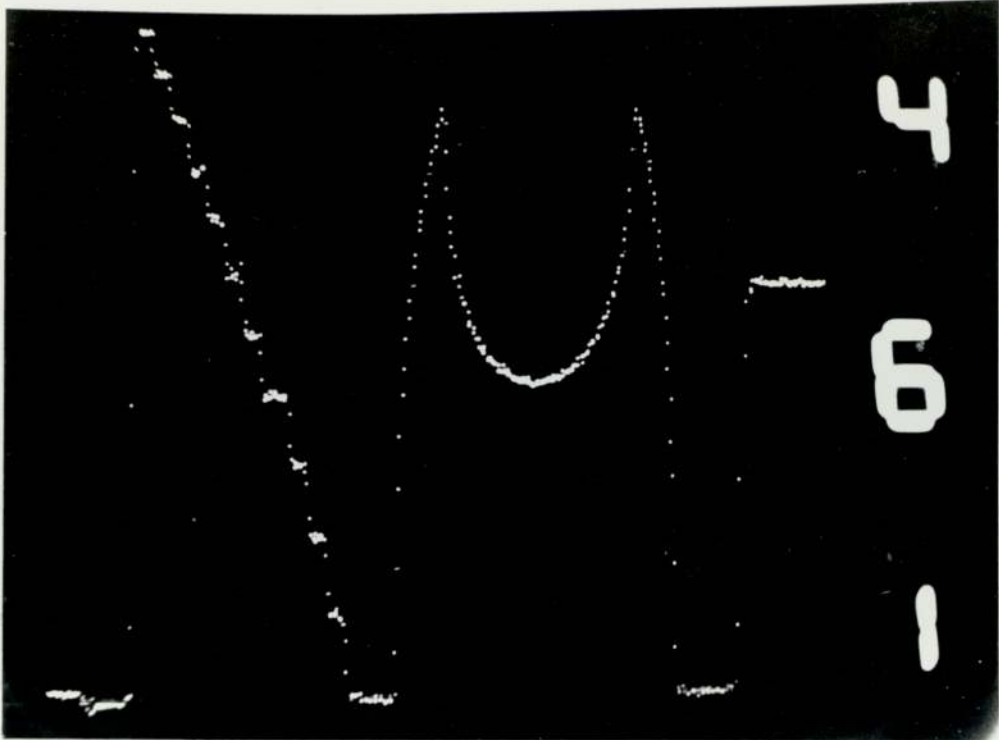
Fig. 4.2   A trace of an artificial bone tube and the step
wedge
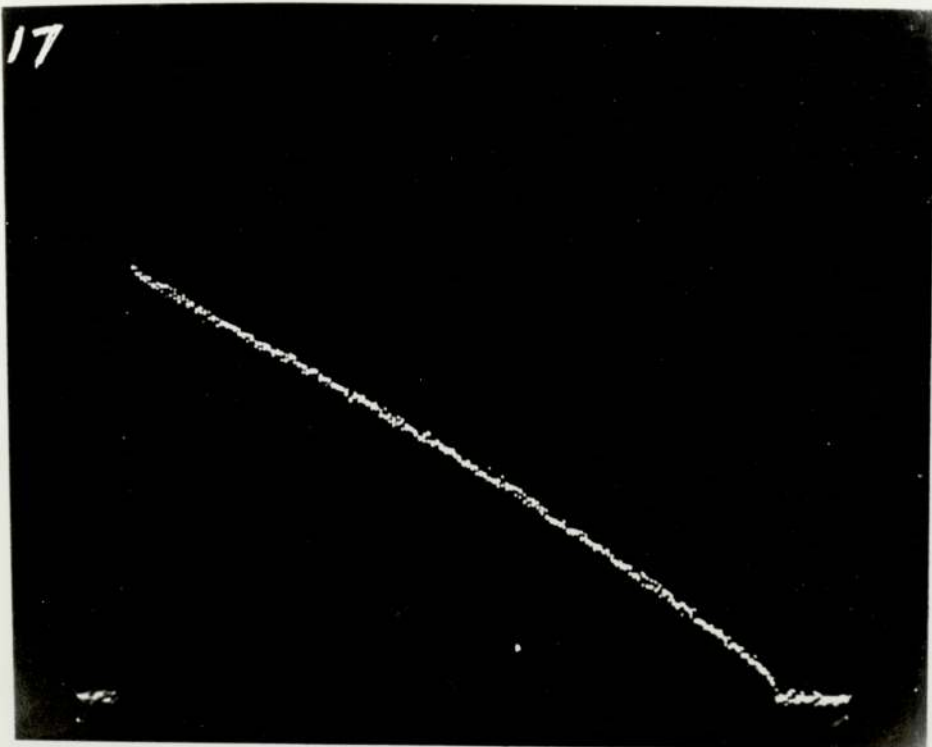
Fig. 4.3   A trace of an ivory wedge of 7.5 mm maximum
thickness

In order to devise a suitable electronic circuit, the signal function should be known. In the beginning it was impractical to try electronic circuits using the scanning machine since this required frequently repeated scans which would heat up the X-ray tube. Therefore, a trace was taken of an ivory wedge having maximum thickness of 7.5 mm (fig. 4.3). As is shown in figure 4.3, the variation of the signal for high ivory thicknesses is nearly linear but for small thicknesses the variation of the signal with wedge height increases. So an electronic circuit with the inverse function of the signal function was required in order to get a straight line function throughout, representing the uniform ivory wedge.

A number of electronic circuits which were expected to give a similar function were examined, but it was found difficult to get the required function. Among the circuits tested were negative feedback amplifiers, multidiodes, combinations of the two and a transistor with multidiodes. Later it was realised that finding a suitable function which could do the linearity correction for the present signal function $(y_{(n)})$ would suffer distortion for any shift in the d.c. level of the signal to which the machine is liable. Because of this difficulty the method was abandoned.

Another technique, which was tried and gave encouraging results, was to enlarge the scan area with a photographic enlarger and then to trace and measure the magnified area with a plamineter for each step separately (see figure 4.4). The magnification was done to decrease planimeter error. Parallel lines representing step signal heights (y_n) were drawn on a developed X-ray film strip to accompany each trace.

Fig. 4.4   The magnified scan area divided into areas
            corresponding to each step

soft tissue only

$n = 0$

ΔSA_1

1

ΔSA_2

2

ΔSA_3

3

y

4

5

6

7

8

9

10

11

$$SA \quad = \sum_{n=1}^{n=11} \frac{\Delta SA_n}{y_n - y_{n-1}}$$

A4 210 x 297 mm
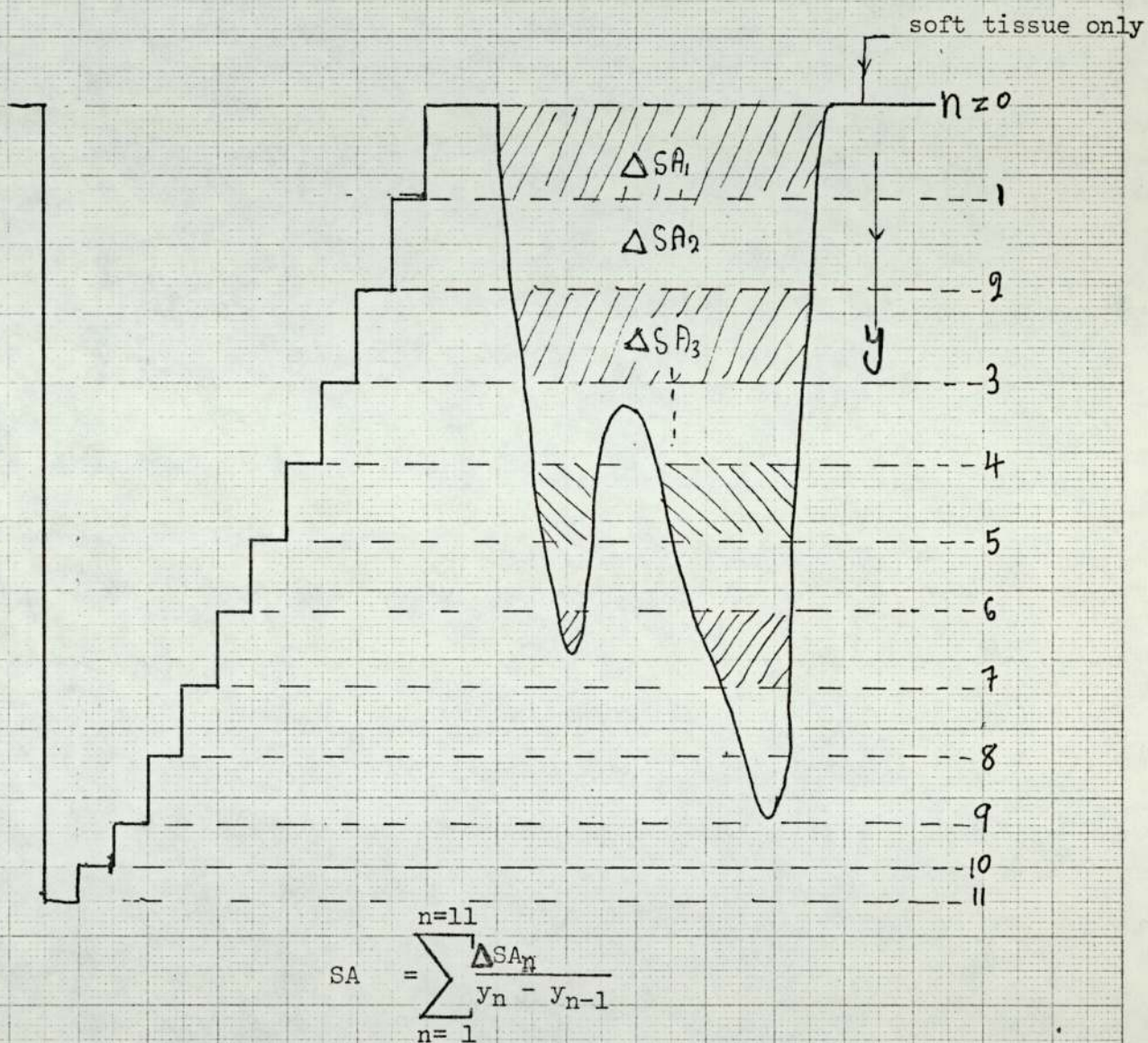
The trace steps were made to match respective lines in the strip. Consequently, the scan area was divided into areas corresponding to each step to enable a simple and accurate tracing of the enlarged areas.

To get equal representation of signal height for all steps (linear relation of signal height to absorber content) each area was divided by its step height $(y_n - y_{n-1})$. The scan area of the trace will be equal to the sum of individual areas.

$$SA_n \; = \; \sum_{n=1}^{n=11} \frac{\triangle SA_n}{y_n - y_{n-1}} \qquad\qquad 4.1$$

Where y_o is zero

and $\triangle SA_n (= SA_n - SA_{n-1})$ is the area corresponding to the nth step.

To check this method, a parallel film strip of 28 mm width was used; on it were marked lines representing the different step heights. The strip area was magnified by 8.2 and each area was traced and measured using a planimeter. Afterwards step areas were corrected for linearity.

Theoretically, the individual areas should now be equal after correcting for the differences in signal heights of the different steps $\dfrac{\triangle SA_n}{y_n - y_{n-1}}$. The individual areas under steps were within ± 1.5% from the mean value and the maximum difference in areas was 2.5%. The expected total error in measuring the scan area of a patient's trace is about 1% which is less than the error in individual areas because any patient's trace covers at least the first four steps and therefore differences in individual areas will tend to compensate for each other.

This technique has the advantage that it is applicable to any
signal function $y_{(n)}$. The only thing required in the case of signal
function variation (which could happen, for example, if the integra-
tion time is altered significalty) is to draw the new 'y_n' lines
representing the signal heights on a transparent or semi-transparent
sheet like, for example, developed X-ray film to accompany each
trace during magnification.

The drawback of this technique was that in measuring a scan
area the area under each step had to be measured separately. This
increased the total work many fold, depending on the maximum height
of the signals of the trace.

4.3   The optical transform method

The third method investigated and later put in operation was
to do the linearity correction by means of an optical transform.
If a fixed object tilted with respect to the axis of a convex lens,
is at a distance (u) greater than the focal length (f) then a real
image will form and the relative image magnification of any point
in the object will depend on its distance from the lens. Under
certain conditions one may be able to get the required relative
magnifications to the different parts of the scan area to give a
linear area representation. If so, the transformed scan area can
be traced on paper and the area measured by a planimeter.

A compound lens together with a light source from an overhead projector were used to give a sharp image. The trace was fixed on a tilted glass plate in front of the lens and was arranged to have the signal height direction (y) along the line of maximum slope of the plate with the line representing the 5th standard step (y_5) at twice the focal length. The image was received on another tilted glass plate (fig. 4.5) covered with white paper with the line image of the fifth step at a distance 2f from the lens.

Areas above the fifth step will be enlarged according to the angle of tilt ($u < 2f$) while those under the fifth step will suffer reduction ($u > 2f$) (fig. 4.6).

Early trials were carried out assuming equal lateral and longitudinal magnifications in working out the conditions for the linear area representation in the image. But it was found experimentally that this gave inaccurate results which indicated the error in assuming equal lateral and longitudinal magnifications. Therefore, it was realised that more accurate analysis of the magnifications had to be undertaken and an investigation had to be made to see whether a linear representation of area could be achieved with this system.

The relation between the signal height (y_n) and its image (y_n^*) was derived and the transformed image of the scan area was worked out in terms of y_n^*, f and Θ. The angle Θ, shown in figures 4.7 and 4.9 is referred to as the angle of tilt. The third step was to assume a linear relation between the transformed scan area (SA) and the step number (n) which is the required condition of the
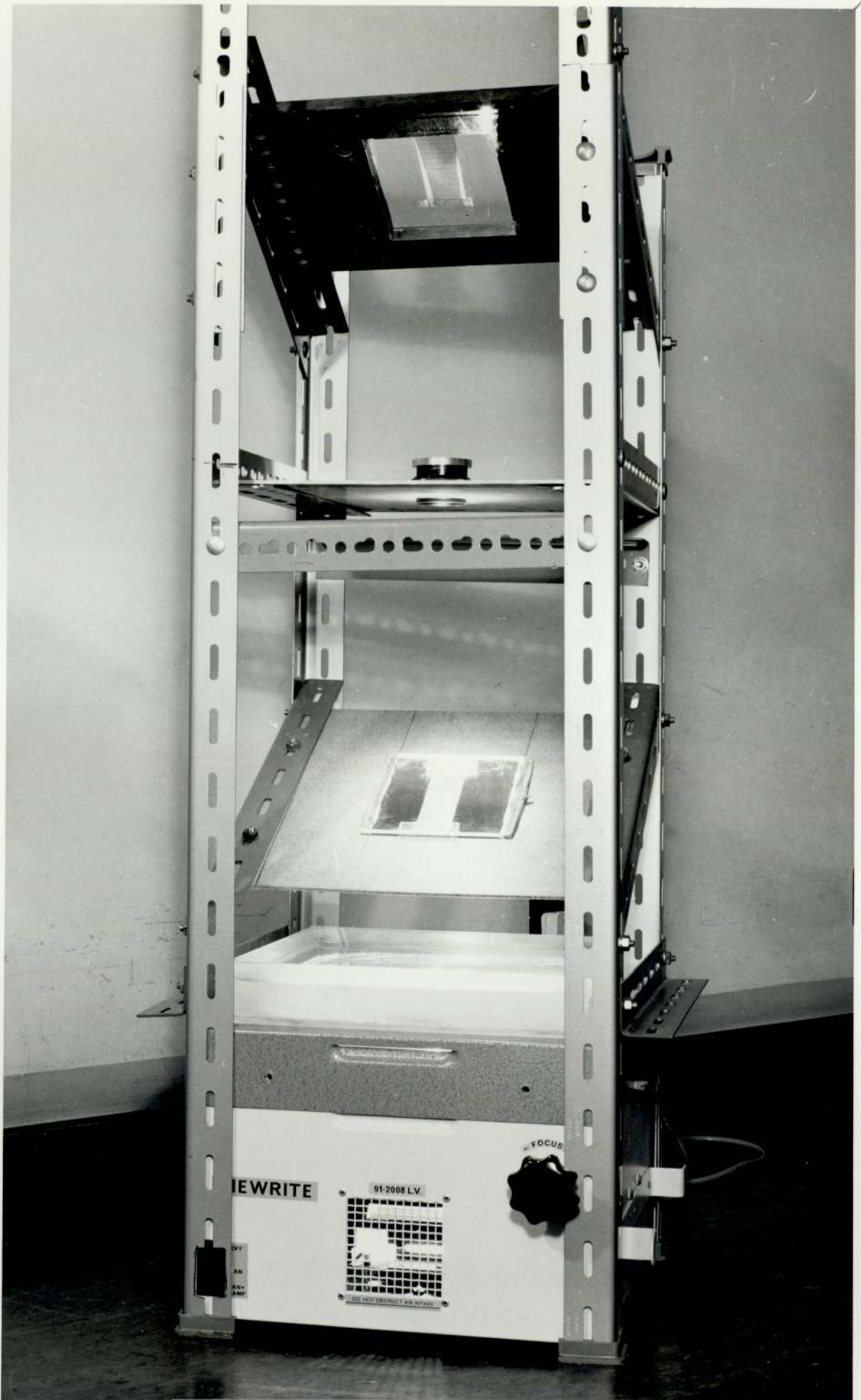
Fig. 4.5   The optical transform system
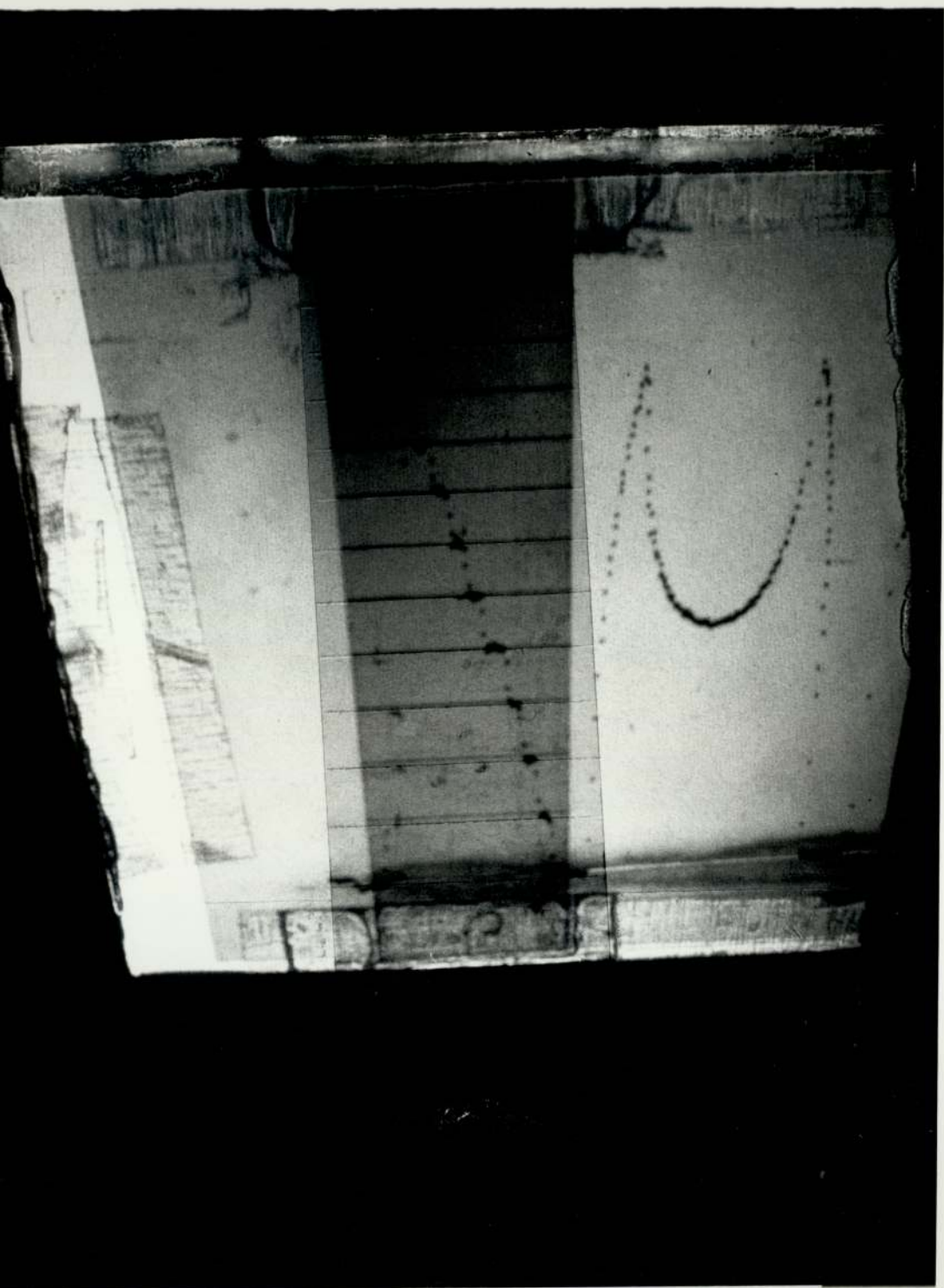
Fig. 4.6   An image transform of a trace of an
            artificial bone tube

optical transform system. From these equations, an equation was derived relating the signal height (y_n) to the step number (n) and by substituting a few measured values of (y_n) for different (n), the constants of the equation were calculated. The equation was

$$y_n = M - \frac{F}{(n + \beta)^{1/2}} \qquad\qquad 4.22$$

Where y_n is the signal height in the trace of step number

n, measured in millimeters from the line representing

attenuation in soft tissue equivalent solution (see

figure 4.1),

and   M, F and ß are constants.

This function was found to fit accurately the signal function $y_{(n)}$ (derived from measurements of the step signal heights in actual traces) which is the required condition in order that the optical transform works. The angle of tilt was worked out from the constants and it was found to be experimentally feasible.

Choosing the right angles and distances of object and image from the lens, it was possible to get the required transform and check the accuracy.

Transformed scan areas of artificial and dead bone pieces were measured. In the measurement of artificial bone, the bone weight derived from the transformed scan area was in agreement with the actual value (section 4.6). In the dead bone piece experiments, good correlations were found between transformed scan areas and both bone weight and bone mineral weight (sections 5.3.3 and 5.3.5).

Details of the method will be given in the following sections.

4.4   The theory and the discussion

The steps followed in deriving the conditions needed to get linear representation of the scan area in the image using the optical transform system will be outlined.

Assume that the trace was fixed on a tilted frame in front of a lens in such a way that the signal height direction (y) was along the line of maximum slope of the frame with one of the signal heights representing the middle step (y_5) at a distance 2f from the lens. The image would be received on another tilted frame, of the same and opposite tilt angle, on the other side of the lens with the line image of the fifth step (y_5^*) at 2f distance from the lens. The magnification of the line representing the fifth step will then be unity.

It was convenient to introduce new parameters (h_n) and (h_n^*) such that the signal heights in both object (y_n) and image (y_n^*) are measured from the line corresponding to step five, i.e.

$$h_n = y_n - y_5 \qquad\qquad 4.2$$

$$h_n^* = y_n^* - y_5^* \qquad\qquad 4.3$$

The relation between the signal height (h_n) and the image height (h_n^*) was derived (equation 4.12) in terms of the focal length and the angle of tilt (θ).

...../

The equation of the transformed scan area for any height (h_n^*) was also derived (equation 4.14) in terms of the focal length and the angle of tilt. From equation 4.14 and using equation 4.12 the relation between image area and signal height (h_n) was derived (equation 4.15).

The fourth step was to assume a linear relation between the transformed scan area (SA) and the step number (n) (equation 4.16) which is the required condition $(\frac{dSA}{dn} = \text{constant})$.

Using equations 4.15 and 4.16, the relation between (y_n) and (n) was derived (equation 4.22) and by substituting three measured values of (y_n) for different (n), it was possible to calculate the constants in the equation. The other values of (y_n) for the rest of the steps were calculated using equation 4.22 and they were found to agree closely with the measured values (Table 4.1).

$(f \sec \theta)$ was among the constants calculated, and from this, the value of the angle of tilt (θ) was worked out after measuring the lens focal length experimentally.

(h_n^*) values were calculated by applying equation 4.12 which should give the required area transform when they were made to match, in the image plane, the corresponding image lines of (h_n) (fig. 4.6).

An achromatic compound lens from a photographic enlarger was used in this system (section 4.5) but for simplicity it is represented by a thin single lens in all figures.

Figure 4.7 shows both object and image drawn in three dimensions together with the lens. In order to show clearly the two magnifications

.../

Fig. 4.7 The object and the image plotted in three dimensions

$GC = f \sec \theta$
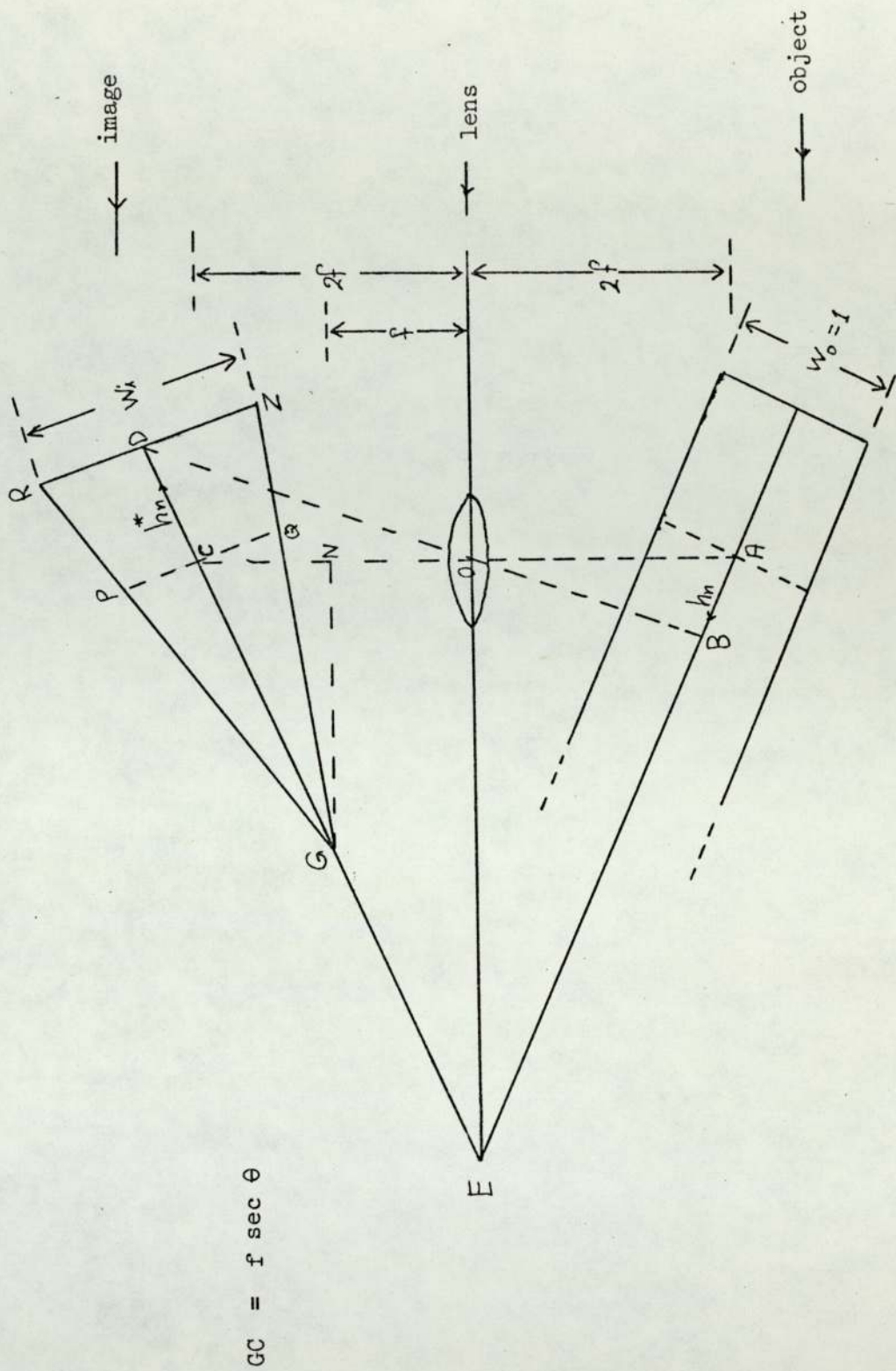
another figure 4.8 shows two lines; one in the longitudinal direction and the other in lateral direction. Each axis is drawn separately in figures 4.9 and 4.10.

In figure 4.7 or 4.9 let

$$OA = OC = 2f$$

Where f is the lens focal length.

Then A and C will be points at unit magnification. A strip of unit width along EA, i.e. the longitudinal axis of the object will give an image of unit width at C. The image will be bordered by two lines which meet at G (fig. 4.7).

To find the image width at any distance (h_n^{*}) from point C along the longitudinal axis of the image, i.e. EGC :

If GN is a vertical line on the lens axis OC then CN = f because at the focal plane the image width is zero.

Therefore, CG = f sec θ. 4.4

From the two similar triangles GPQ and GRZ in figure 4.11

$$\frac{w_i}{1} = \frac{CG + h_n^{*}}{CG} \qquad 4.5$$

From equations 4.4 and 4.5

$$w_i = \frac{f \sec \theta + h_n^{*}}{f \sec \theta}$$

or

$$w_i = 1 + \frac{f \sec \theta + h_n}{f \sec \theta} \qquad 4.6$$

h_n^{*} + ve   away from G . . . magnification

h_n^{*} - ve   towards   G . . demagnification

From figure 4.10 :

$$\frac{w_i}{w_o} = \frac{v}{u} \qquad 4.7$$

i stands for image and o for object.

Fig. 4.8   Object and image planes with two object and two image lines

AB and CD in the longitudinal direction

BT and DS in the lateral direction
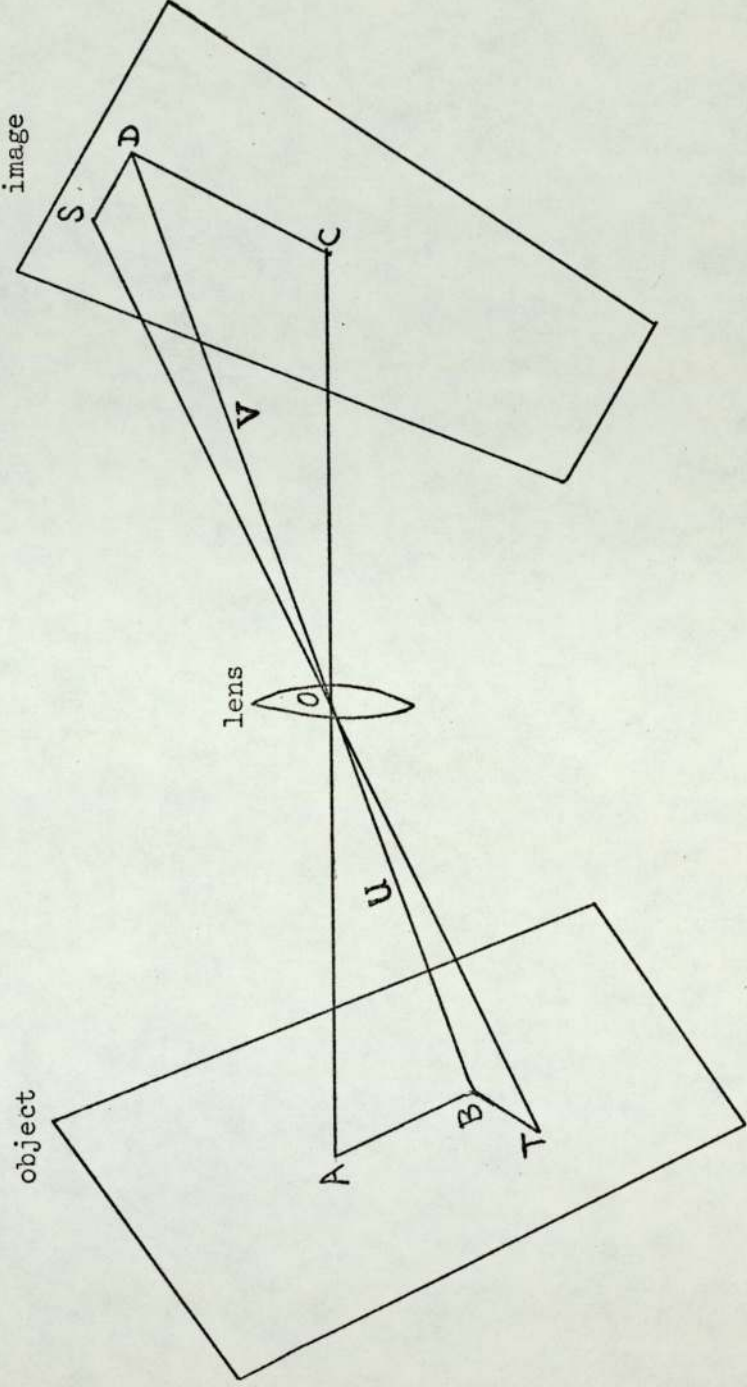
Fig. 4.9   Object and image lines in the longitudinal
direction
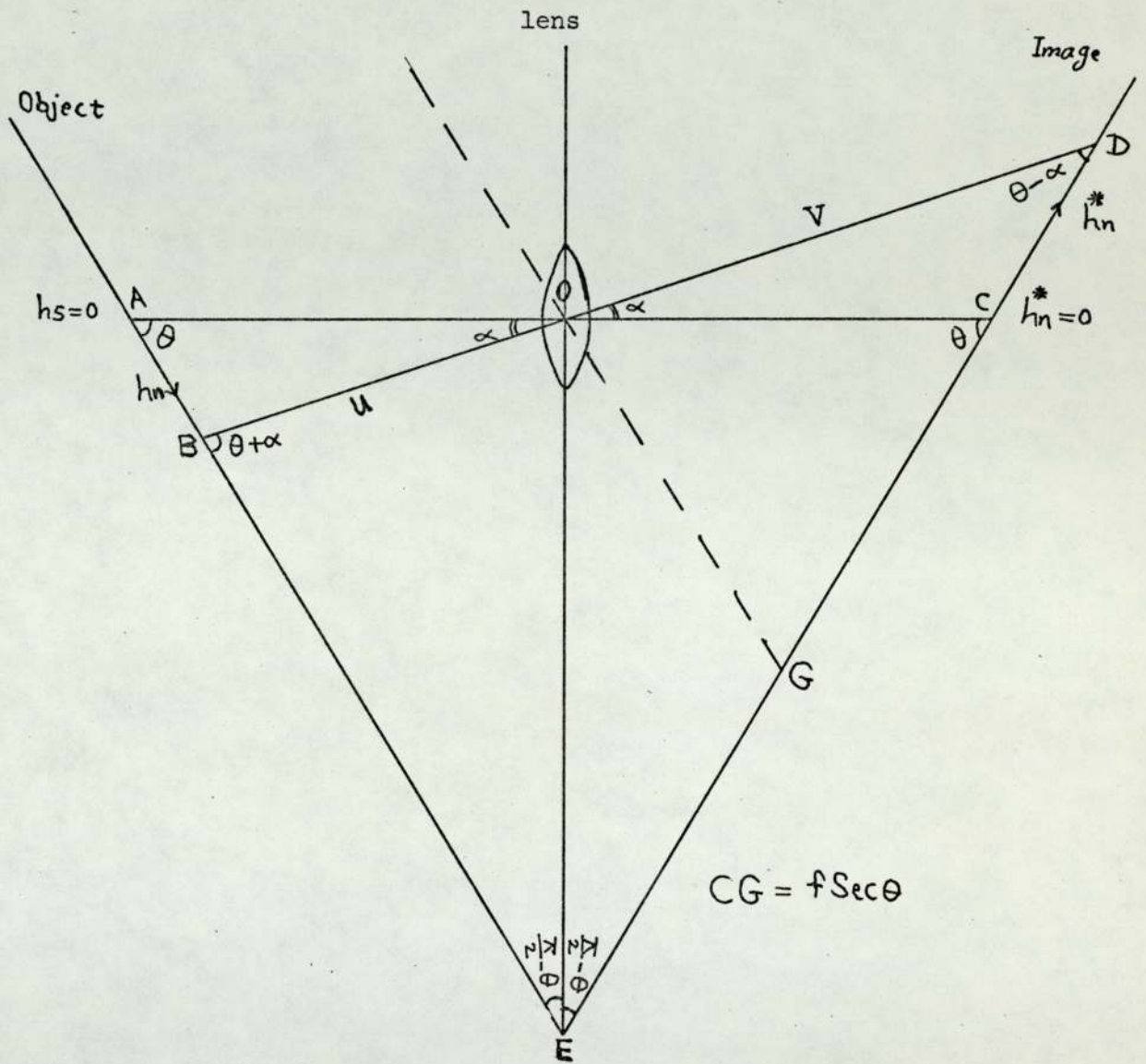
In triangle AOB $\dfrac{h_n}{\sin \alpha} = \dfrac{u}{\sin \theta}$

In triangle DOC $\dfrac{h_n^*}{\sin \alpha} = \dfrac{v}{\sin (180 - \theta)}$

$\therefore \qquad \dfrac{h_n^*}{h_n} = \dfrac{v}{u}$

Fig. 4.10 Object and image lines in the lateral direction

lens

S

$\frac{w_i}{2}$

B

u

O

v

D

image

$\frac{w_o}{2}$

$\frac{w_i}{w_o} = \frac{v}{u}$

T

object

R

w_i

Z

$+h_n^+$

P

C

Q w_i

$-h_n^*$

f sec θ

G
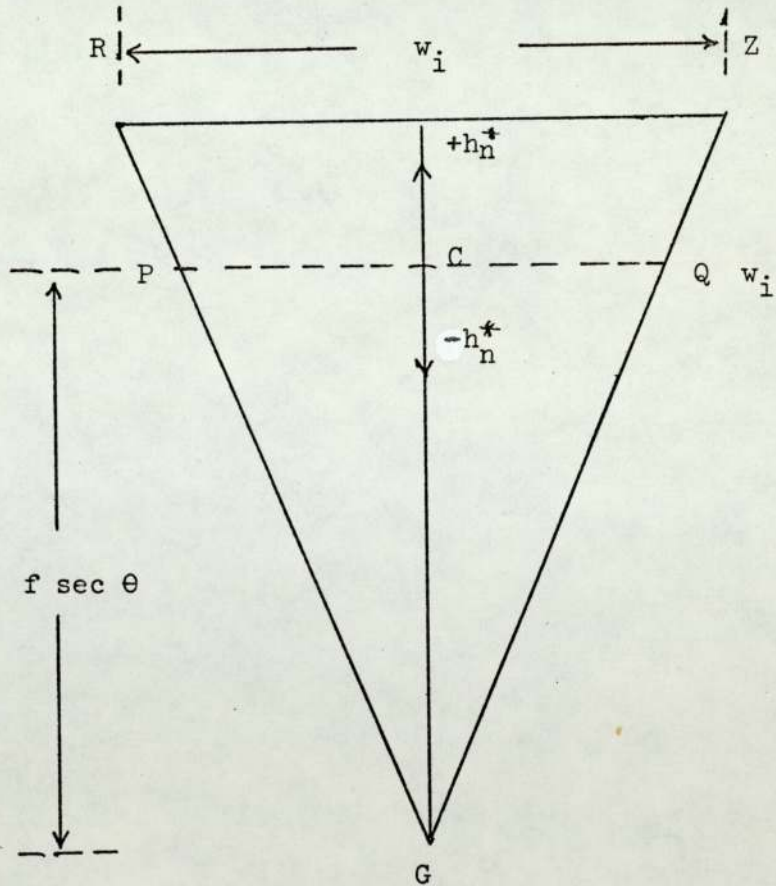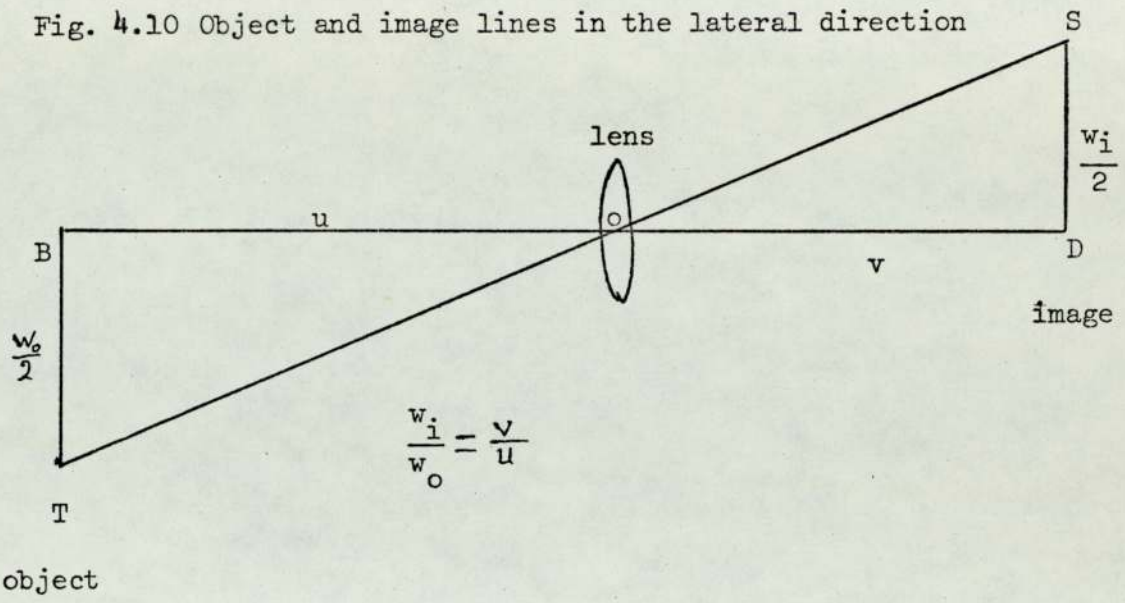
Fig. 4.11   The image area of a unit width strip along EA
(in fig. 4.7)

From equations 4.6 and 4.7

$$\frac{v}{u} = \frac{w_i}{1} = 1 + \frac{h_n^*}{f \sec \theta}$$ 4.8

From figure 4.9:

in triangle AOB   : $\dfrac{h_n}{\sin \alpha} = \dfrac{u}{\sin \theta}$ 4.9

in triangle DOC   : $\dfrac{h_n^*}{\sin \alpha} = \dfrac{v}{\sin (180 - \theta)}$ 4.10

The two latter equations 4.9 and 4.10 give

$$\frac{h_n^*}{h_n} = \frac{v}{u}$$ 4.11

From equations 4.8 and 4.11, it can be easily shown that

$$h_n^* = \frac{1}{1/h_n - 1/f \sec \theta}$$ 4.12

In this equation f can be measured but it remains to find the angle of tilt θ which will give a linear representation of area in the image. Knowing θ, the values of h_n^* which will satisfy the required transform can be calculated from equation 4.12.

A rectangular strip on the object plane, along EA, gives rise to a trapezium shaped image in the image plane (fig. 4.6). It was required to find the equation relating the transformed area (SA) to the height h_n^* (fig. 4.11). In order to do this, the transformed area of a unit width strip along EA was calculated. The transformed area for height h_n^* is

$$SA_n = \frac{1}{2} w_i (h_n^* + f \sec \theta)$$ 4.13

but from equation 4.6 $w_i = 1 + \dfrac{h_n^*}{f \sec \theta}$

.../

Therefore $\quad SA_n = \dfrac{\cos\theta}{2f}\,(h_n^{\,*} + f\sec\theta)^2 \qquad$ 4.14

or using equation 4.12

$$SA_n = f\,\frac{\sec\theta}{2}\left[1 - \frac{h_n}{f\sec\theta}\right]^{-2} \qquad 4.15$$

For the image in the optical projected scan area SA_n to be linear with n, then a formula of the following form should hold:

$$SA_n = \alpha\,(n + \beta) \qquad 4.16$$

Where $\quad \alpha$ and β are two constants.

By substituting the value of SA_n (equation 4.16) in equation 4.15, a relation between n and y_n was derived.

$$\alpha\,(n + \beta) = f\,\frac{\sec\theta}{2}\left[1 - \frac{h_n\cos\theta}{f}\right]^{-2} \qquad 4.17$$

$$1 - \frac{h_n\cos\theta}{f} = \left[\frac{f\sec\theta}{2\,\alpha\,(n+\beta)}\right]^{1/2} \qquad 4.18$$

$$f\sec\theta - h_n = \frac{(1/2\,f\sec\theta)^{1/2} \; x \; f\sec\theta}{\alpha^{1/2}\,(n+\beta)^{1/2}} \qquad 4.19$$

or $\quad h_n = f\sec\theta - \dfrac{\sqrt{1/2}\;(f\sec\theta)^{3/2}}{\alpha^{1/2}\,(n+\beta)^{1/2}} \qquad 4.20$

but by definition $h_n = y_n - y_5$ (equation 4.2)

Therefore $\quad y_n = y_5 + f\sec\theta - \dfrac{\sqrt{1/2}\;(f\sec\theta)^{3/2}}{\alpha^{1/2}\,(n+\beta)^{1/2}} \qquad 4.21$

or $\quad y_n = F - \dfrac{M}{(n+\beta)^{1/2}} \qquad 4.22$

Where $\quad$ F and M are two constants.

$$M = \sqrt{1/2} \; \frac{(f \sec \theta)^{3/2}}{\alpha^{1/2}} \qquad \qquad 4.23$$

$$F = f \sec \theta + y_5 \qquad \qquad 4.24$$

Equation 4.22 should fit the signal function (y_n) if the optical transform is to work.

To find M, F and ß values three equations were needed and to try to satisfy the signal function $y_{(n)}$ using these constants, three measured values of y_n for different n values were substituted in equation 4.22. For a good fit over the range of the signal function, the y_n values for n = 0, 5 and 10 were taken from typical traces (the mean values of y_n measured from two typical traces).

n	=	0	y	=	0
n	=	5	y	=	40.15 mm
n	=	10	y	=	68.10 mm

Table 4.1

These give

F	=	316.7	mm
ß	=	16.053	
M	=	1288.88	mm^{-1}

Using these constants, the other values of y_n were computed and compared with the measured values from the trace as shown in Table 4.1. From Table 4.1 it can be seen that the calculated y_n values fitted, with good precision, the measured figures and the discrepancy was within the differences in the measured values of y_n from the different traces (which was found equal to ± 0.2 mm).

The experimental accuracy of measuring y_n on the trace was found equal to $\pm$ 0.1 mm maximum from the mean.

To find the corresponding value of θ, equation 4.24 was used.

$$F = y_5 + f \sec \theta$$

$$316.7 = 40.15 + f \sec \theta$$

$$f \sec \theta = 276.55 \text{ mm}$$

The experimentally measured value of f was 130 mm.

Therefore $\sec \theta = \dfrac{276.55}{130} = 2.127$

Hence $\theta = 62°$

To calculate h_n^* values, equation 4.12 was used by substituting value of $f \sec \theta$.

$$h_n = \frac{1}{\dfrac{1}{h_n} - \dfrac{1}{276.55}} \qquad\qquad 4.25$$

The values of y_n^* were calculated from h_n^* in equation 4.3.

$$y_n^* - y_5^* = h_n^*$$

The values of h_n, h_n^*, y_n and y_n^* corresponding to the different values of n are shown in Table 4.2.

The y_n and y_n^* values were plotted on two X-ray film strips and put in the object and image positions respectively (see figure 4.5). The object and the image plates were made approximately 28° (90° - θ) to the horizontal. The lines representing step five in both object and image films were put, as near as possible, in line with the lens axis at 2f distance from the principal planes on the two sides.

With the present optical frame (fig. 4.5 and section 4.5) it
is difficult to set accurately by measurement the object and the
image plates at the required distances and angles. Therefore,
they were set, as accurately as possible, in the required positions
and then a slight variation in angles, distances and film positions
were carried out until the line images of y_n optimally matched with
y_n^* lines in the image plate (fig. 4.6).

There is a point which is worth mentioning here. For tilted
object and image lines it can be shown that

$$\frac{1}{u} + \frac{1}{v} = \frac{\cos \alpha}{f} \qquad 4.26$$

for α : see figure 4.9.

The largest value of α was calculated to be 8.9° for which
$\cos \alpha = 0.988$. So there is very little departure from ideal
focus over the whole image surface in spite of the tilted conjugate
planes.

4.5 The optical frame

The object, lens and image plates were fixed above the light
source, in that order. Four long handy angle ('angle') (100, 100,
114.5, 114.5 cm) were used for this purpose. They were secured
vertically in the corners of the projector light box. Six angle
pieces (33.6 and 36.3 cm) were applied to clamp the four vertical
rods to each other and to the light box (see figure 4.5). The
three plates of object, lens and image were bolted with screws to
the four vertical rods.

An achromatic compound lens was employed which has a 3.2 cm aperture. An aluminium cap with a hole in the middle (1.6 cm diameter) was put on the lens to increase the depth of field. A 'dural' plate (1/8 in thick) was used to support the compound lens. A threaded hole was made in the middle of the aluminium plate to screw the compound lens in position. The lens was put at the light source focus and aligned with it.

The object and image plates were placed obliquely to the vertical rods so that they made equal acute angles with these rods. A cardboard plate(3.2 mm thick) was used in supporting the object screen whilst a stiffer plate made from bakelite (12.7 mm thick) was particularly chosen to uphold the image screen. The stiff plate prevented any possible bend in the image screen during tracing the transformed scan ares. Square openings (11 x 13 cm) were made in both the object and image plates where thin glass screens (o.48 x 12.4 x 13.7 cm) were fixed (fig. 4.5).

Angular and positional variation in the plates' positions could be made by easing the four screws connecting the plates to the vertical members and adjusting the screws to other positions in the rectangular holes of the vertical rods.

In order to decrease the amount of heat dissipated in the X-ray trace when tracing the transformed scan area, a perspex water bath was made from 6.4 mm thick perspex of dimensions 28.9 x 28.9 x 5 cm (see figure 4.5).

.../

4.6 Calibration of scan areas to artificial bone

In in-vivo measurements, it is worthwhile to calibrate the scan area to a more meaningful unit like artificial bone volume, weight or calcium content. This could be done by assuming that the bone scanned has a similar composition to that of artificial bone (section 3.1.3) and the surrounding soft tissue has a similar composition and equal density to the tissue equivalent solution (section 3.2), which is incorrect. There are differences in the composition of bone and soft tissue among healthy people in one site and the differences in bone composition in metabolic bone disorders are expected to be even higher. Even though this is so, the approximate values will give an idea of the amount of bone in the scanned site.

$$SA_n = \frac{\cos \theta}{2f} (h_n^* + f \sec \theta)^2 \qquad 4.14$$

$$\Delta SA_n = SA_n - SA_{n-1}$$

$$\Delta SA_n = \frac{1}{2 f \sec\theta} \left[(h_n^* + f \sec \theta)^2 - (h_{n-1}^* + f \sec \theta)^2 \right] \qquad 4.27$$

By substituting f, θ and h^* values (section 4.4) in equation 4.27, it can be easily shown that

$$\Delta SA_n = 6.568 \text{ mm}^2 \qquad 4.28$$

.../

SA_n is the scanned area (SA) for one step of artificial bone (AB) which was 1.2 mm high, 9.5 mm long and 1.0 mm wide (appears as 2 mm in the trace). The volume of the artificial bone scanned was

$$= 1 \times 1.2 \times 9.5$$
$$= 11.4 \ mm^3 \hspace{3cm} 4.29$$

From equations 4.28 and 4.29

$$1 \ mm^2 \ SA = 1.736 \ mm^3 \ AB \hspace{2cm} 4.30$$

Since every 500 mm^2 area was represented by 205×10^{-3} (written just 205) of planimeter reading (PR) units (section 4.7), therefore

$$1 \ PR \ unit = 2.439 \ mm^2 \hspace{2cm} 4.31$$

Therefore, the measurement of the planimeter had to be multiplied by the two factors in equations 4.30 and 4.31 to get the reading in mm^3 of artificial bone. $1PR \ unit = 4.234 \ mm^3 \ AB$ \hspace{1cm} 4.32

This figure (equation 4.32) could be multiplied by the artificial bone density (1.735 g/cm^3) to get it in grammes weight.

$$1 \ PR \ unit = 0.00732 \ g \ AB \hspace{2cm} 4.33$$

or this value (equation 4.33) could be multiplied by the weight percentage of calcium in AB to get the reading in terms of calcium content.

A check was done of artificial bone weight from a trace of artificial bone tube (of 15 mm and 10 mm external and internal diameters) using the optical transform system. The value was compared with the actual artificial bone weight scanned and the difference was 0.3% which is within the accuracy of measuring

the scan area by the planimeter.

4.7   The planimeter accuracy

Two methods were applied to measure the transformed scan area. The first method implemented was to trace the area on a uniform celluloid sheet of thickness 0.253 $\pm$ 0.003 mm and then to cut this area using a sharp pointed steel rod. Five similar areas (about 6 cm^2) were cut in this manner then the weight of each area was measured with a sensitive balance.

The maximum percentage difference between the five individual measurements was 1.65% ($\pm$ 0.8% difference from the mean value).

The same area was measured five times using a disc planimeter (precision disc planimeter, Stanley and Company Limited) with the tracer arm adjusted to its shortest length to give a high scale reading. The maximum percentage difference between individual measurements was 1.03% ($\pm$ 0.52% difference from the mean).

Comparing the error in the two methods, the planimeter method compared favourably with celluloid method. Also, the planimeter method was preferred because it is the quicker and easier measurement.

An area of 5 cm^2 gives a planimeter reading of about 205×10^{-3}. It was decided that the maximum acceptable differences in individual measurements of one area would not exceed 3×10^{-3} of planimeter reading scale. If the difference happened to be greater

.../

than 3×10^{-3}, more readings were taken. Therefore, the maximum possible error in the individual planimeter readings is about 1.3% for 5 cm^2 area and it is inversely proportional to the area.

In planimeter measurement of transformed scan areas the mean of at least three readings was taken. In order to estimate the error in the mean of the three planimeter measurements, a small area of about 1.8 cm^2 was measured nine times. The mean of each three successive readings were calculated and compared with each other. The planimeter reading was 75×10^{-3} with a maximum difference in the mean of 1×10^{-3}. Using this value, the plani-meter error for different sizes of areas can be calculated (see Table 4.3).

4.8   The total accuracy

In any measurement of a transformed scan area the total error is due to three different causes. Systematic errors include those of adjustment of the angle of the object and the image planes. Similarly, the distances 'AO' and 'OC', i.e. object and image distances from the lens focal planes, might not be made exactly equal to twice the focal length. The third possible systematic error is in the alignment of step five in both object (y_5) and image (y_5^*) with the lens axis (see figure 4.7).

Systematic errors could be detected by the inaccurate matching of y_n line images with the respective y_n^* lines in the image screen. Other methods of identifying frame setting error

.../

are failure in obtaining unit lateral magnification in the fifth

step as well as the contrast of the measured value of 'f sec θ'

to the previously calculated value. 'f sec θ' could be measured

experimentally by extending the two image bordering lines (PR and

QZ in fig. 4.7) of a parallel object strip until they meet at 'G'

and then measuring the vertical distance from 'G' to the image line

of the fifth step (GC).

The second source of error is that due to tracing. The

tracing error will be more significant in small areas than in large

ones. This error can be decreased to the minimum by careful

tracing of image points and joining these points in a smooth curve.

The third kind of error springs from the implementation of

the planimeter and is also area dependent and can be estimated

(section 4.7).

To check the accuracy of the optical transform system two

measurements were carried out on two different sizes of transformed

areas, with separate and collective measurements of areas corres-

ponding to individual steps (step image areas). The first

measurement made was on a parallel X-ray film strip, 28 mm wide,

where all 'y_n' lines were plotted. Transformed area of each step

was traced and measured. Similarly, collective areas of the first

step plus the second step $(A_{n\ 1\ +\ 2})$, the first step plus the

second step and the third $(A_{n\ 1\ +\ 2\ +\ 3})$ and so on, were measured

(Table 4.4). The mean unit transformed areas, i.e. $\dfrac{A_{n\ 1\ +\ 2\ .\ .\ +\ n}}{n}$

were calculated in order to compare values easily.

                                                              .../

In individual areas, the maximum difference was 6% with a difference of ± 3% from the mean value. The planimeter error in these small areas was about 1.4%, and any tracing error here will be significant.

In collective step transformed area measurements, i.e. $A_{n\ 1\ +\ 2\ .\ .\ +\ n}$ which is similar to the case in patients' trace, differences in individual step areas will partially compensate for each other. The maximum difference between these areas (normalised to one step area, i.e. $\frac{A_{n\ 1\ +\ 2\ .\ .\ +n}}{n}$) dropped to 2.36%. Planimeter errors in these relatively large areas were small except for the fir st three areas (A_{n1}, $A_{n1\ +\ 2}$, $A_{n1\ +\ 2\ +\ 3}$) where the error values were 1.4%, 0.7% and 0.46% respectively (section 4.7).

Generally in patients' traces the areas cover at least the first five steps (see section 4.10); thus the error in the transformed scan areas ranging from the fifth step onwards will be only 1.1% (Table 4.4). Also in patients the mean width of ulnas, in the site scanned, was found equal to 11 mm, which appeared as twice this width in the trace. In collective measurements done on the transformed areas of a 22 mm wide strip a similar accuracy of about 1% was found.

The second measurement was carried out on a larger area of film strip 80 mm wide. Heights representing steps 0, 3, 6, 9 and 11 were drawn. The transformed areas were traced and measured (Table 4.5). In these large areas the planimeter error was negligible and tracing error will be less significant. The maximum difference in collective areas measured ($A_{n1\ +\ .\ .\ +\ 3}$, $A_{n1\ +\ .\ .\ +\ 6}$,

...../

$A_{n1 + .. + 9}$, $A_{n1 + .. + 11}$) was 1.2% and this agreed with the
first measurements done on the thinner strip for areas higher than
the fourth step.

Other measurements were carried out on the same area to check
the accuracy in the linearity of the transformed areas for different
heights h_n. To do this, areas corresponding to steps 1, 2 and 3
($SA_{n1 + .. + 3}$), $A_{n4 + 5 + 6}$, $A_{n7 + 8 + 9}$ and $A_{n10 - 11}$ were
measured separately. A maximum discrepancy of 2.4% was found
between these areas after normalising (see Table 4.5) which is mainly
due to forementioned systematic error.

4.9   The conclusions

A rough estimation of 29 transformed scan areas of patients'
traces revealed that the smallest one was $4 \ cm^2$. The rest of the
areas ranging from $5 \ cm^2$ and upwards. Simultaneously, the mean
heights of these traces were estimated. In all these traces the
mean height ranged from step five upwards save for one trace in
which the mean height was found to be equal to the fourth step.

In the present setting of the planimeter's arm-tracer, $4 \ cm^2$
is represented by 167×10^{-3} reading in the planimeter scale
(PR units). So the maximum planimeter error in the measurements
of the transformed scan areas in patients traces is 0.6%. The
rest of the error $(2.36 - 0.6 = 1.76\%)$ is mainly systematic.

.../

In the present frame it is not easy to set accurately the required distances and angles because of the difficulties of appropriate adjustment of the object and image plates. Even though this is so, with the present setting it was possible to get 1.1% accuracy for traces with heights ranging from the fifth step which is mostly the case in patients' traces. An extra uncertainty of 1% could occur in the measured scan areas because of the variation in the angle of declination of the base line (section 2.11). This made the total accuracy to be 2.1% in the transformed scan areas of patients' traces.

From the results arrived at it can be concluded that the optical transform system is a feasible technique to do the linearity correction for patients' traces which will enable one to measure, with good accuracy, scan areas representing total mineral content in the site scanned.

Table 4.1

Calculated and measured values

of y_n

n	y_c mm	y_m mm	$y_m - y_c$ mm
0	0	0	0
1	9.43	9.65	0.22
2	18.06	18.25	0.19
3	26.0	25.95	-0.05
4	33.34	33.20	-0.14
5	40.15	40.15	0
6	46.5	46.4	-0.1
7	52.42	52.43	0.01
8	57.97	57.85	-0.12
9	63.19	63.1	-0.09
10	68.1	68.1	0
11	72.74	72.7	-0.04

Table 4.2

Calculated values of y, y^*, h and h^*

n	y_c mm	y^* mm	h mm	h^* mm
0	0	0	-40.15	-35.06
1	9.43	7.41	-30.72	-27.65
2	18.06	15.6	-22.09	-20.46
3	26.00	22.6	-14.15	-13.46
4	33.34	29.42	- 6.81	- 6.64
5	40.15	35.06	0	0
6	46.5	41.56	6.35	6.5
7	52.42	47.9	12.27	12.84
8	57.97	54.11	17.82	19.05
9	63.19	60.19	23.04	25.13
10	68.1	66.15	27.95	31.09
11	72.74	72.00	30.59	36.94

Table 4.3

Maximum expected error in the mean of three planimeter measurements,

for different sizes of areas

Area cm^2	PR mean reading x 10^3	Maximum expected error %
2	83	1.2
4	161	0.6
6	250	0.4
8	346	0.29
10	433	0.23
12	516	0.19

Table 4.4

Individual and collective measurements of transformed areas of a

28 mm wide object

n	A_n PR unit x 10^3	$A_{n4 + . . + n}$ PR unit x 10^3	$\dfrac{A_{n1 + . . + n}}{n}$ PR unit x 10^3
1	71.8	72.7	72.7
2	72.7	145.0	72.5
3	71.3	216.5	72.2
4	71.8	287.7	71.1
5	73.8	362.0	72.4
6	70.3	432.0	72.0
7	74.8	509.0	72.7
8	71.5	580.3	72.5
9	74.0	654.5	72.7
10	73.0	727.3	72.7
11	72.5	800.6	72.8
	Mean value $\dfrac{A_{n1 + . . + 11}}{11}$ $= 72.5$		Maximum Difference = 2.36%

Table 4.5

Transformed area measurements of an 80 mm wide

object

n	A_n PR unit x 10^3	$\dfrac{3A_n}{n}$ PR unit x 10^3	Maximum % Difference
1 + 2 + 3	620.3	620.3	
1 + ..+ 6	1244.0	622.0	
1 + ..+ 9	1879.0	626.3	1.2
1 + ..+ 11	2298.0	627.8	
1 + 2 + 3	620.3	620.3	
4 + 5 + 6	624.0	624.0	
7 + 8 + 9	635.0	635.0	2.4
10 + 11	419.0	628.3	

CHAPTER FIVE

In-vitro Measurements

5.1   Survey of bone indices

The measure resulting from a bone scan (scan area 'SA') is given by equation 1.5 in g/cm:

$$\int Bdw = \frac{P_b}{M_b - M_s} \int \ln \frac{I_2}{I_1} \, dw$$

Where M_b, M_s are the linear attenuation coefficients in cm^{-1} of bone and soft tissue respectively

P_b is bone density in g/cm^3,

I_1 is the X-ray attenuated beam in soft tissue only,

I_2 is the X-ray attenuated beam in bone and soft tissue,

dw is an element of width of bone in the site scanned in cm,

B is the bone mineral mass per unit area in radiation beam path in g/cm^2,

and $\int Bdw$ represents total mineral content per centimeter length of bone. Other investigators call it integral area, area under the curve, area under the trace, bone mass and bone index.

The scan area is a useful measure in serial observations on one patient which often is the case in bone densitometry. It is also useful for checking the reproducibility of the machine. However, when making comparisons of bone mass among individuals or groups, some type of allowance for bone size is generally made in order to reduce the variation and assure that any result showing

.../

differences is not attributable to differences in bone size alone.
It would be ideal to know the volume so that bulk density could be
derived; however, it is difficult to measure this volume in-vivo,
especially in small bones like the ulna and the radius, due to the
significant error involved. The measurements of the bone size
obtained in the scanning technique are overall width and the width
of the medullary cavity.

Smith et al, 1974, and many other investigators (Johnston
et al, 1968, West and Reed, 1970) using monochromatic photon sources
and a detector, adjusted the scan area (SA) to a certain width (w).
Smith, Johnston and Pao-Lo Yo, 1972, reported that the coefficient
of variation of the population was reduced from 14% in SA to 9%

in $\frac{SA}{w}$ for cortical bone, but only a minimal reduction is obtained
in trabecular bone scans. Similar results were reported by Johnston
et al, 1968, who have done scans, using a monochromatic source, on
a large number of radius bones at two sites — at 3 cm distance from
the distal end of the radius which measures primarily cancellous bone
and at 8 cm distance where the bone is mainly compact. The coefficients
of variation were approximately 16% for 8 cm (SA) and 11% for $\frac{SA}{w}$.
Higher coefficients of variations were found for the cancellous site
with 20% coefficients of variation for both (SA) and $\frac{SA}{w}$. The high
variations in (SA) and $\frac{SA}{w}$ in cancellous sites could be due to the
difficulty in positioning the arm in the required place, together
with the rapid changes in bone shape in these sites.

West and Reed, 1970, proposed an index in units of g/cm^3 by
dividing the scan area by the external cross sectional area of the
bone. They called this the 'effective bone density' which is the

.../

overall density of the site scanned including medullary cavity.

The obvious criticism of this unit is that, by expressing the cross-section as $\frac{\pi w^2}{4}$ (where W is the bone width in the scanned site), the bone is taken to be of circular cross-section which is not true. West, R R, 1969, mentioned that although calculating the area from one dimension does not give a true value, it does have the correct dimensions and the correct order of magnitude.

Strandjord and colleagues, 1966, 1970, also used monochromatic photon sources (^{125}I, ^{241}Am) in their in-vivo scanning measurements of the phalanx and os calcis. They measured the scan areas in these sites and expressed their results as the overall linear absorption coefficient (cm^{-1}) of bone. The thickness of the bone was measured from a radiograph. A bone of equal width, but of thinner cortex, would give a lower linear coefficient of absorption. Osteomalacia would also give a lower linear coefficient of absorption. A distinction, there-fore, cannot be made between osteoporosis and osteomalacia (Strandjord et al, 1970).

Many investigators using bone radiography (Barnett and Nordin, 1960, 1961, Anderson, Shimmins and Smith, 1966, Pridie, 1967) have used the cortical thickness for the radiographical assessment of osteoporosis. McGrace , Glas and Sweet, 1967, mentioned that measurable change in cortical thickness appears relatively late in the course of developing osteoporosis. They added that a diagnostic method which depends entirely on the measurement of this change must therefore be regarded as an insensitive procedure.

West and Reed, 1970, defined a further index namely 'cortical bone density' by dividing the (SA) from the scan tracing by the cortical cross-section area, assuming a simple circular geometry ($\frac{SA}{\pi (w-c)c}$, where c is the mean cortical thickness). One of the problems of this index is the inaccuracy in the measurements of the cortices, especially in the case of small bones. With the high spatial resolution of the Aston scanning machine (section 1.2.3.5) which is much higher than that of the radioisotope methods (Table 1.1), it is possible to get better accuracy in measuring cortical thicknesses.

In the absence of accurate in-vivo measurements of bone volume, (SA) and $\frac{SA}{w}$ are so far presumably the best in following an individual, and in detecting differences from normal populations, respectively.

Many investigators (Grace, Glas and Sweet, 1967, Evens et al, 1969, Strandjord et al, 1970, Smith and Cameron, 1972) have started studies with a view to relate bone indices to patholgies of patients, by making value comparison with normal subjects of similar age, sex and race.

5.2   The dead ulna experiments

The techniques discussed in this thesis and many other techniques are based on measurements made on the ulna a few centimeters from the distal end (ulnar styloid).

In order to obtain an idea of the significance of arm re-
positioning errors on scan area and to determine the position in
the trace giving least variation of measured parameters, a number
of measurements were carried out on dead ulnas. The ulnas were
removed from deceased geriatric hospital patients. In all cases the
surrounding tissue has been removed and when not in use the specimens
were kept in formalin in an air-tight container to avoid dehydration
of the bone and marrow.

There are two possible repositioning errors in fixing the
ulna: angular rotation and longitudinal movement. Scans were made
on the ulnas at different angles and distances around the pre-
determined position 3 cm from the ulnar styloid, which is the normal
position used for scanning. A special frame was made for this purpose
to enable accurate rotation and movement of the ulna. Parts of right
and left ulnas (⁓15 cm long) including the ulnar styloid, were
individually fixed in glass tubes at the far end from the ulnar
styloid using wax. Each ulna was fixed accurately horizontal in the
glass tube and a position indicator was fixed with bostik on to the
glass tube (see fig. 5.1). The indicator was made from 6 mm thick
perspex in the shape of a ring with a pointer attached. The hole
of the ring was cut such that the indicator fitted tightly onto the
glass tube holding the ulna. A line was made dividing the pointer
longitudinally to be used as the reference line in rotating the ulna.
A rectangular brass block was made to accommodate the tube of the dead
ulna in the uniform 3.6 cm diameter hole that runs horizontally
through the block. Two (2BA) nylon screws penetrating through two
holes on top of the brass to secure the ulna in position during scanning.
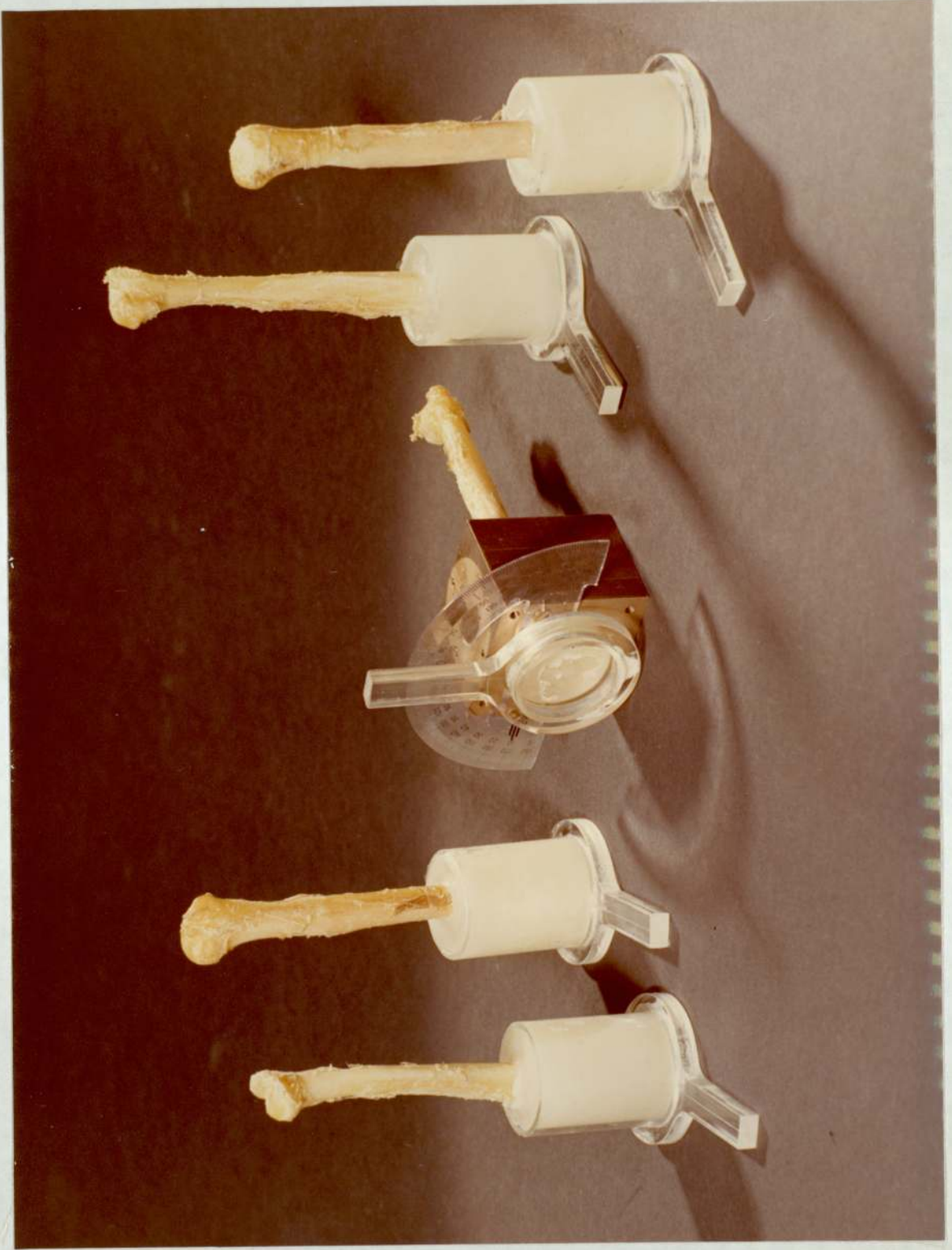
.../

Fig. 5.1   The dead ulnas and the holder

A protractor was fixed to the back of the brass block with two (6BA) counter sunk brass screws as shown in figure 5.1 to enable accurate reading of the angle of rotation.

For the longitudinal movement of the ulna, parallel lines were drawn on the two sides of the perspex frame of the artificial bone stepwedge (fig. 3.9) at 2.5 mm apart, so that the brass block movement, i.e. the ulna will be measured against the scale of this stationary stepwedge frame. In performing a scan the side of the brass block was pushed until it butted against the stepwedge frame.

A total of five ulnas were scanned: three from left arms and two from right arms. Typical traces are shown in figures 5.2, 5.3, 5.4, 5.5. The two peaks heights representing maximum attenuation of X-rays by the ulna were read from the trace against the steps of the stepwedge scanned with it (Tables 5.1 and 5.2). The water level height is equivalent to the zero step. The scan areas of the traces were also measured (Chapter Four) at the different distances from the predetermined position (Table 5.3). The percentage variations of the scan areas at the different positions were calculated with reference to the measured scan area of the ulna, in the predetermined position.

Two figures were plotted showing the peak heights: the first with respect to the ulna position (fig. 5.6) and the second with respect to the angle of rotation (fig. 5.7). A third figure was plotted showing the variation of the scan areas, i.e. the transformed with position (fig. 5.8).

.../

Figs. 5.2, 5.3, 5.4, 5.5   Typical traces of dead ulna at
different distances (D) and angles (θ)

Fig. 5.2   D = 0, θ = 90°

Fig. 5.3   D = 0, θ = 85°
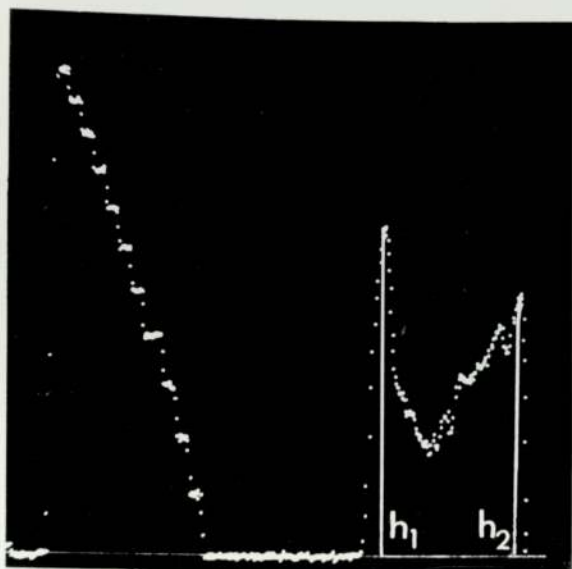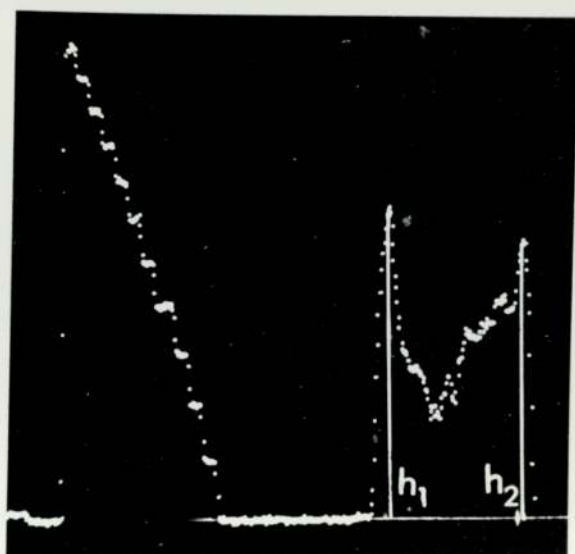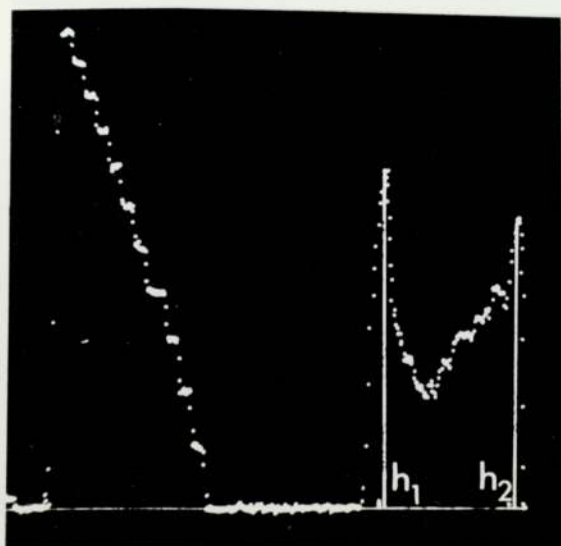
Fig. 5.4   D = 2.5 mm
θ = 90°
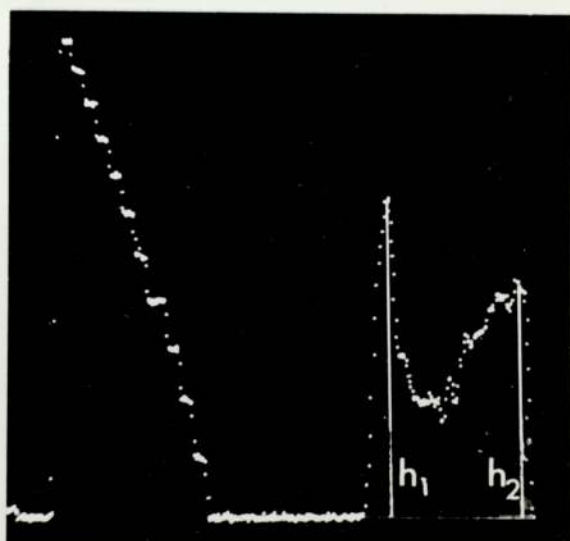
Fig. 5.5   D = -2.5 mm
θ = 90°
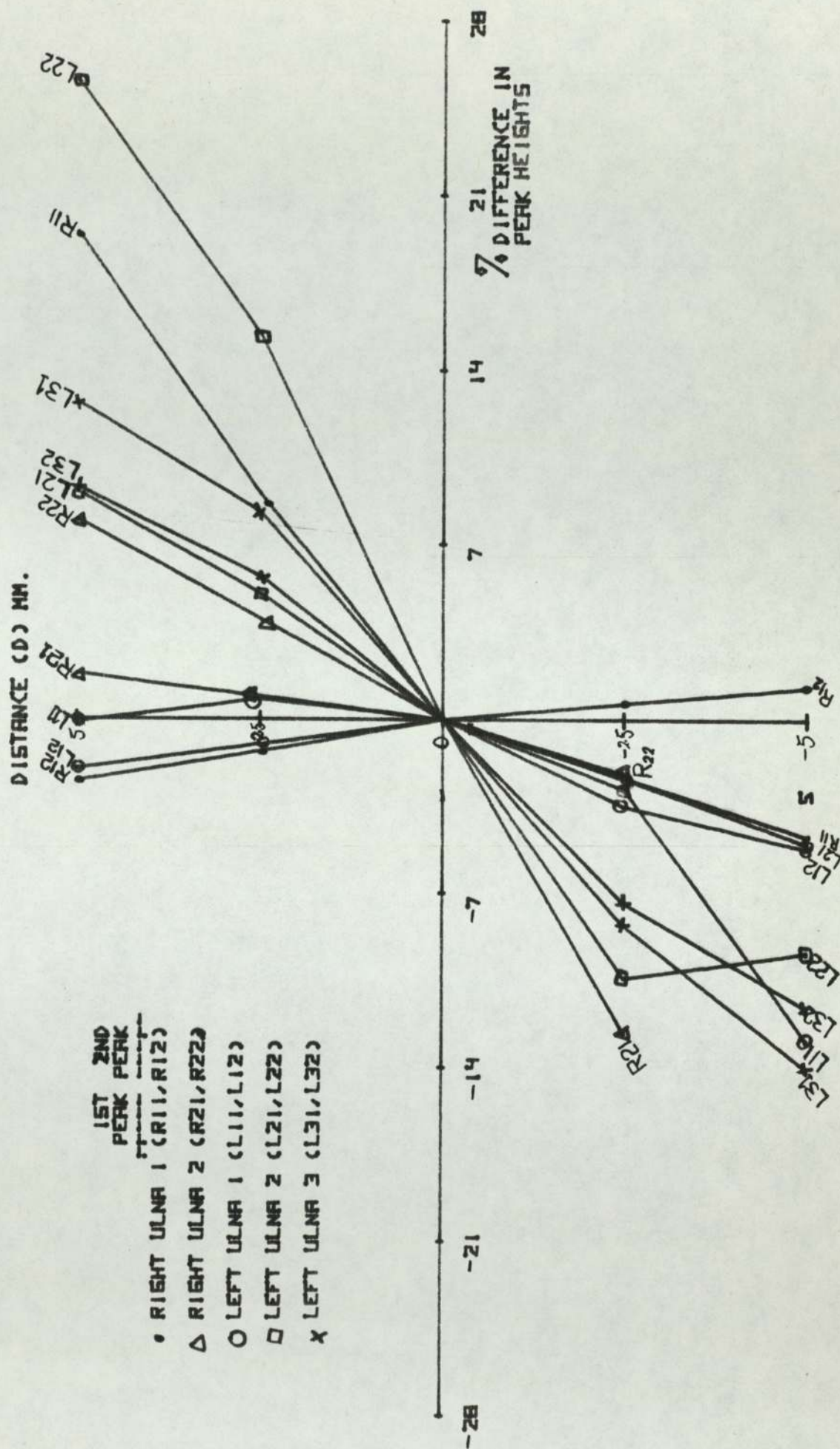
FIG.(5.6) VARIATION OF PEAK HEIGHTS ROUND THE
PREDETERMINED POSITION (D= 0)

ANGLE (B°)

% DIFFERENCE IN PEAK HEIGHTS
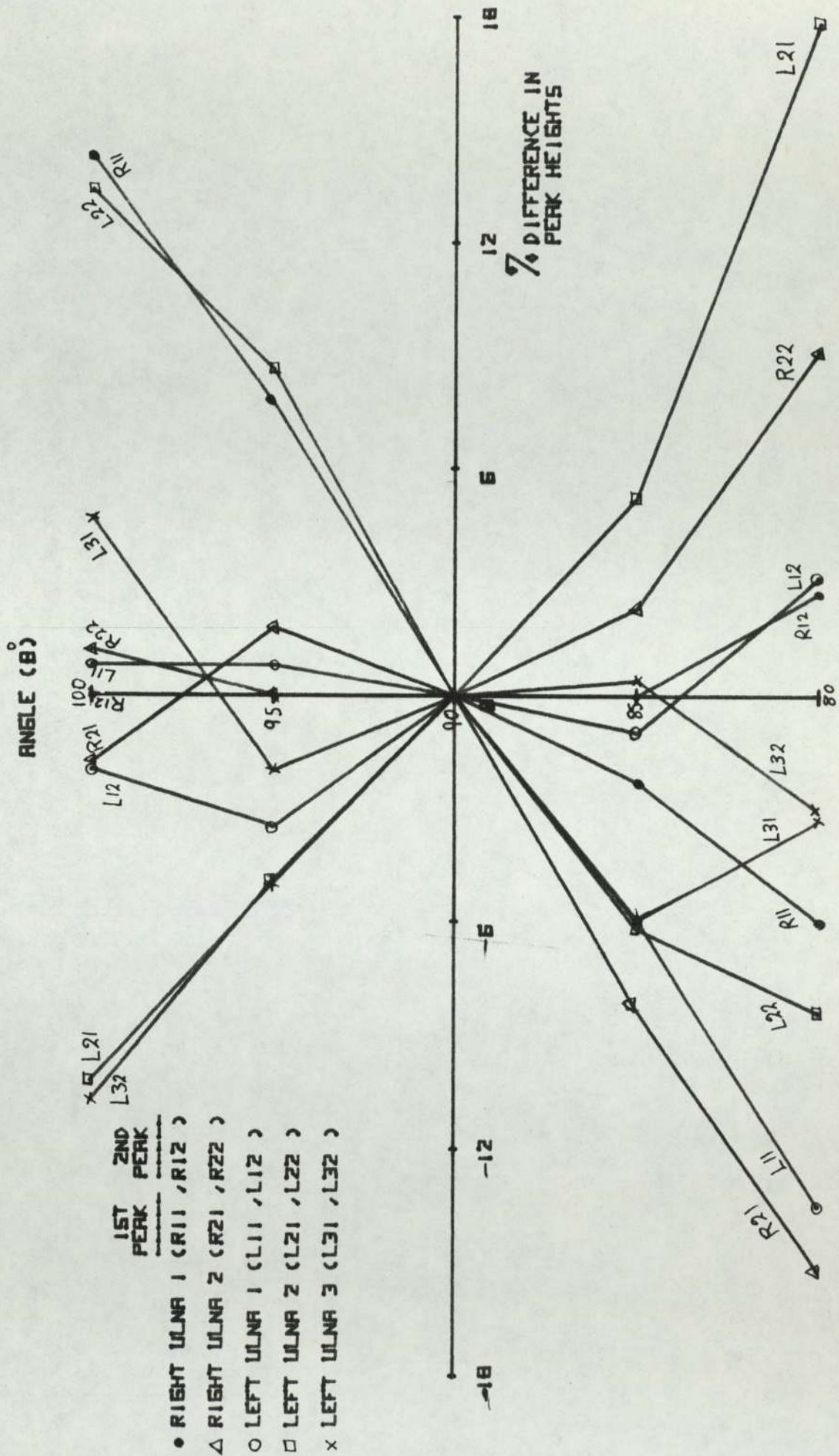
FIG.(5.7) VARIATION OF PEAK HEIGHTS WITH ROTATION (B)

	1ST PEAK	2ND PEAK
● RIGHT ULNA 1	(R11	,R12)
△ RIGHT ULNA 2	(R21	,R22)
○ LEFT ULNA 1	(L11	,L12)
□ LEFT ULNA 2	(L21	,L22)
× LEFT ULNA 3	(L31	,L32)
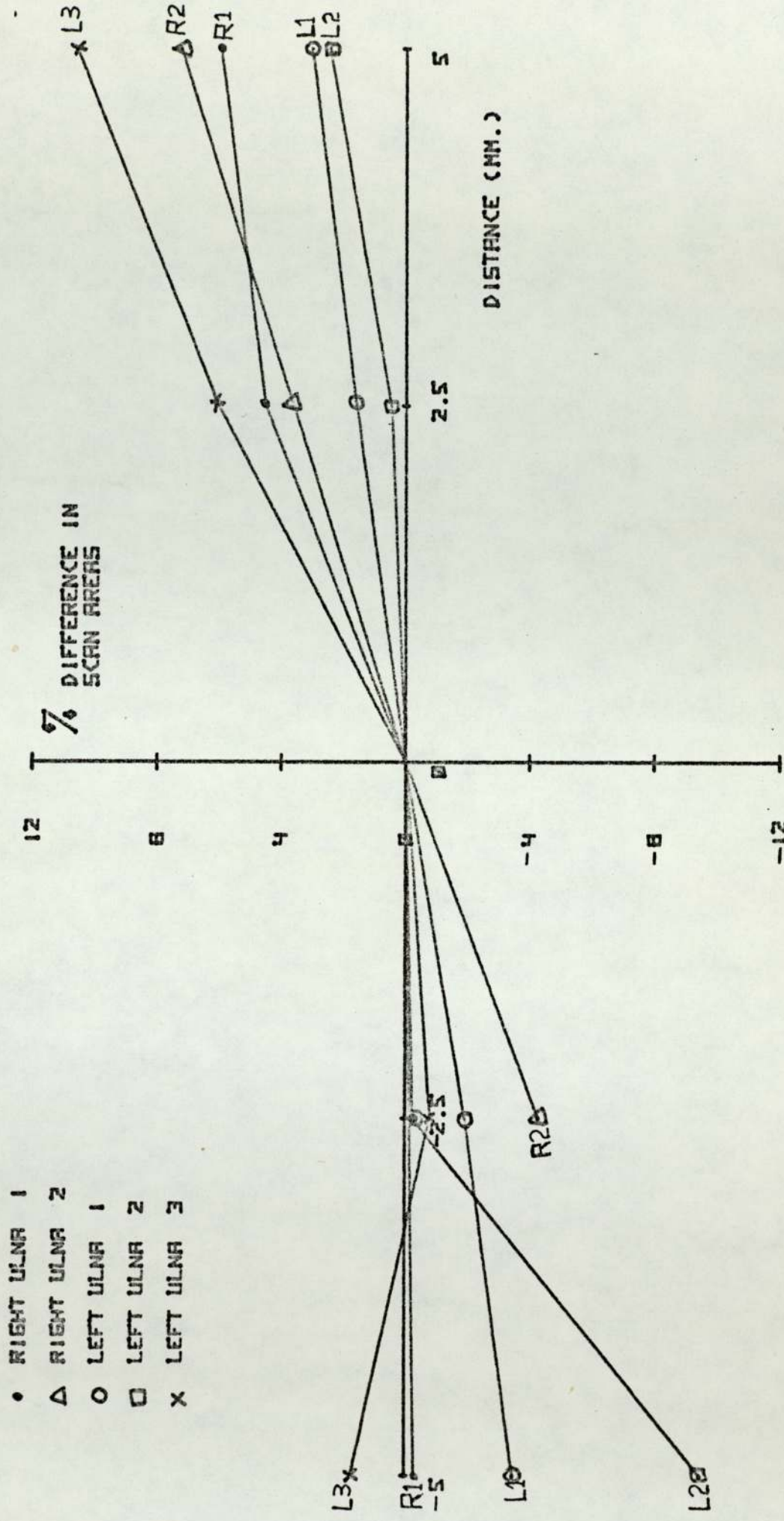
FIG.(5.8) VARIATION OF SCAN AREAS ROUND THE PREDETERMINED POSITION (D=0)

The following conclusions could be derived from figure 5.8.
There are increases in scan areas in the 5 mm movements of the ulna
towards the elbow of 10.6% maximum and there are decreases in scan
areas in moving the ulna 5 mm towards the ulnar styloid of 9.5%
maximum (except in one measurement 5 mm from the predetermined position
where there is 1.7% increase in scan area.) The total variation of
the scan areas in the 10 mm movements of the five ulnas varies from
6% to 12% (Table 5.3). Therefore an error of the order of 1% per
millimeter may result from inaccurate longitudinal positioning.
Introducing bone width (w) to the measured scan areas (SA), i.e.
$\frac{SA}{W}$ did not decrease the differences on measurements of individual
ulnas, but it did decrease differences between the scan areas of
the different ulnas. This was found valid in peak height variations
also. The scan areas at different angles of rotation and the same
position, which should be constant, were measured and the values
were found to be within the experimental accuracy of measuring the
scan areas (section 4.9).

In figure 5.6 of peak height variations with movement, for
both right and left ulnas there are increases in the heights of the
peaks when the scanning position is moved far from the ulnar styloid,
except in two peaks (R_{12}, L_{12}), and vice versa, except in one peak
(R_{12}). Of the five scanned ulnas, the change in the peak heights
(in each ulna) varied from 0 up to 27% with movement of 5 mm either
way in the first peak and, from 0 up to 36% in the second peak.
These increases in peak heights and the increases in scan areas,
mentioned earlier, are due to the increase in the size of the ulna when
moving towards the olecranon. From this result, an increase could

.../

be predicted in peaks with the forward movement of ulna and vice versa. Therefore, if the mineral status of the bone is assessed from peak heights alone, an error of the order of 1.5% per millimeter may result from incorrect longitudinal positioning.

In figure 5.7 the total change in the peak heights (first and second) for the $\pm$ 10° rotation varied from 0 up to 23%. Therefore, if the mineral status of the bone is estimated from peak heights alone, an error of the order of 1% per degree may result from incorrect angular positioning. Looking at the peaks variation with rotation (fig. 5.7) there is nothing in common between the five ulnas and from this result it can be concluded that peak heights are less predictable in terms of angle variation than in terms of ulna position.

From the peak height measurements (Tables 5.1, 5.2), it was found that in four of the five ulnas, the first peak was greater than the second. In the fifth ulna (L_3) the second peak (L_{32}) was significantly greater than the first peak (L_{31}).

The significant differences in the variation of the peak heights (first and second) with the angular and positional changes, reveals the fact that the bone cross-sections differ in shape from one individual to another. This indicates the great inadequacy in using bone width to correct for bone size.

5.3   The relation of the scan areas to in-vitro bone measurements

Measurements were carried out on a number of bone pieces cut from four dead ulnas in order to find the relation between the scan

areas and various in-vitro measurements made on the bone.

The optical transform system was used to give the linear area representation of the scan areas of the traces which were then measured with a planimeter.

A programmable calculator was used in plotting the figures of scan areas with each of the following: bone weight, dry fat-free weight, mineral (ash) weight and calcium content. The correlation coefficients and the fit equations were also calculated.

Good correlations were found between the scan areas and each of bone weight, dry fat-free weight and mineral weight (sections 5.3.3, 5.3.4, 5.3.5). The best correlation was found between scan areas and mineral weight (r = 0.98). The relation of the scan areas to calcium content was also investigated (section 5.3.6).

5.3.1 The preparation of the bone pieces

The ulnas used were removed from deceased geriatric hospital patients. Each ulna section was about 12 cm long including the ulnar styloid. Pairs of ulnas were put horizontal in a rectangular box of cardboard and then the box was filled with a plaster of Paris which was mixed with water to secure the ulnas in position preparatory to cutting. The plaster of Paris was left to dry before cutting the ulnas accurately with a milling machine. The ulnas were greased with vaseline before putting in the cardboard box to enable easy release of the plaster of Paris from the bone pieces. The pieces were washed afterwards with water to remove the remaining plaster of Paris. The length of the bone pieces was cut to 0.5 mm less than the length of

the detector slit which is 9.5 mm, in order to ensure the scanning of the whole piece.

A special perspex frame was made for fixing the bone pieces in the right position above the detector slit during the scanning (section 5.3.2). All the dead bone pieces were immersed in water for ten days to get rid of all the air bubbles in the pieces before doing scane.

Figures 5.9, 5.10, 5.11 and 5.12 show traces of dead bone pieces taken from different ulnas.

5.3.2   The fixing frame

A simple perspex frame was made for securing the bone pieces accurately in the scanning position. The frame consisted of a sheet of perspex 1 mm thick, machined so as to fit tightly into the front gap in the arm fixing frame, i.e. on the scanning side. The perspex sheet was 15.2 cm long and 10.3 cm wide. Two small perspex blocks each with a threaded hole in the middle of each side were fixed onto the perspex sheet (in front of the stepwedge position) using perspex cement   . The perspex blocks were 2.75 cm apart and their holes were made facing each other parallel to the steps of the step-wedge. Two (2BA) screws were threaded in the two holes from outside. The nylon screws were 2.54 cm long each with a perspex ring fixed in front of each screw to its tip. Each perspex ring was 1.9 cm in diameter and 0.3 cm thick.

.../

Figs. 5.9, 5.10, 5.11, 5.12   Typical traces of dead ulnar
                              sections
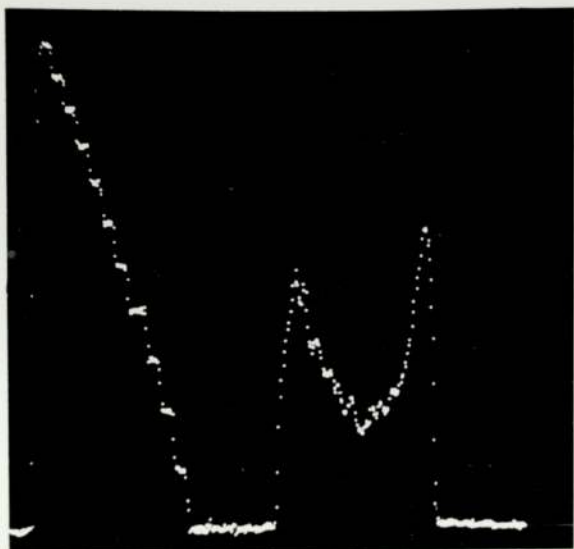
Fig. 5.9
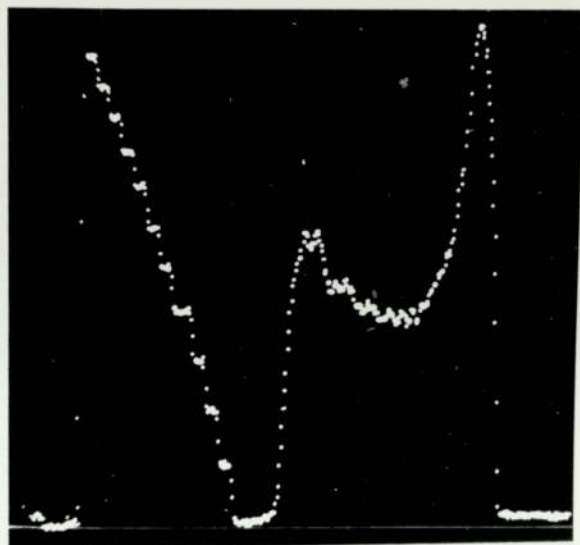
Fig. 5.10
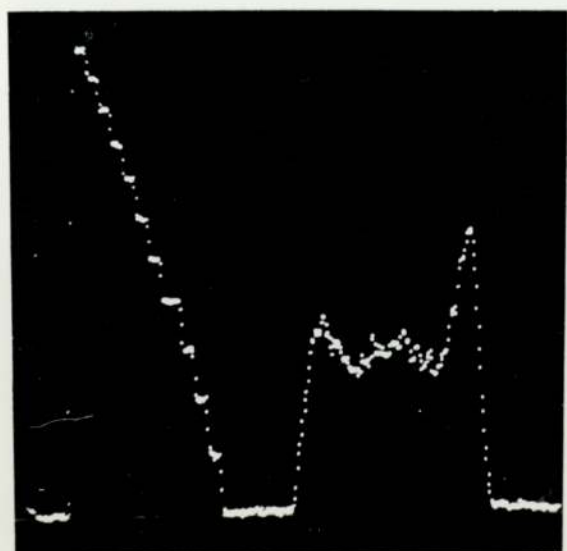
Fig. 5.11
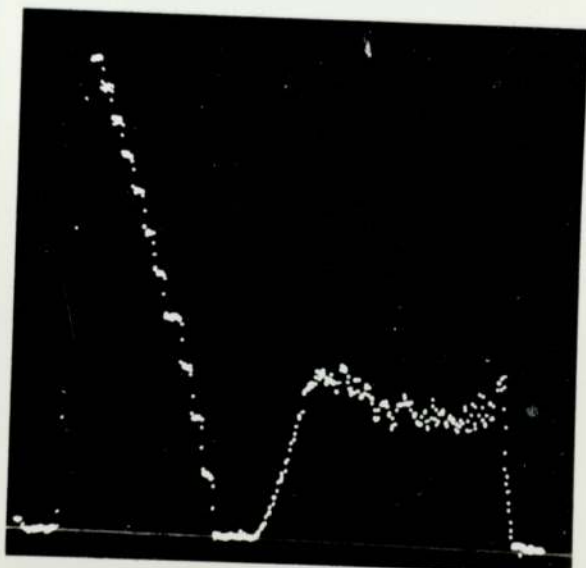
Fig. 5.12

The bone pieces were secured in between the two rings, one by one for scanning. The nylon screws with the perspex rings were used for the alignment of the bone pieces exactly above the slit of the detector. In order to ensure that the whole bone piece is scanned, i.e. the bone piece is exactly above the detector slit, a rectangular 'dural' block was scanned first. The 'dural' block was 9 mm wide, 18 mm long and 8 mm in height. After setting the water bath in position and fixing the arm frame, the perspex fixing frame was inserted with the 'dural' block being fixed widthwise in between the two perspex rings. The X-ray machine was put on manual operation for two seconds exposure. The moving trolley was stationary in a position so that the 'dural' block was in the way of the X-ray ribbon. The output signal was recorded on the oscilloscope screen. The position of the 'dural' block was varied by the use of the two screws until minimum signal was recorded, that was when the 'dural' block caused maximum obstruction of the X-ray beam. There was a possible movement of 0.5 mm in the 'dural' block, where there was no variation in the signal values due to the differences between the slit length and the block width, mentioned earlier. One nylon screw was then left un-touched and all the fixing of bone pieces was done using the second screw. Thirty eight bone pieces were scanned using the perspex frame. The frame can be used for other scanning purposes.

The effect of the 0.5 mm width of the perspex rings which was scanned with each bone piece was found experimentally to cause negligible signal attenuation.

5.3.3 The relation of the scan areas to the bone weight

Nine bone pieces were used in this experiment. The pieces
were left to dry in air for a few days after scanning, then were
weighed separately. The error in weighing is negligible. The
scan areas (Table 5.4) were calibrated in cm^3 artificial bone volume
(section 4.6).

The scan areas are plotted against the bone weight in figure
5.13. The straight line relates the two measured quantities
according to standard linear regression analysis. It is expressed
by the equation

$$SA = -0.203 + 1.392 \, W \qquad\qquad 5.1$$

Where SA is the scan area expressed in cm^3 AB,

and W is the bone piece weight in grammes.

The correlation between the scan areas and the bone weight is high
$(r = 0.96)$.

5.3.4 The relation of the scan areas to the dry fat-free
bone weight

In this experiment twenty one bone pieces were used. Each
one was scanned and the scan area was measured.

To dissolve the bone fat, a solvent solution was prepared by
mixing 50% carbon tetrachloride with 30% acetone and 20% isopropyl
alcohol. Carbon tetrachloride is a good fat solvent. Similarly,
acetone and isopropyl alcohol are two fat solvents but they have the
advantage of mixing with water which enables the carbon tetrachloride
to be in contact with the bone fat since the latter does not mix

SCAN AREA (CALIBRATED
TO ARTIFICIAL BONE
VOLUME ((CM.↑3))
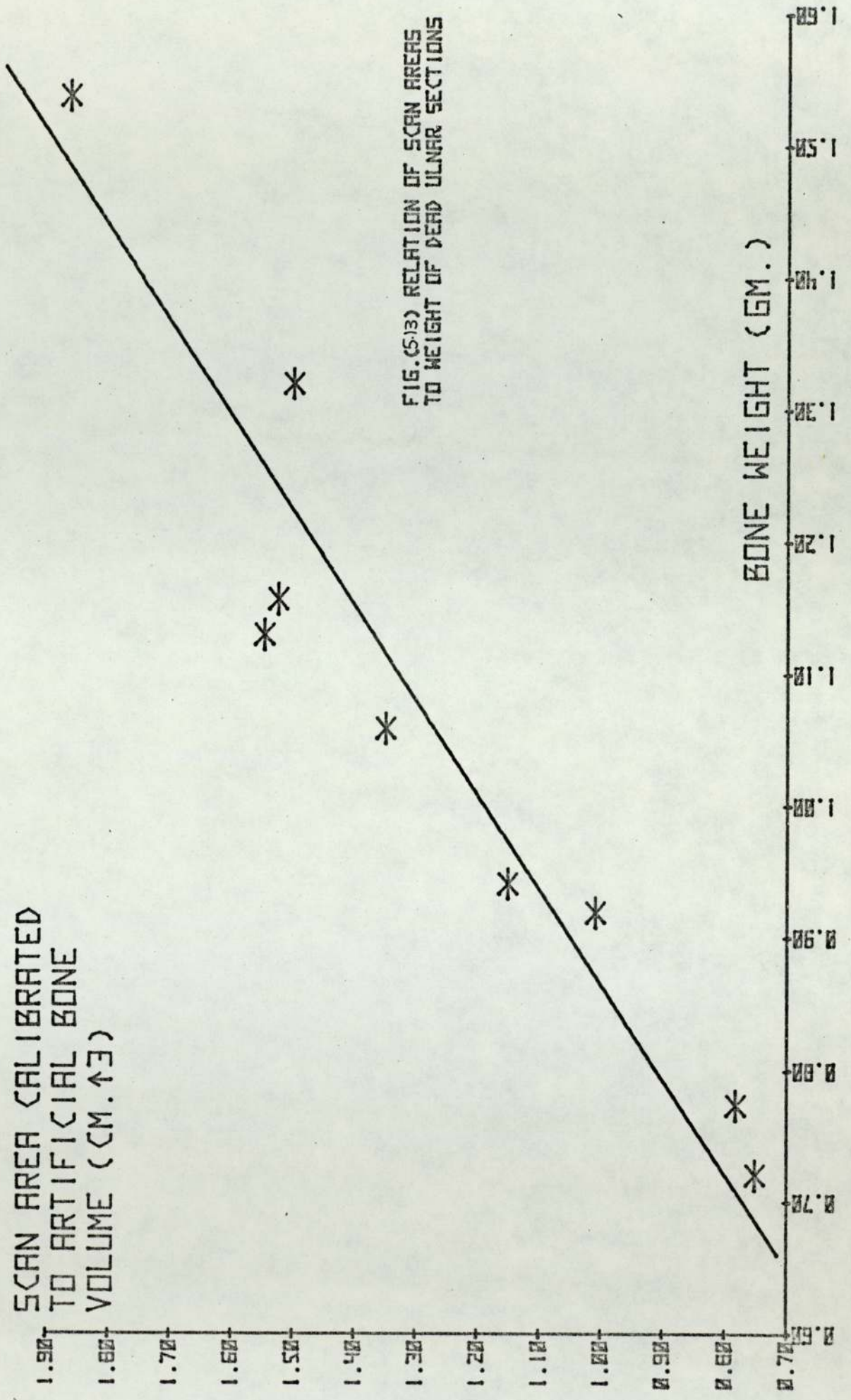
FIG.(5.13) RELATION OF SCAN AREAS
TO WEIGHT OF DEAD ULNAR SECTIONS

BONE WEIGHT (GM.)

easily with water. Solvents like pure acetone or ether and alcohol (1 : 1) were used by other investigators (Cameron, Mazess and Sorenson, 1968).

Each bone piece was put in a test tube containing 20 cc of the fat-solvent solution for a week and the test tubes were sealed. A daily shaking of the test tubes was carried to ensure good diffusion of the solvent solution in the bone. After the end of the week the solvent solution was replaced by fresh solution and left for another week in the test tube.

To dry the bone pieces each was put in a small numbered glass boat and these were placed in an oven at temperature of $104^{\circ}C$. The bone pieces were left in the oven for 24 hours and then were transferred to small sealed weighing bottles. Each bottle was weighed with and without the bone and from these measurements the dry fat-free weight of the bone piece was calculated (Table 5.5). The accuracy of the measured dry fat-free bone weight is about 2% and the uncertainty was caused by moisture absorption.

Figure 5.14 shows the scan areas against the dry fat-free bone weight. The straight line which relates the two measured quantities is expressed by the equation:

$$SA \quad = \quad -0.104 \quad + \quad 1.625 \, W \qquad\qquad 5.2$$

Where   SA is the scan area calibrated in cm^3 AB,

and   W is the dry fat-free bone weight in grammes.

The correlation coefficient is 0.96.

The correlations between the scan areas and both of the dry bone weight (not defatted) and the fat -free (not dried) bone weight were found also to be high (r = 0.96 and 0.95 respectively).

.../

SCAN AREA (CALIBRATED
TO ARTIFICIAL BONE
VOLUME ((CM.↑3)

FIG.(5-14) RELATION OF SCAN AREAS
TO DRY FAT-FREE WEIGHT OF DEAD
ULNAR SECTIONS
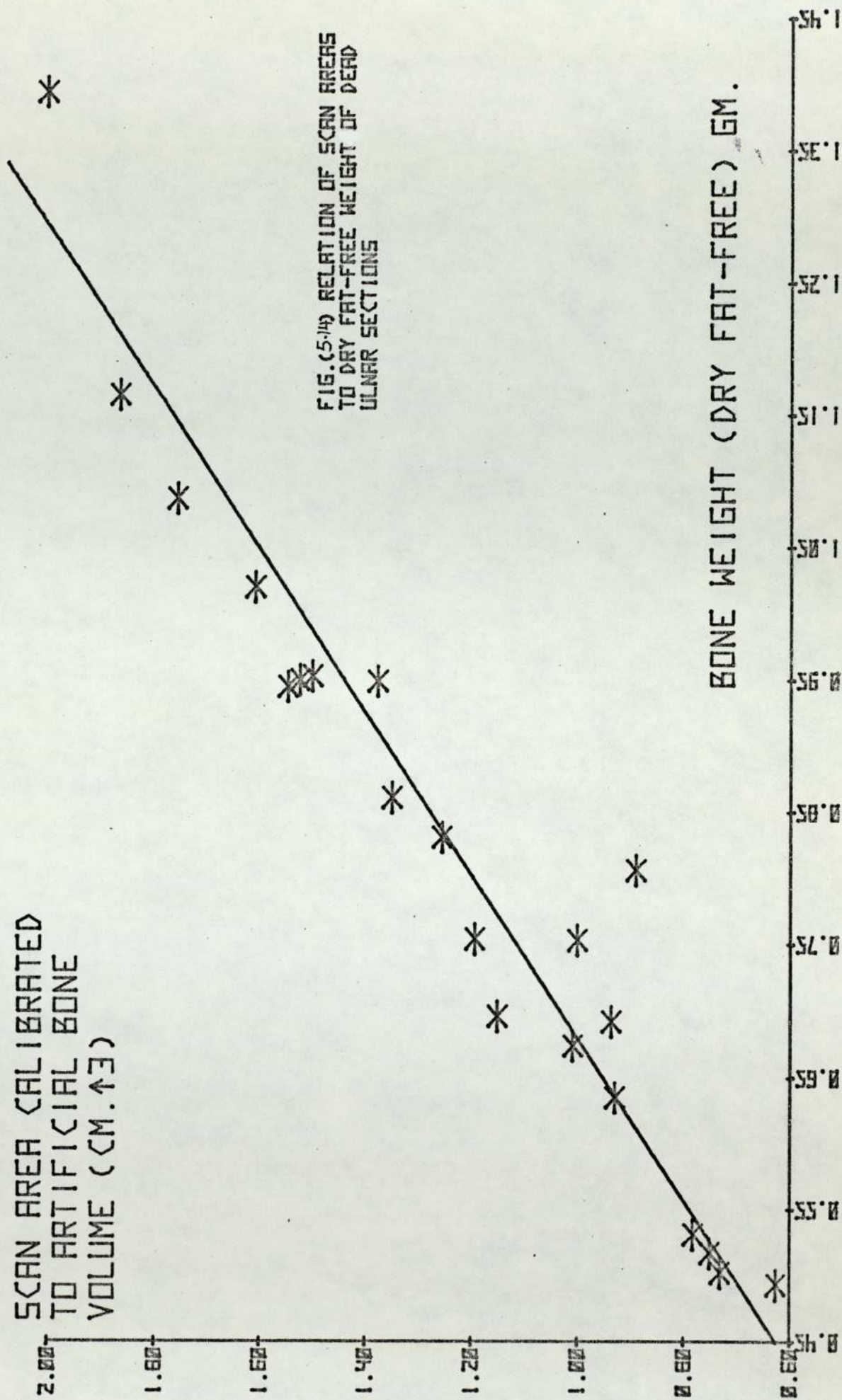
BONE WEIGHT (DRY FAT-FREE) GM.

5.3.5   <u>The relation of the scan areas to the bone mineral</u> <u>weight</u>

The scan area represents the total mineral content of the scanned bone (section 1.2.2). To find experimentally the correlation between the scan areas and the bone mineral weight, twelve bone pieces were put in crucibles and were ashed in a furnace (890° for two hours). The crucible was weighed with and without the mineral from which the latter was determined. The bone samples showed no evidence of having fused with the surface of the silica crucibles in which they were heated and the error in mineral measurements is negligible.

Table 5.6 shows the mineral weight of the different bone pieces together with the scan areas. Figure 5.15 shows the two measurements plotted and the regression line. It is expressed by the equation

$$SA \quad = \quad 2.303 \; W \qquad\qquad\qquad 5.3$$

Where   SA is the scan area calibrated in cm^3 AB,

and   W is the bone mineral weight.

The line passes through the origin. The scan areas were highly correlated with mineral weight ($r \;=\; 0.98$) which shows that the X-ray scan is a good measure of total mineral content of bone. Sorenson, Cameron and Wisconsin, 1967, and other investigators (Shimmins et al, 1972, Smith et al, 1974) used monochromatic photon sources instead of polychromatic sources,and have reached a similar correlation of scan areas to mineral weight.

FIG.(5.5) RELATION OF SCAN AREAS TO WEIGHT OF BONE MINERAL IN SECTIONS OF DEAD ULNAE
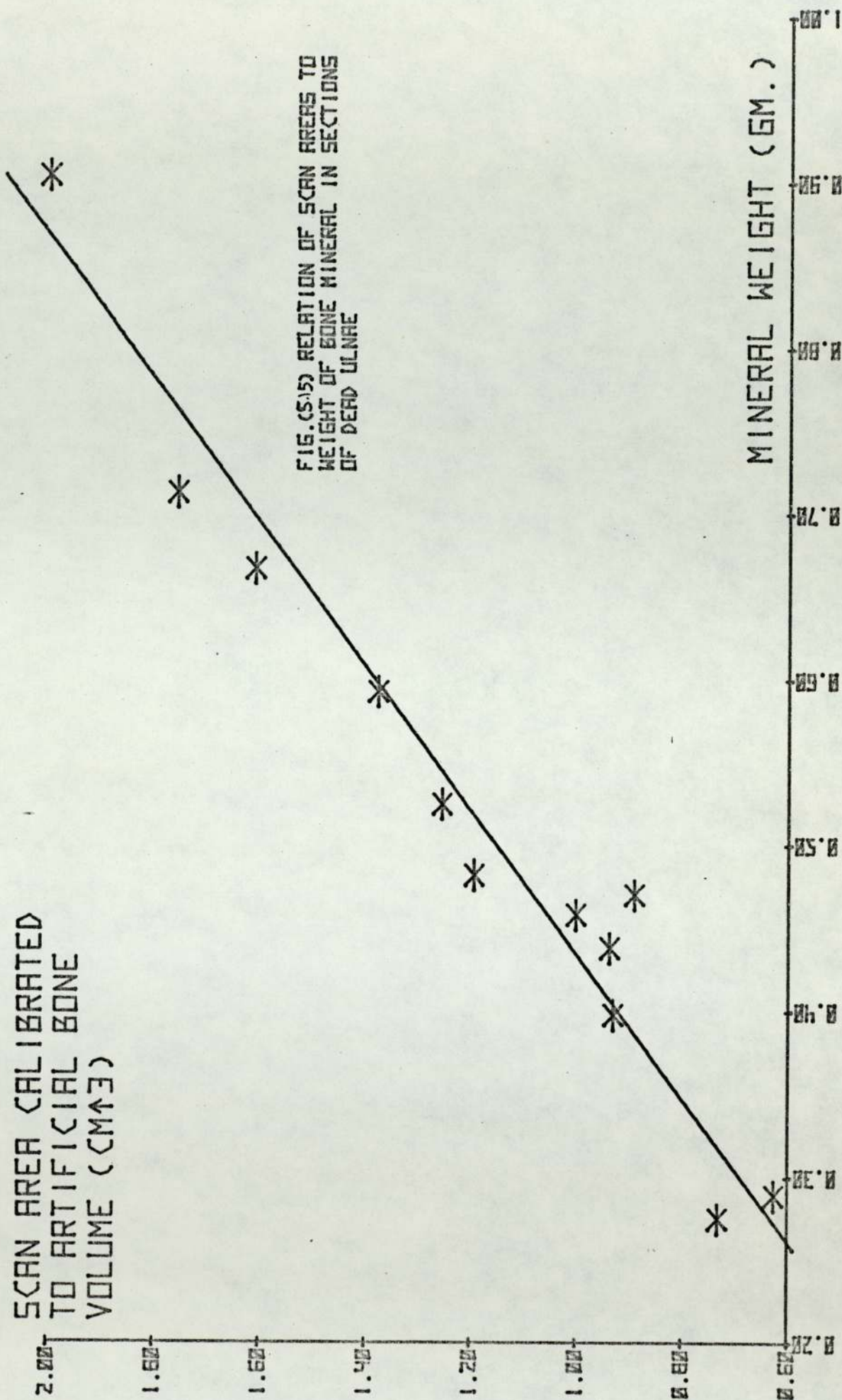
5.3.6   The relation of the scan areas to the bone calcium content

The mean feature in most bone diseases like osteomalacia, rickets or osteoporosis is lack of calcium in the patient's bones. Calcium is one of the main contributors in the absorption of X-rays in bone in the energy range (30 - 90) keV (Table 3.1). Assuming that calcium content is directly proportional to the total mineral content of bone, the calcium content can be calculated from the scan area because the latter is highly correlated to total mineral content (section 5.3.5).

The calcium content for a number of bone pieces, which were scanned, were estimated by neutron activation method (section 5.3.6.1). The correlation of the calcium content to the scan areas may test the assumption that the calcium content is proportional to total mineral.

5.3.6.1   The method

There are different methods of measuring the calcium content of the bone pieces, such as neutron activation analysis and chemical analysis. For the purpose of simplicity and accuracy, neutron activation analysis was chosen using the ^{48}Ca (n, γ)^{49}Ca reaction. The characteristic γ-ray from the decay of ^{49}Ca is 3.1 MeV. Calcium-48 isotope forms only 0.18% of the element and the reaction (with neutrons) does not have high absorption cross-sections. For these reasons, to achieve sufficient ^{48}Ca activation, i.e. low statistical error of small bone pieces, they were activated in the Universities Research Reactor at Risley.

Nine bone pieces were used for this irradiation and four small artificial bone samples were used as standards to calculate the absolute calcium content in each bone piece. In each irradiation, two bone pieces and one artificial sample were irradiated together in a 'rabbit' for one minute. The irradiation time was automatically controlled. The 'rabbit' base was wide enough to take only two pieces and the third artificial bone sample sat above them. Correction was made for the neutron flux variation along the length of the 'rabbit' (section 5.3.6.2). The ninth bone piece was irradiated with one artificial bone sample.

To achieve satisfactory resolution a lithium drifted germanium $[$Ge (Li) $]$ detector was used. The activity was measured for two hundred seconds live time. The total counts of the peak were calculated by a computer connected on line to the counting system.

5.3.6.2   The calculation of bone calcium content

To calculate the calcium content of the bone pieces the following procedure was adopted.

1)   The correction for the differences in actual 'clock' counting time.

The actual 'clock' counting time for each activated piece (Table 5.7) depends on its total activity which determines the dead time of the counter. Differences in actual 'clock' counting times cause varying decay in the activity of the isotope which introduces an error in the measured activity. The correction for the differences of actual 'clock' counting times of the artificial and the real bone

.../

pieces was made by finding the time of 'mean count rate' for each counting time. The following equation was used in determining the time of 'mean count rate'.

$$C_o \, e^{-\lambda t`} = \frac{\int_o^T C_o \, e^{-\lambda t} \, dt}{T} \qquad 5.4$$

Where C_o is the count rate at the beginning of count (t = 0),

t` is the time of 'mean count rate',

$\lambda = \dfrac{0.693}{t_{1/2}}$ is the radioactive decay constant in min^{-1},

and T is the actual 'clock' counting time in minutes
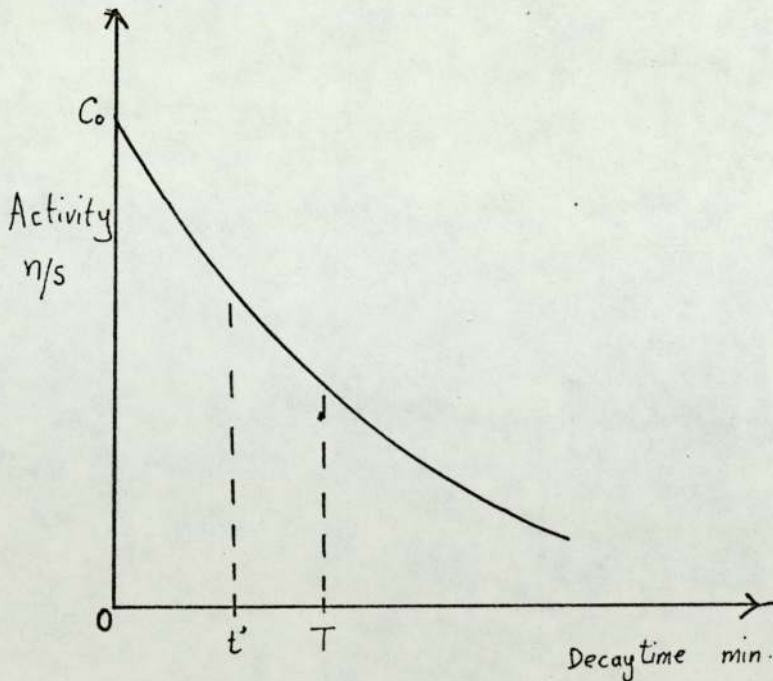
Fig. 5.16 The radioactive decay curve

By integration of equation 5.4

$$t^{\star} = \frac{t_{1/2}}{0.693} \quad \ln \left[\frac{0.693}{t_{1/2}} \frac{T}{(1 - e^{-\frac{0.693T}{t_{1/2}}})} \right] \quad 5.5$$

$t^{\star}$ was calculated using equation 5.5 for each piece and was then added to the recorded decay time (t) (the time from the end of irradiation until the moment of starting counting). The percentage decay for each total decay time ($t^{\star}$ + t) was obtained using the following equation.

$$\left[\frac{I}{C_o} = e^{-\frac{0.693 (t^{\star} + t)}{t_{1/2}}} \right] \quad x \quad 10^2 \quad 5.6$$

Where I is the measured count rate.

2) The correction for the variation in the thermal neutron flux.

The artificial bone samples and the bone pieces were irradiated near the core of the reactor where the thermal neutron flux is approximately 3.6×10^{12} n cm^{-2} sec^{-1}. The artificial bone sample sat above the two bone pieces, which were nearer to the core, in the 'rabbit'. The decrease in thermal neutron flux along the length of the 'rabbit' is approximately 4% per centimeter. Since the length of the bone piece was 0.9 cm (section 5.3.1), the total count of the artificial bone samples were multiplied by $\frac{100}{96}$ to correct the decrease in thermal neutron flux.

3)   The total count rate (TCR) per 1.735 gm (1 cm^3) of artificial bone was calculated using the following formula.

$$AB(TCR) = \frac{1.735}{AB \text{ weight}} \times \frac{1}{\text{\%age decay}} \times \frac{100}{96} \times \text{measure count rate (I)}$$

5.7

Each 1.735 gm of artificial bone contains 0.333 gm calcium (Table 3.5).

4)   The total calcium content in each bone piece was calculated as follows.

$$\text{Calcium content} = \frac{0.333}{AB(TCR)} \times \frac{1}{\text{\%age decay}} \times \text{measured count rate (I)}$$

5.8

Calcium content for the different bone pieces together with the scan areas are shown in Table 5.8.

5.3.6.3   Discussion of the result

Figure 5.17 shows the measured calcium content of the bone pieces plotted against the scan areas. The linear regression equation is:

$$SA = -0.204 + 7.797 \, W \qquad 5.9$$

Where   SA is the scan area in cm^3 AB

and   W is the calcium content measured by N.A.A. method. The correlation is moderate (r = 0.83). It is less than the correlation of the scan areas to bone or mineral weights (sections 5.3.3 and 5.3.5).

.../
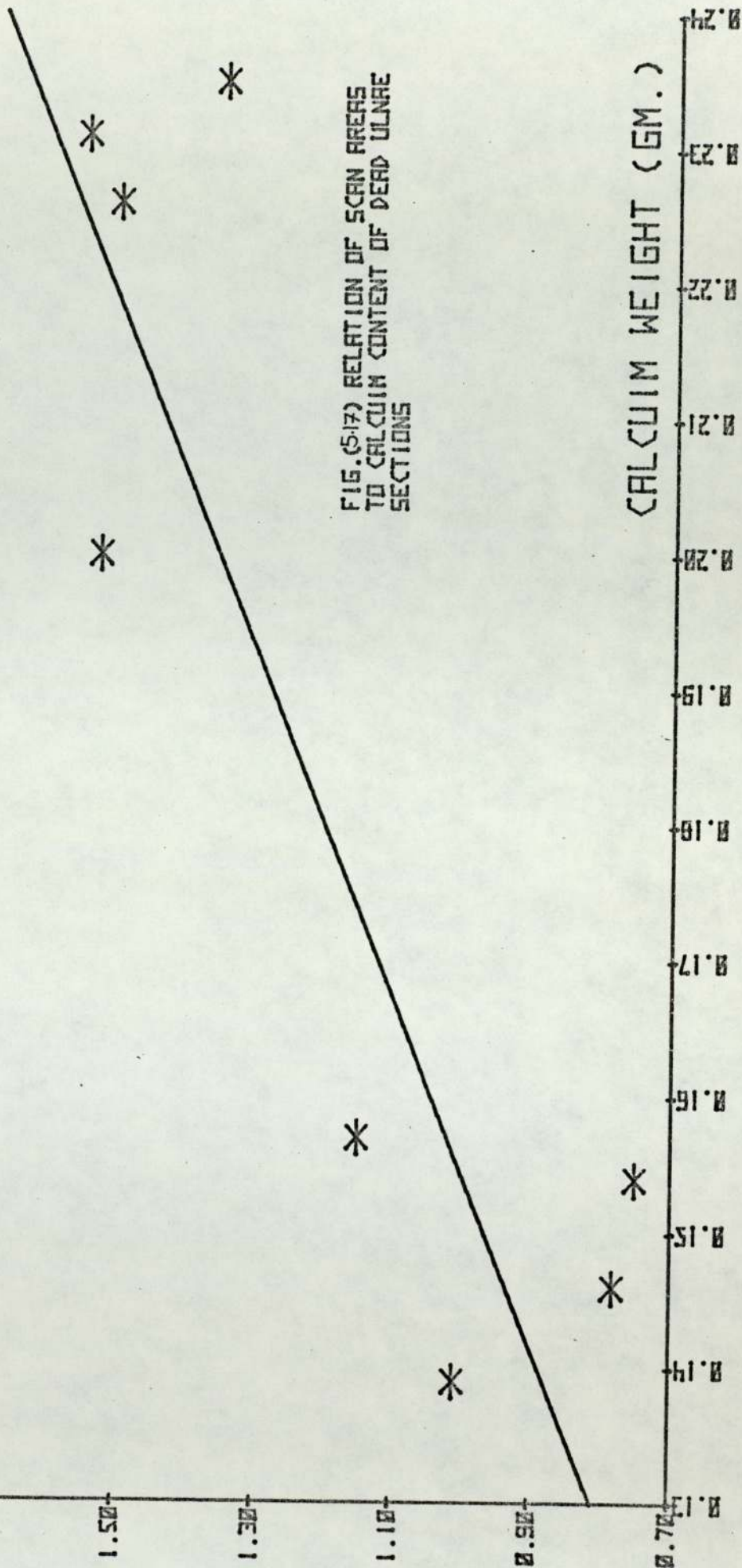
FIG.(5:17) RELATION OF SCAN AREAS TO CALCUIM CONTENT OF DEAD ULNAE SECTIONS

The accuracy of the calcium measurement by the N.A.A. is less than the accuracy of the measurements of the bone weight, dry fat-free bone weight and the bone mineral weight due to the statistical error in total count. The total standard error of deviation includes statistical error of count plus small errors like an estimate of that due to the drop in thermal neutron flux across the piece and the effect of the pieces' configurations on detection efficiency. The total standard error of deviation is equal to

$$D = \pm \sqrt{D_1^2 + D_2^2 + D_3^2 + D_4^2} \qquad 5.10$$

Where D_1 is the standard deviation in the count of the
          artificial bone sample irradiated with the bone piece
          and it is expressed as fractional error.
          D_2 is the standard deviation in the count   of the
          bone piece expressed as a fractional error,
          D_3 is the fractional error due to the drop in thermal
          neutron flux across the bone piece (estimated 1%),
and D_4 is the fractional error in detection due to
          differences in the shapes of the bones (estimated 1%).

The total standard error of deviation in the measured calcium content of each bone piece was calculated (Table 5.8) and were drawn in figure 5.18 to show the possible values of calcium content. The standard error in measuring the scan areas is $\pm$ 1% (section 4.9).

For better understanding of the relationship between the above-mentioned measurements, more accurate calcium measurement is required. High correlation will support the theory that calcium in bone is in a main salt which is the same in the different individuals. If the

SCAN AREA (CALIBRATED
TO ARTIFICIAL BONE
VOLUME (CM.↑3)
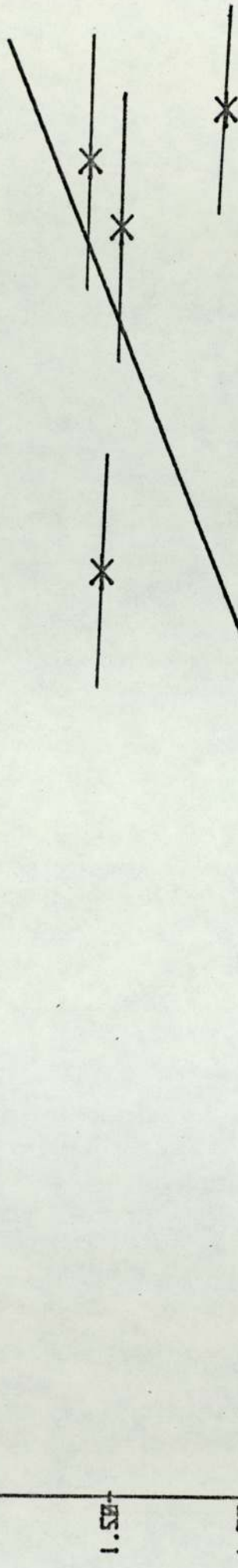
FIG.(5·18) RELATION OF SCAN AREAS
TO CALCUIM CONTENT OF DEAD ULNAR
SECTIONS

CALCUIM WEIGHT (GM.)

correlation is not high this could be explained by the presence of different calcium compounds in bone having different calcium percentages and their contribution in bone varies from one individual to another.

5.4   The right measurements to make

In the Aston technique the displayed trace on the oscilloscope is photographed on an X-ray film. For a quick comparison of two or more results, the traces (negatives which are partially transparent) can be superimposed and changes in bone mineral content or dimensions may readily be seen. However, for an assessment of the changes in mineral content, the scan areas have to be measured to compare the values. Bone calcium content can also be estimated from the scan areas (section 4.6) and compared.

In order to have an accurate comparison of bone densities in different individuals with different sized bones, the bone volumes (in the site scanned) need to be obtained together with the scan areas. Without an accurate measure of volume, the measurement of photon beam transmission tells us nothing about bone density what-ever, the photon source or detector. Bone volume can be estimated from other measurements, that is, from a set of radiographs made at different angles (X-ray tomography). The accuracy of these measure-ments in-vivo is still poor specially for small bones like the ulna. Research is being conducted at Aston University by A I Bashter to develop an ultrasonic machine with a view to drawing the external circumference of bones in-vivo, hopefully with greater accuracy.

Until the availability of such a machine, which is intended to be an integral part of the scanning technique, bone width could be used as a type of correction for bone size by adjusting the scan areas to a chosen width. This tends to decrease the coefficient of variation of the population especially for cortical bone sites (see section 5.1) as is the case in our measurements carried out about 3 cm proximal to the ulnar styloid.

Table 5.1

The first and second peak heights (h_1 and h_2) measured against the
standard stepwedge in traces of dead ulnas done at and around the
predetermined position (D = 0)

Ulna	Trace No.	Position D min	h_1 step	$\dfrac{h_1 - h_{10}}{h_{10}}$ %	h_2 step	$\dfrac{h_2 - h_{20}}{h_{20}}$ %
Right 1			R_{11}		R_{12}	
	328	0	6	0	5.57	0
	335	2.5	6.54	9	5.50	-1.3
	336	5.0	7.17	19.5	5.43	-2.5
	337	-5.0	5.72	-4.7	5.64	+1.3
2			R_{21}		R_{22}	
	338	0	9.73	0	7.33	0
	343	5.0	9.91	1.8	7.92	8.0
	344	-2.5	8.5	-12.6	7.17	-2.2
Left 1			L_{11}		L_{12}	
	348	0	9.92	0	8.08	0
	357	2.5	10.00	0.8	8.0	-1.0
	358	5.0	9.91	-0.1	7.92	-2.0
	355	-2.5	9.64	-2.8	7.8	-3.5
	356	-5.0	8.64	-12.9	7.66	-5.2
2			L_{21}		L_{22}	
	398	0	6.58	0	5.0	0
	405	2.5	6.91	5.0	5.77	15.4
	406	5.0	7.18	9.1	6.28	25.6
	407	-2.5	6.42	-2.4	4.48	-10.4
	408	-5.0	6.25	-5.0	4.53	-9.4
3			L_{31}		L_{32}	
	409	0	6.0	0	9.83	0
	410	2.5	6.5	8.3	10.39	5.7
	411	5.0	6.76	12.7	10.74	9.3
	412	-2.5	5.5	-8.3	9.1	-7.4
	413	-5.0	5.16	-14.0	8.69	-11.6

Table 5.2

The first and second peak heights (h_1 and h_2) measured against the
standard stepwedge in traces of dead ulnas at the predetermined
position at different angles

Ulna	Trace	Angle θ	h_1 step	$\dfrac{h_1 - h_{10}}{h_{10}}$ %	h_2 step	$\dfrac{h_2 - h_{20}}{h_{20}}$ %
Right 1			R_{11}		R_{12}	
	328	90	6.0	0	5.57	0
	329	85(left)	6.46	7.7	5.57	0
	330	80	6.86	14.3	5.57	0
	331	95 (rt)	5.86	-2.3	5.57	0
	332	100	5.64	-6.0	5.72	2.7
2			R_{21}		R_{22}	
	338	90	9.73	0	7.33	0
	339	85	9.91	1.8	7.33	0
	340	80	9.55	-1.8	7.42	1.2
	341	95	8.92	-8.3	7.5	2.3
	342	100	8.25	-15.2	8.0	9.1
Left 1			L_{11}		L_{12}	
	348	90	9.92	0	8.08	0
	351	85	10.00	0.8	7.8	-3.5
	352	80	10.00	0.8	7.92	-2.0
	349	95	9.33	-5.9	8.0	-1.0
	350	100	8.58	-13.5	8.33	3.1
2			L_{21}		L_{22}	
	398	90	6.58	0	5.00	0
	401	85	6.25	-5.0	5.43	8.6
	402	80	5.91	-10.2	5.67	13.4
	399	95	5.92	5.2	4.69	-6.2
	400	100	7.75	17.8	4.58	-8.4
3			L_{31}		L_{32}	
	414	90	6.0	0	9.88	0
	417	85	5.88	-2.0	9.4	-4.9
	418	80	6.28	4.7	8.82	-10.7
	415	95	5.64	-6.0	9.92	0.4
	416	100	5.8	-3.3	9.6	-2.8

Table 5.3

The measurements of the scan areas for five dead ulnas done at and around the predetermined position 3 cm from the ulnar styloid

Ulna		Trace No	Position D mm	Scan Area PR unit x 10^3	$\dfrac{A_D - A_O}{A_O}$ %
Right	1	328	0	165.8	0
		335	2.5	175.7	5.97
		336	5.0	173.3	4.52
		337	-5.0	166.3	-0.3
	2				
		338	0	245.2	0
		343	5.0	263.0	7.26
		344	-2.5	234.7	-4.28
Left	1				
		348	0	370.6	0
		357	2.5	376.5	1.59
		358	5.0	381.9	3.05
		355	-2.5	363.5	-1.92
		356	-5.0	357.7	-3.48
	2				
		398	0	210.5	0
		405	2.5	211.5	0.48
		406	5.0	215.7	2.47
		407	-2.5	210.0	-0.24
		408	-5.0	190.6	-9.45
	3				
		409	0	161.9	0
		410	2.5	171.7	6.05
		411	5.0	179.1	10.62
		412	-2.5	160.6	-0.8
		413	-5.0	164.7	1.73

Table 5.4

Scan areas and weight for different dead ulnar sections

(The scan areas are calibrated to AB volume)

Trace No.	Bone Weight W gm	Scan Area SA PR.unit x 10^3	Scan Area SA cm^3 AB x 1/2
436	1.538	440.0	0.931
438	0.919	238.3	0.504
439	0.941	271.8	0.575
442	0.721	177.5	0.376
443	0.774	184.8	0.391
441	1.130	365.3	0.773
454	1.132	354.3	0.750
455	1.059	318.7	0.675
459	1.157	360.0	0.762

Table 5.5
Scan areas and weight (dry fat-free) for different dead ulnar sections

(The scan areas are calibrated to AB volume)

Trace No.	Bone Weight (dry fat-free) W gm	Scan Area SA PR.unit x 10^3	Scan Area SAcm^3 AB x 1/2
429	0.692	221.3	0.468
430	1.394	472.0	0.999
431	0.806	210.3	0.445
435	0.949	325.0	0.688
437	0.753	236.3	0.500
440	0.831	296.3	0.627
445	0.635	219.7	0.465
446	1.087	414.7	0.878
447	1.020	379.8	0.804
449	0.502	173.0	0.366
451	0.493	148.0	0.313
456	0.754	281.7	0.596
436	1.165	440.0	0.931
438	0.674	238.3	0.504
439	0.696	271.8	0.575
442	0.517	177.5	0.376
443	0.531	184.8	0.391
441	0.945	365.3	0.773
454	0.953	354.3	0.750
455	0.861	318.7	0.675
459	0.950	360.0	0.762

Table 5.6

Scan areas and mineral weight for different dead ulnar sections

(The scan areas are calibrated to AB volume)

Trace No.	Bone Mineral Weight W gm	Scan Area SA PR.unit x 10^3	Scan Area SA cm^3 AB x 1/2
429	0.438	221.3	0.468
430	0.904	472.0	0.999
431	0.470	210.3	0.445
435	0.593	325.3	0.688
437	0.458	236.3	0.500
440	0.525	296.3	0.627
445	0.398	219.7	0.465
446	0.713	414.7	0.878

Table 5.7

Measured activities of ^{49}Ca for different AB and bone 'B' pieces together with $T^{(1)}$, $t^{`(2)}$, $t^{(3)}$ and the percentage decay in time $(t^{`} + t)^{(4)}$

Piece No	Weight gm	T min	t` min	t min	t` + t min	% decay in(t+t`)	Measured count rate I-count/min
AB 1	1.7514	4.383	2.113	20	22.113	17.5	945
B 455		4.65	2.243	14.33	16.573	27.11	1064
B 459		5.833	2.802	3.0	5.802	63.33	2119
AB 2	1.7611	4.6	2.221	21.0	23.221	16.06	1291
B 436		5.9	2.823	14.0	16.823	26.58	1442
B 438		5.417	2.617	7.0	9.617	46.88	1615
AB 3	1.7546	4.583	2.265	15.0	17.265	25.67	1397
B 441		5.083	2.451	9.0	11.451	40.58	1573
B 439		5.45	2.629	2.0	4.629	69.44	1832
AB 4	1.7592	4.65	2.243	14.0	16.243	27.99	1468
B 442		4.467	2.157	8.0	10.157	44.94	968
B 443		4.9	2.366	2.0	4.366	70.92	1608
AB 1	1.7514	4.617	2.231	13.0	15.231	30.00	1508
B 454		5.5	2.649	5.0	7.649	54.73	1844

(1)   T is 'actual' counting time

(2)   t` is time of 'mean count rate'

(3)   t is recorded decay time

(4)   t` + t is total decay time

Table 5.8

Scan areas and calcium weight for different dead ulnar sections

(The scan areas are calibrated to AB volume)

Trace No.	Scan Area SA PR.unit x 10^3	Scan Area SA cm^3 AB x 1/2	Calcium Wt W gm	Standard Error of Deviation (in W) %
436	440	0.931	0.219	4.8
438	238.3	0.504	0.139	4.4
439	271.8	0.575	0.157	4.1
441	365.3	0.773	0.231	4.2
442	177.5	0.376	0.154	4.7
443	184.8	0.391	0.146	4.1
454	354.3	0.750	0.226	4.1
455	318.7	0.675	0.235	4.9
459	360.0	0.762	0.200	4.5

CHAPTER SIX

Clinical Experience

6.1   Scanning the subject

This has to be done quickly and with the minimum inconvenience to the subject. The subject was first told briefly and simply how the machine operates and what he was required to do. The subject's sleeving was then removed or folded away to expose the majority of the arm (Edwards, J, 1973). The height of the patient was then estimated (section 2.8) to see whether any platform was needed for him to stand on. With the artificial bone stepwedge in position, the arm was immersed in the bath (which was filled with warm water containing small amounts of NaCl and KCl) and it was in such a position that the ulnar styloid resting firmly against the perspex block (fig. 2.18). This was done just before the start of the scanning (to minimise discomfort to patient) by releasing the compression spring adjacent to the ulnar styloid.

After allowing the subject to adopt the most convenient position, the respective straps over the thumb and the fifth finger were carefully tightened until the arm was held firmly in a supinated position. The depth fixer was inserted over part of the arm to be examined and a note was taken of the position of the ulnar styloid (see section 2.7).

Two to three traces were taken at sites 3 mm apart after which the arm was released from the bath and negative films developed.

A check-list was consulted in doing a scan.

.../

6.2   In-vivo measurements

The scanning technique of bone mineral measurement has been used on a few volunteers and on several cases involving metabolic changes in calcium level. Several measurements include patients who are undergoing regular dialysis by the artificial kidney and patients diagnosed as osteoporotic and osteomalacic. Some of the patients were undergoing medical treatment like vitamin D and calcium supplement and others were on low protein diets. In the majority of the cases, total calcium measurements by neutron activation analysis were done about every six months in Birmingham University. The results are not sufficient to make a comparison with the N.A.A. measurements in all cases.

At this early stage of the measurements, it is not possible to give a complete clinical analysis of the traced collected.

Traces of three healthy people of different ages are shown in figures 6.1, 6.2 and 6.3. In the early scanning measurements, the ivory stepwedge was used as a calibration standard (figs. 6.1 and 6.2) but later a stepwedge from the artificial bone was used instead (fig. 6.3).

The variation in the signals representing transmitted X-rays in the arms' soft tissues plus the extra tissue equivalent liquid, is apparent in all the traces which shows the differences in their composition. Part of the variation is due to inaccuracy in the over-laying tissue equivalent liquid (section 3.2) to stimulate soft tissues in X-ray attenuation.
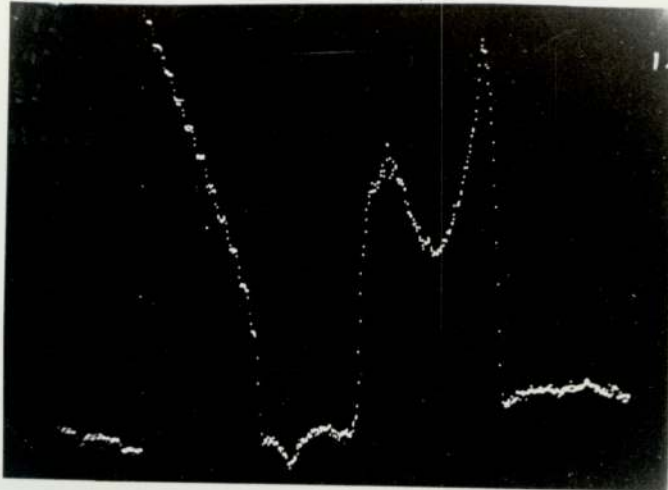
Fig. 6.1   A trace of an in-vivo ulna of a healthy
           subject, 56 years old, and the ivory
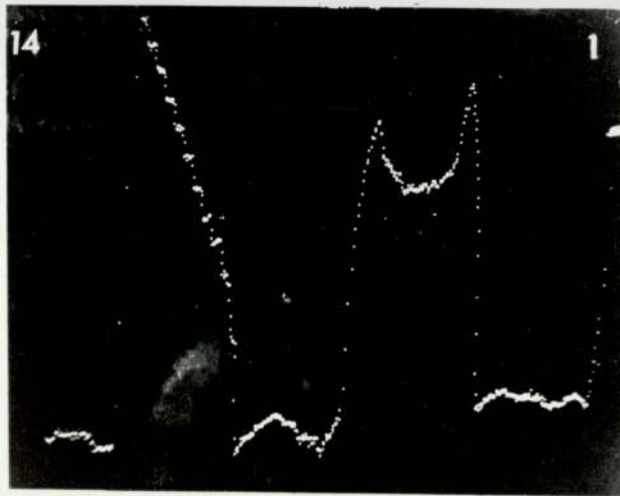

Fig. 6.2   A trace of an in-vivo ulna of a healthy
           subject, 25 years old, and the ivory
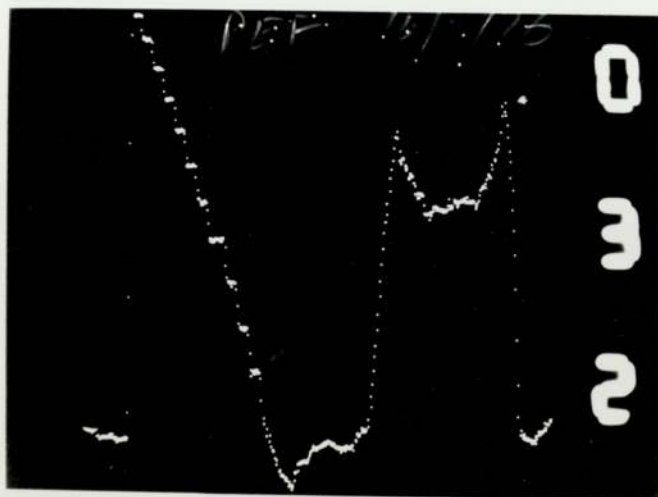   step wedge

Fig. 6.3   A trace of an in-vivo ulna of a healthy
           subject, 47 years old, and the artificial
           bone step wedge

In metabolic bone diseases, a loss of a certain fraction of bone density may occur either as a loss of cortical bone density (porosity) or as cortical thinning (West, R, 1969). The two losses may co-exist (Barnett and Nordin, 1961). Figure 6.4 shows a scan of a pregnant women (7 - 8 months), 19 years old, who suffers from a severe osteomalacia. It appears that there is a decrease in mineral content throughout the cross-section of the bone with a significant decrease in the first peak.

Figure 6.5 shows a scan of an old woman, 72 years of age, who was suspected of developing osteoporosis. The cortex widths are rather small in comparison with the bone width.

Figure 6.6 is a trace of a woman patient who had kidney failure and was put on low protein diet. The first peak (representing the first maximum attenuation of X-rays in the ulna) is level with that representing the X-ray attenuation in the middle of the ulna which includes the medulla.

In two measurements carried out six months apart, on two dialysis patients who are receiving vitamin D and calcium supplements, it seems that there was an increase in overall mineral as shown in figures 6.7 and 6.8. In the two cases the patients felt an improvement in their cases.

Generally speaking, in all patients' cases examined there are decreases in mineral content throughout the bone (in comparison with traces of healthy people) which differ in degree from one individual to another and it appears that there are also new distributions of mineral throughout the bone. Vogel and Anderson, 1969, who used a rectilinear scanner with a monochromatic photon source have studied
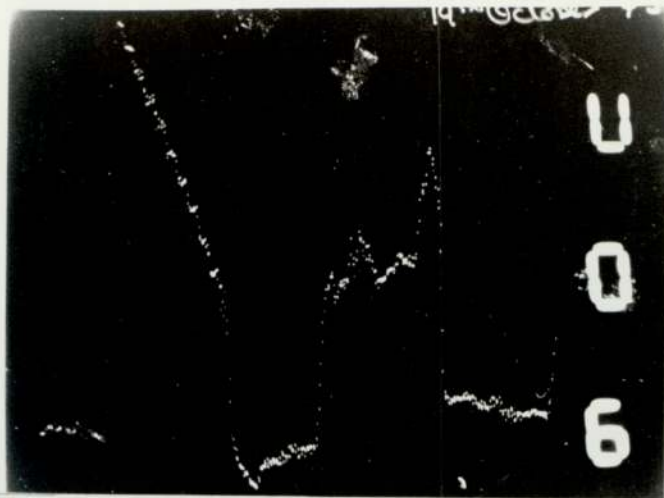
.../

Fig. 6.4   A trace of an in-vivo ulna of an
            osteolamacic patient, 19 years old
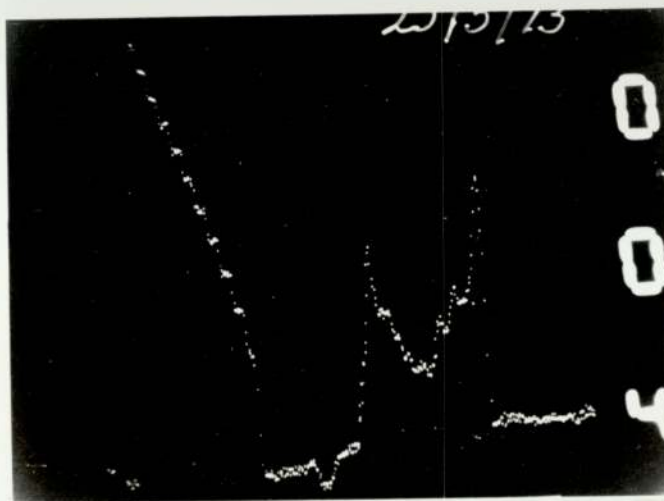
Fig. 6.5   A trace of an in-vivo ulna of an
            osteoporotic patient, 72 years old

Fig. 6.6   A trace of an in-vivo ulna of a
            dialysis patient, 26 years old,
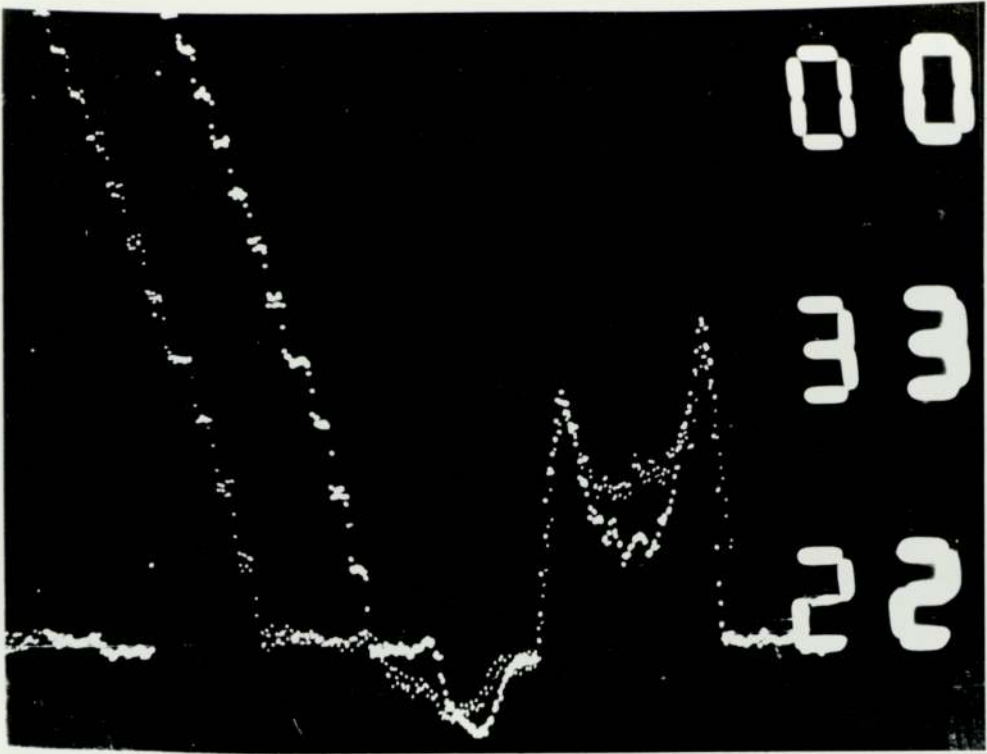   on a low protein diet

Fig. 6.7 Two superimposed traces (6 months interval) of an in-vivo ulna of a dialysis patient, on a new Vitamin D
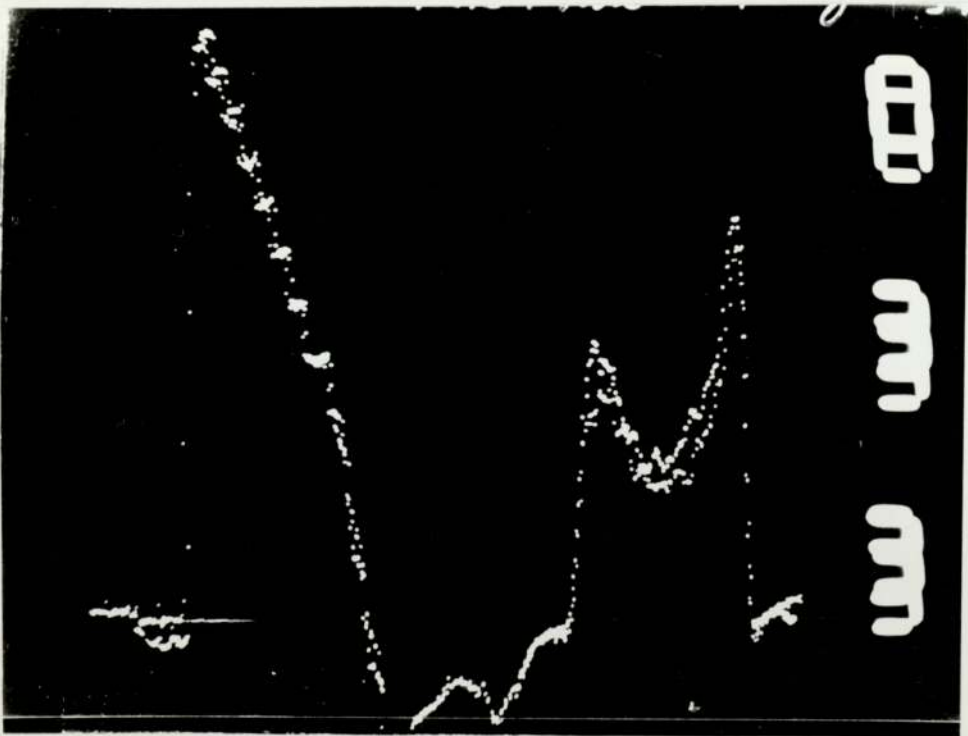

Fig. 6.8 Two superimposed traces (6 months interval) of an in-vivo ulna of a dialysis patient, 49 years old, on a new Vitamin D

the mineral content in the os calcis in volunteers during a period of bed rest. They found lack of uniformity in loss as well as regain (after ambulation) of mineral which they thought suggests a remodelling activity within the os calcis.

In measurements done on traces of 32 patients, the following information was found: the mean width of the ulnas in the site scanned was 11 mm and the maximum width wa s 13.5 mm. The minimum width was 9.5 mm. In 76% of the traces the second peak (representing the second maximum attenuation of X-rays in the ulna) was higher than the first peak by different percentages, 12% of the cases showed the two peaks were equal and the first peak was higher than the second in another 12%. Similar results were found from measurements done on dead ulnas.

6.3   Hand positioning

The fixing frame with the accessories (section 2.2) was made to hold the patient's arm accurately in position. The elbow fixer (section 2.7) was made to ensure reproducibility. Two traces were taken on a healthy subject to check the reproducibility in positioning. A scan was taken after fixing the arm in place (fig. 6.1) then it was released and another trace was taken after a time (fig. 6.9). As is shown in figure 2.10, the two traces are superimposed.

Some patients were in a weak state and they could not stand long enough or they required some help to stand; in these cases fast fixing was required (since fixing is the main contributor in total scanning time which is about two minutes) and a difficulty arose in
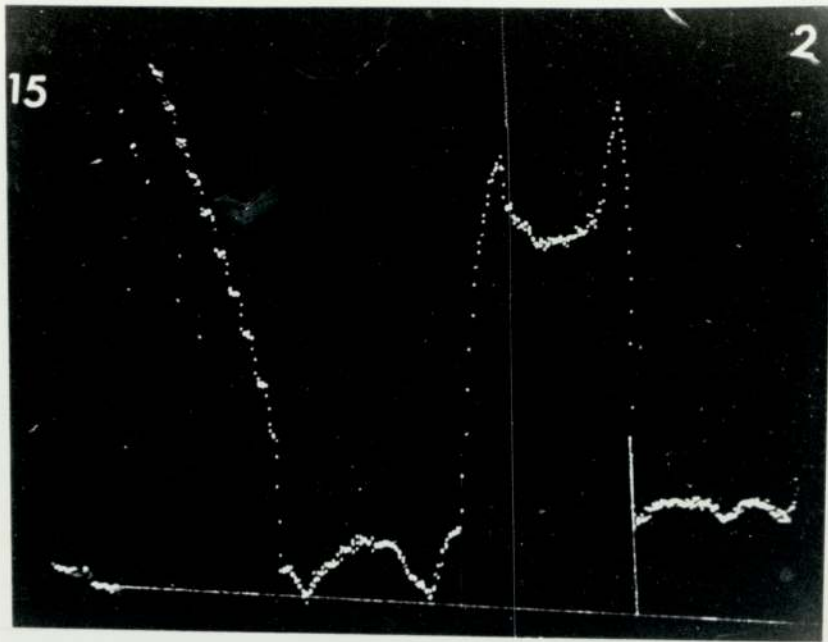
...∕

Fig. 6.9   A trace of an in-vivo ulna (fig. 6.2) made
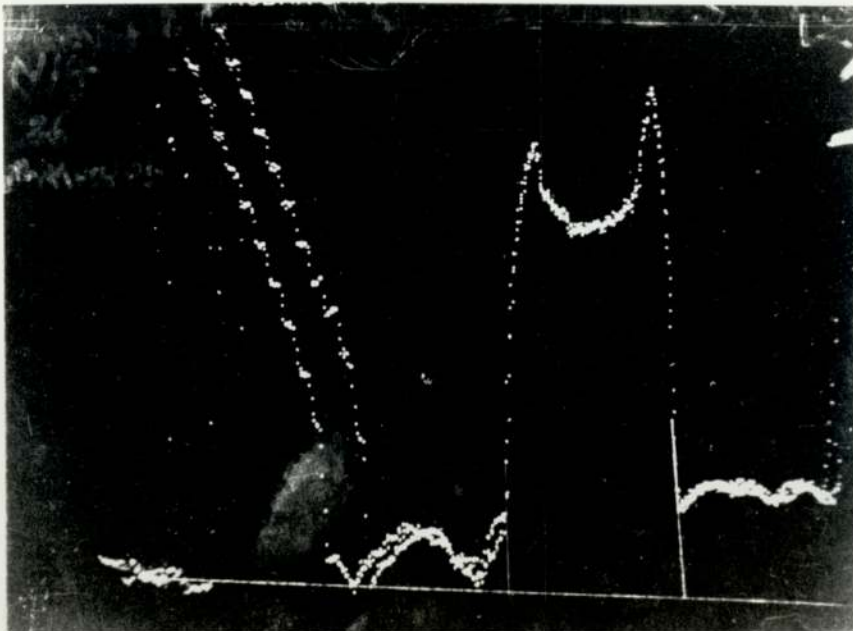   during a second and separate examination

Fig. 6.10   Figures 6.2 and 6.9 superimposed

repositioning the arm accurately. Error in repositioning the arm produced traces of different sites which could not be easily compared. A possible solution is to do scans at closely spaced intervals, a few millimeters along the length of the bone (in one fixing) and to measure the mean total mineral content. Sorenson, Cameron and Wisconsin, 1967, have applied this approach to measurements made near the distal end of the radius. Taking more than one· scan at different sites of the bone has another advantage, that is, they will confirm more accurately the change in total mineral content. This approach has been applied recently to patients.

6.4   The X-ray film

The X-ray film required in every scan is a 12.5 x 10 cm sheet. This is the main part of the running cost and the other part is the small quantities of NaCl and KCl required to make the tissue equivalent solution. The film which was used, cut from a large size film to get nine small films with very little waste. Sometimes it happened that when developing the film in the automatic machine it got stuck. This could not only damage the film since the film has to be removed manually, but it could spoil the following film by getting stuck onto it.

It was recognised that this is caused by the sharp corners of the film. A simple solution is to get the required size from the manufacturer if possible or the film could be cut from a smaller size of X-ray film to make four films each with rounded corners. The film should be pushed with the rounded corner looking to one side of the developing machine.

CHAPTER SEVEN

Conclusions and Suggestions

7. Conclusions and suggestions

This chapter contains a brief review of the main achievements of the experimental work together with some suggestions for future work.

The improvements made to the scanning machine (Chapter Two) include decreasing the spot splitting on the output signal appearing on the trace, by using the X-ray tube in a tilted position. A better limb positioning was provided using the elbow fixer and the standing platform. An effective magnetic screening was made for the two detector boxes. In a future design of the scanning machine, it would be useful to put all electronic equipment in a copper box or other suitable metal to ensure maximum attenuation of external interference.

An artificial bone standard was made (Chapter Three) which is homogeneous, machinable and has elemental composition and density similar to real bone. The attenuation coefficients are accordingly similar. The artificial bone standard is also stable and does not absorb water. It can be used in the calibration of other techniques of bone densitometry and bone radiography. Artificial bone standards of slightly different composition can be made by the same method to represent different bones. It will be desirable to make new artificial bone specimens using purer calcium orthophosphate powder, if available, with the other powders.

The optical transform system discussed in Chapter Four provides accurate measurement of scan areas which represent total mineral content in the sites scanned. The scan area is the main parameter

in scanning measurements. For a better accuracy in the optical
transform system an easier positioning adjustment of object and
image plates is required. Also it would be better to draw the
h and h^x lines directly on the object and the image glass plates
instead of using developed X-ray films on top of the plates, which
were found to displace with time.

Chapter Five established the relationship between the scan
areas and various in-vitro bone measurements. Good correlations
were found between scan areas and each of the following; bone weight,
dry fat-free bone weight and mineral weight. The correlation between
scan areas and bone calcium content has been studied. However, for
better understanding of the relationship between the latter two, a
more accurate measurement of calcium is required. The effect of
limb positioning errors on trace and scan area measurements was
studied. An error of the order of 1% per millimeter may result
from inaccurate longitudinal positioning of the limb.

The in-vivo measurements reported in Chapter Six give an idea
of the expected shapes of traces and how the changes in mineral
content in patients compare with healthy people. It is very important
to continue these measurements on different groups of patients,
especially those who have regular total body calcium measurement (by
N.A.A.) in order to establish the exact correlation of the changes
in mineral content in the bone site and total body calcium.

As clinical experience builds up it will become possible to
establish the normal range of bone mineral content as a function of
sex, age and build.

.../

Early recognition of disorders, e.g. osteomalacia may then be possible. It may also be possible to institute screening of groups at risk, for instance in pregnancy, particularly in the immigrent community.

BIBLIOGRAPHY

1.   Archer-Hall, Carpenter, Edwards and Francois
      B.J.R.   Vol. 46   1973

2.   Atomoenergi isotop service
      S-61101 Nykoping Sweden Bone Scanner 7102

3.   Ardran G.M.
      B.J.R.   Vol. 24   1951

4.   Atkinson P.J.
      J.Obstet. Gynecol. Brit. Commonwealth 77 1970

5.   Anderson, Osborn, Tomlinson, Newton, Rundo, Samon, Salmon & Smith
      Lancet 2   1964

6.   Appleby, Burkinshaw, Marshall, Oldroyd and Oxby
      N.A.T. in Life Science, LAEA - 5M - 157 - 17   1972

7.   Atkinson, West, Parsons and Reed
      B.J.R.   Vol. 3   1970

8.   Anderson, Shimmins and Smith
      B.J.R.   Vol. 39   1966

9.   Atkinson, Weatherell and Weidmann
      J. of bone and joint surgery 44B, 496   1962

10.   Boddy, Al-Hashimi and Boyle
      S.R.R.C. 30/68   1968

11.   Bywaters, E.G.L.
      Opacity. Clin. Sci. 6, 281, 1948

12.   Barnett and Nordin
      B.J.R. Vol. xxxiv No. 407 1961

13.   Barnett and Nordin
      Clin. Radiol Vol. II No. 166 1960

14.   Bethhard, Schmitt, Olehy, Kaplan, Ling, Smith and Molle
      Neutron activation techniques in life science   1967

15.   Boddy, Holloway and Ellott
      Int. J.A.R.I.   Vol 24   1973

16.   Boddy, Holloway and Ellot
      Phys. Med. Biol. Vol. 19 No. 3 1974

17. Boddy, Wilson and Alexander
9th Symp. Radioactive Isotopes in Clinical Medicine
and Research.   Munich   1970

18. Boddy, Holloway, Ellott, Glaras, Robertson and East
Symp. N.A.T. in Life Science.   LAEA – SM – 157/20   1973

19. Boddy, Glaras and Robertson
Phys. Med. Biol. Vol. 20 No. 1 1975

20. Boddy, Robertson and Glaras
Phys. Med. Biol. Vol. 19 No.6 1974

21. British Authors
Text book of radiology Vol. IV 3rd edition 1959

22. BIP Chemicals Limited
Resin Department, Private communication

23. Boddy and Glaras
International J. of radiation and Isotopes Vol. 24 1973

24. Coggle J.E.
Biological effects of radiation 1971

25. CIBA – GEIGY (UK) Limited
Plastic division, Private communication

26. Cameron, Mazess and Sorenson
Investigation Radiology Vol. 3 No. 3 1968

27. Camberlain, Fremlin, Peters and Philip
Brit. Medical J. Vol. 2 1968

28. Cameron and Sorenson
Science   Vol. 142   1963

29. Cohn, Shukla, Dombrowski and Fairchild
Symp. N.A.T. in Life Science LAEA – SM – 157/63 1973

30. Cohn, Fairchild and Shukla
Phys. Med. Biol. Vol. 18 No. 5 1973

31. Cohn and Dombrowski
J. of Nuclear Medicine Vol. 12 No. 7 1971

32. Catto, McIntosh and Macleod
Phys. Med. Biol. Vol. 18 No. 4 1973

33. Clark and Van Dyk
Phys. Med. Biol. Vol. 18 No. 4 1973

34. Chesnut, Manske, Baylink and Nelp
    Proc. Int. Conf on Bone Mineral Measurement 1973

35. Cᵏamberlain, Fremlin, Peters and Philip
    9th Int. Symp. in Radioactive Isotopes in Clinical
    Medicine and Research   Munich   1970

36. Engstrom and Wein
    Acta Radiology 31 1949

37. Evens, Pak, Ashburn and Bartter
    Investigation Radiology Vol. 4 1969

38. Edwards J.P.N.
    PhD thesis, The University of Aston in Birmingham 1973

39. Fourman and Royer
    Calcium Metabolism and the Bone 2nd edition 1968

40. Fischer and Porter Company
    Warminster, Pennsylvania U.S.A.

41. Glasser, Quimby, Morgan and Weatherwax
    Physics Foundations of Radiology 3rd edition 1961

42. Goldsmith, Johnston, Ury, Vose and Colbert
    The J. of Bone and Joint Surgery Vol. 53A No. 1 1971

43. Garn S.M.
    American J. of Clinical Nutrition Jan. 1962

44. Harold E.J.
    The Physics of Radiology 2nd edition

45. Harris and Heaney
    Skeletal Renewal and Metabolic Bone Diseases

46. Henny G.C.
    Radiology 54   1950

47. Hubbell J.H.
    NSRDS National Bureau of Standards 29 1969

48. Helela and Virtama
    Sym. Oss. European Association of Radiology
    Editors Jelliffe and Strickland 1970

49. Henrikson C.
    Iodine-125 as a radiation source for odetological
    roentgenology Report 1967

.../

50. Jackson W.P.U.
     Calcium Metabolism and Bone Diseases   1967

51. Jackobson B.
     American J. of Roentgenology   Vol. 191   1964

52. Jurist J.M.
     Phys. Med. Biol.   Vol. 15   No. 3   1970

53. Johnston, Smith, Pao-Lo Yo and Deiss
     Metabolism   Vol. 17   No. 12   1968

54. Kaye and Laby
     Tables of Physical and Chemical Constants   14th edition   1973

55. Long C.
     Biochemists' Handbook   1961

56. Lundbery and Nilsson
     Clin. Orthop.   60.   1968

57. Meredith and Massy
     Fundamentals of Physics and Radiology   2nd edition   1972

58. Mayneord W.V.
     Acta of the Internation Union against Cancer   2   1937

59. Mazess R.B.
     U.S.   A.E.C. Report   COO-1422-30   1968

60. Mason R.L.
     Science   Vol. 150   1965

61. Mayer, Trostle, Ackerman, Schraer and Doyle Sittler
     Radiation Research   Vol. 13   1960

62. McGrace, Glas and Sweet
     B.J.R.   Vol. 40   1967

63. Nillson Bo. E.
     Acta Orthopaedica Scandinavica Supplementum
     Vol. 37   No. 91   1966

64. National Bureau of Standards
     N.B.S. Handbook   85   1964

65. Nillson Bo. E.
     Symp. Oss. European Association of Radiology
     Editors Jelliffe and Strickland   1970

66.   Nelp, Denney, Murano, Hinn and Chesnut
      Symp. N.A.T. in Life Science LAEA-SM-157/66

67.   Nelp, Palmer, Murano, Pailthorp, Hinn, Rich, Williams,
      Rudd and Denney
      J. Lab. Clin. Med. 7 1970

68.   Osbas E.
      PhD Thesis The University of Birmingham 1975

69.   Private communication with Dr J Archer-Hall
      The University of Aston in Birmingham

70.   Palmer, Nelp, Murano and Rich
      Phys. Med. Biol. Vol. 13 No. 2 1968

71.   Pridie R.B.
      B.J.R. Vol. 40 1967

72.   Progress in methods of bone mineral measurement, Bethesda,
      U.S. Department of Health, Education and Welfare p. 532 1968

73.   Richards A.G.
      J. Dent. Res. 32 1953

74.   Ramo, Whinnery and Van Duzer
      Fields and Waves in Communication Electronics 1965

75.   Reed, West and Atkinson
      Symp. Oss. European Association of Radiology
      Editors Jelliffe and Strickland 1970

76.   Simon G.
      Principles of Bone X-ray Diagnosis 3rd edition 1973

77.   Stein I.
      American J. of Roentgenology 37 1937

78.   Sorenson, Witt and Cameron
      U.S. A.E.C Report COO-1422-9 1966

79.   Smith, Johnston and Pao-Lo Yo
      J. of the American Medical Association Vol. 219 1972

80.   Spiers F.W.
      B.J.R. Vol. 19 1964

81.   Sorenson, Cameron and Wisconsin
      J. Bone Surgery Amer. Vol. 49A 1966

.../

82. Strandjord N. M. et al
    N ASA SP-64 p. 115 -

83. Strandjord, Forhand, Lawrence and Cox 1970
    Symp. Oss. European Association of Radiology
    Editors Jelliffe and Strickland   1970

84. Shimmins, Smith, Aitken, Anderson and Gillespie
    Clin. Radiol. Vol. 23   1972

85. Sorenson and Cameron
    Symp. Oss. European Association of Radiology
    Editors Jelliffe and Strickland   1970

86. Smith, Horton, Aitken and Smith, A.
    B.J.R. Vol. 47   1974

87. Smith and Cameron
    Bone Mineral Analyzer, Norland Instruments (USA) 1972

88. Virtama P.
    Acta. Anat. Supple. 29 1957

89. Virtama and Mahoven
    B.J.R. Vol. XXXIII No. 385 1960

90. Virtama, Gastrin and Telkka
    Clin. Radiol Vol. 13 1962

91. Vose G.
    Radiology 71 1958

92. Vose G.
    Lab. Invest. Vol. 8 1959

93. West R.R.
    PhD Thesis, The University of Leeds 1969

94. West R.R.
    B.J.R. Vol. 46 1973

95. West and Reed
    B.J.R. Vol. 43 1970

96. Watt and Cameron
    US A.E.C. Report COO-1422-42 1969